H24/3137

MONASH UNIVERSITY
THESIS ACCEPTED IN SATISFACTION OF THE
REQUIREMENTS FOR THE DEGREE OF
DOCTOR OF PHILOSOPHY

ON.................................. 1 March 2002 ....

....

for   Sec. Research Graduate School Committee

Development of a realistic *in vitro* model for studying the energetics of cardiac papillary muscles

Linda Jane Mellors

B.A. B.Sc. (Hons)

A thesis submitted to the Faculty of Medicine, Monash University
for the degree of
Doctor of Philosophy

Department of Physiology
Monash University
Victoria 3800
AUSTRALIA

October 2001

Table of contents

List of figures

List of tables

List of abbreviations

ATP	Adenosine triphosphate
BDM	2, 3-butanedione monoxime
CSA	Cross-sectional area
ΔG	Change in free energy
ΔH	Change in enthalpy output
ΔQ	Change in heat output
ΔT	Change in temperature
ΔW	Change in work output
ε_{Net}	Net mechanical efficiency
FLA	Force-length area
L_{max}	Muscle length at which isometric force is maximal
L_{opt}	Muscle length at which sinusoidal work output is maximal
P_0	Active isometric force (*i.e.* excluding passive force)
P_{O_2}	Partial pressure of oxygen
PCr	Phosphocreatine
PVA	Pressure-volume area
V_{O_2}	Rate of oxygen consumption
ΣW	Total work output

Summary

The primary aim of this thesis was to improve the realism of protocols used to study the energetics of isolated papillary muscles. Experiments were performed *in vitro* using left ventricular papillary muscles from adult male rats. Measurements of force output, muscle length change and muscle temperature change were used to calculate the work and heat produced during and after each protocol. Net mechanical efficiency was defined as the proportion of the energy (enthalpy) liberated by the muscle that appeared as work.

The first study was designed to determine whether the efficiency of rat papillary muscles is protocol-dependent by comparing the efficiency measured using two established contraction protocols. In the current study, the mean efficiency of preparations performing low frequency afterloaded isotonic contractions (10 twitches at 0.2 Hz) was 21.1 ± 1.4 %, 13.2 ± 0.7 % when performing sinusoidal length change contractions (40 twitches at 2 Hz) and 21.5 ± 1.0 % when performing high frequency afterloaded isotonic contractions (40 twitches at 2 Hz). Additional experiments designed to measure work output unambiguously indicated that the method used to calculate work output in isotonic contractions overestimated actual net work output due to the inclusion of the work done by parallel elastic elements. When the true net work output was used to determine efficiency in afterloaded isotonic contractions, efficiency was similar to that for sinusoidal contractions. It was concluded that the maximum net mechanical efficiency of rat papillary muscles was not protocol-dependent and was between 10 and 15 %.

Net mechanical efficiency of the heart *in vivo* has been estimated to be 20-25 %. One possible reason for the difference between the values calculated for the isolated muscles and those for intact hearts is that the pattern of length changes used in isolated muscle studies bear little resemblance to those observed *in vivo*. The second study aimed to develop a realistic strain protocol, based on published measurements of contracting papillary muscles *in situ*, for use with isolated preparations. A standard contraction protocol (27°C; 40 twitches at 2 Hz) that followed the strain dynamics of papillary muscles *in situ* was developed. The realism of the protocol was enhanced further by incorporating isometric relaxation and thus the model could simulate the main mechanical features of ventricular function. The most notable result from these experiments was that the enthalpy output per twitch was relatively constant despite the various alterations made to the protocol including differences in shortening amplitude, isometric duration, shortening-lengthening duty cycle and contraction frequency. Due to the relatively constant enthalpy output, changes in mechanical efficiency reflected changes in work output per twitch. The strain parameter that affected work output per twitch the most was the amplitude of shortening. Using the realistic strain protocol, the maximum net mechanical efficiency of rat papillary muscles was ~15 %. This supports the idea that efficiency is not protocol-dependent since the efficiency of muscles performing afterloaded isotonic, sinusoidal and realistic contraction protocols was 10-15 %.

In the final study, the realistic strain protocol was used to study the effects of hypothermia (15 or 8°C) on rat papillary muscles following rewarming to 30°C. Hypothermia is used routinely during cardiac bypass surgery but the effects of the cold period on the muscle have not been well-characterised. The contraction protocol consisted of 40 twitches at 2.2 Hz. The work output from the rewarmed muscles was depressed relative to the control measurement throughout the post-rewarming recording period. Work output was more depressed following 8°C hypothermia (~60-70 % of the pre-cooling value) than following 15°C hypothermia (~90-98 % of the pre-cooling value). Work output was depressed due to a decreased ability of the muscle to generate force and altered force-velocity properties. Following the 8°C hypothermia, enthalpy output was closely matched to work output and so the net mechanical efficiency of the muscles remained reasonably close to the pre-cooling values.

Declaration

This thesis contains no material that has been accepted for the award of any other degree or diploma in any university, or other institution, and to the best of my knowledge, it contains no material published previously or written by another person, except where due reference is made in the text. All experiments reported in this thesis complied with the Australian Code of Practice for the Care and Use of Animals for Scientific Purposes and had approval from the Monash University Animal Welfare Committee.
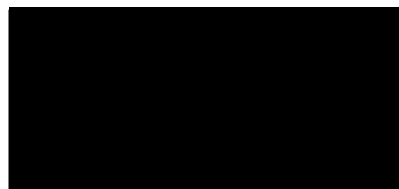
Linda Mellors

List of publications

The following publications are listed in support of this thesis:

Papers

Mellors, L.J. and Barclay, C.J. (2001). The energetics of rat papillary muscles undergoing realistic strain patterns. *Journal of Experimental Biology (in press)*.

Mellors, L.J., Gibbs, C.L. and Barclay, C.J. (2001). Comparison of the efficiency of rat papillary muscles during afterloaded isotonic contractions and contractions with sinusoidal length changes. *Journal of Experimental Biology* **204**: 1765-1774.

Abstract

Mellors, L.J., Gibbs, C.L. and Barclay, C.J. (2001). Is the efficiency of rat papillary muscle dependent on contraction protocol? *Journal of Muscle Research and Cell Motility* **21(8)**: *(in press)*.

Acknowledgments

Firstly, I would like to express my sincere gratitude to my supervisor, Dr Chris Barclay. I have been incredibly fortunate to have been introduced to the world of muscle energetics by such a talented and patient teacher. Thank you for teaching me everything I needed to know to complete my Ph.D. and for providing me with constant encouragement to achieve my goals. Thank you also for making the lab such an interesting and friendly place to work.

Sincere thanks also to Prof Colin Gibbs for supporting my candidature, providing comments on various parts of this thesis and for drawing on his vast expertise to assist me in sourcing information.

Special thanks to Peter Arnold for constructing the thermopiles, constructing and modifying equipment and answering my thermopile questions. I would also like to thank Will Brenton for repairing and modifying electronic equipment and David Caddy for statistical advice.

The diagram in Figure 2.2 was prepared by Michelle Mulholland. The photographs in Figures 2.3, 2.4 and 2.5 were taken by Rachel Mellors and scanned by Carole Rushton and Dr Chris Barclay. Thank you all for allowing me to benefit from your expertise.

Sarah Mellors did a wonderful job proof-reading the entire thesis and I am extremely grateful for her contributions. Thank you also to Julie Walshe and Rachel Mellors for making themselves available to Sarah for consultation on 'difficult' sentences.

Chapter 1: Introduction

The primary aim of this thesis was to characterise the energetics of isolated rat papillary muscles using a contraction protocol that closely matched the *in vivo* activity of these muscles. The following introduction will briefly identify some important issues in the measurement of cardiac energetics.

The basic function of almost all muscles is to convert the energy obtained from carbohydrates and fats into mechanical energy. The processes involved in this energy conversion are the focus of the field of study known as muscle energetics. In the heart, the mechanical energy produced by the ventricular muscles powers the movement of blood around the body. There have been many studies of various aspects of the energetics of the heart and cardiac muscle. Studies of cardiac energetics using whole hearts, either *in vivo* or *in vitro*, have the advantage of investigating the heart functioning in, or close to, its normal manner. However, due to the complexity of the heart's structure, it is difficult to relate measurements of whole heart energy consumption and work output to, for example, the energy consumption and work output of ventricular work *per se*. To obtain precise measurements of energy consumption and work output of ventricular muscle, the use of isolated cardiac muscle preparations is preferable. Both the energy consumption and mechanical work output of such preparations can be measured very accurately, with excellent time resolution and can be easily related to the mass of tissue actually performing the work. However, in most studies to date, the contraction protocols used with isolated cardiac muscles have been designed to facilitate the laboratory study of the

muscles rather than to simulate the normal activity of the muscle. There are several reasons for this: (1) to ensure that diffusive oxygen supply is adequate, most studies have used low contraction frequencies, (2) the interpretation of energetic aspects of contraction is more simple when force output or muscle length are held constant and (3) until relatively recently, it was difficult to alter muscle length using the complicated patterns of normal cardiac contraction.

The overall aim of this thesis was to develop a protocol for studying isolated papillary muscles *in vitro* that closely matched *in vivo* muscle activity and to characterise the energetics of rat papillary muscles using the protocol. Specifically, this involved using higher contraction frequencies than those used in previous studies of energetics and matching the pattern of length changes to those observed *in situ*. To overcome the difficulties outlined above, split papillary muscles of low cross-sectional area were used to enhance diffusive oxygen supply and to allow high contraction frequencies to be used. To reproduce the complicated patterns of length change that occur *in vivo*, a computer-controlled motor was used to accurately control muscle length. Energy consumption was calculated from measurements of muscle temperature change during a contraction protocol. Temperature change was measured using a thermopile with excellent time resolution characteristics. Detailed explanations of the materials and methods used in the current study are given in Chapter 2.

The first step towards developing a new, realistic protocol for use with isolated papillary muscle preparations was to compare two protocols that have been used previously to measure cardiac mechanics and energetics. To this end, the conventional afterloaded isotonic protocol was compared with the most recent attempt at a realistic protocol, a sinusoidal length change protocol (Chapter 3). This study aimed to clarify reported differences in the energetic characteristics of rat papillary muscles using the two protocols and to determine whether mechanical efficiency was really protocol-dependent as suggested by the results of earlier studies.

The measurements of papillary muscle energetics using these traditional protocols were used as a background for characterising the energetics of these muscles during a much more realistic contraction protocol (Chapter 4). The realistic strain (*i.e.* length change) pattern was based on published measurements of papillary muscle dynamics *in situ*. The strain pattern was varied to encompass the common *in situ* characteristics. The energetic

profile of rat papillary muscles was determined with muscles contracting according to this strain pattern.

This contraction protocol was then used to investigate the effects on the energetics of rat papillary muscles resulting from spending 1-2 hr at a low temperature (Chapter 5). Low temperatures are commonly used during cardiac bypass surgery but the consequent alterations in the energetics of cardiac muscle directly resulting from the hypothermia have been only poorly characterised. The realistic protocol not only allowed the effects of hypothermia on the energetics of the muscle to be characterised but also provided insights into the mechanisms underlying the observed changes in muscle function.

Chapter 2: Materials and methods

This chapter provides details of the materials used and the general methodology followed for the experiments presented in this thesis. Where a particular method or protocol specific to a set of experiments has been used, details are presented in the relevant chapter.

2.1   Animals

Adult male *Sprague-Dawley* rats aged between 12 and 16 weeks were obtained from Monash University Animal Services and housed in the Department of Physiology's Animal House. Rats within this narrow age range were chosen since the mechanical properties of the heart are consistent during this period (Capasso *et al.*, 1982). Only male rats were used to avoid potential interpretative complications due to gender differences. Although Leblanc *et al.* (1998) reported that hearts of male and female rats aged 2-4 months exhibit similar contractile profiles, Wang *et al.* (1998) reported that the force-Ca^{2+} relationships for papillary muscles from 3-4 month old male and female rats were different.

All rats had free access to standard laboratory rat chow and water for the duration of the study. The environmental surroundings of the rats were monitored from birth. The temperature range was 20-22°C with a relative humidity of ~50 %. The rats were exposed to a 12 hr light/dark cycle.

All procedures involved in the handling and care of animals were in accordance with the Australian Code of Practice for the Care and Use of Animals for Scientific Purposes and were approved by the Monash University Animal Welfare Committee.

2.2 Papillary muscle preparation and dissection

Rats were killed by cervical dislocation whilst under deep chloroform anaesthesia and the chest cavity was opened to expose the beating heart. The heart was rapidly excised and immersed in a series of beakers containing room temperature ($\sim$22-23°C), oxygenated (95 % O_2 - 5 % CO_2) Krebs-Henseleit solution (see Section 2.3 for composition) and was gently massaged to remove remaining blood. The aortic stump was cannulated to allow back-perfusion through the coronary circulation with 10 ml oxygenated Krebs-Henseleit solution (at room temperature) containing 30 mM 2,3-butanedione monoxime (BDM; Sigma Chemical Co., St Louis, MO, USA). This rapidly caused the heart to cease contractile activity and allowed viable, split papillary muscle preparations to be dissected (see Section 2.3.1).

The outer wall of the right ventricle was separated from the remainder of the ventricle and a straight cut was made along the length of the septum. The left ventricle was carefully opened and pinned back taking care not to damage the papillary muscles situated on the opposite wall of the ventricle. The heart was then allowed to rest in the BDM solution for 20 min before dissection of the papillary muscles commenced. This was found to have a beneficial effect on the mechanical performance of the muscle once it was mounted in the experimental chamber.

Suitable papillary muscles from the left ventricle were selected on the basis of their length and overall appearance while viewed under a microscope (×20 magnification; Zeiss, Germany). These muscles were trimmed and/or split longitudinally if necessary and the underside separated from adhering tissue. Small platinum wire loops were tied to either end of each preparation with braided, non-capillary silk thread (5/0, Dynek Pty. Ltd., Australia). Preparations were removed from the ventricle while maintaining a passive tension of $\sim$5 mN using a C-shaped spring clip.

Papillary muscles are convenient to use in isolated muscle experiments given their natural shape. The muscles have myocytes arranged in parallel along the length of the muscle, can be readily dissected and can have ties or clips attached to either end allowing attachment to apparatus for measuring mechanical properties.

2.3 Solutions

Preparations were bathed in Krebs-Henseleit solution with the following composition (mM): 118 NaCl; 4.75 KCl; 1.18 KH_2PO_4; 1.18 $MgSO_4$; 24.8 $NaHCO_3$; 1.6 $CaCl_2$; 10 glucose. Where mentioned in the text, 30 mM BDM was added to this solution. All solutions were bubbled continuously with carbogen gas (95 % O_2 - 5 % CO_2) to ensure that the muscle received a constant supply of oxygen and that the pH was maintained at 7.4.

2.3.1 Effects of BDM on cardiac muscle

The addition of BDM to dissecting solutions allowed papillary muscles to be split without any impairment of function following wash-out (Kiriazis and Gibbs, 1995). The precise mechanism of the protective effects of BDM is unknown but appears likely to be due to inhibition of mechanical activity by BDM. The mechanisms of inhibition of force production in cardiac muscle by BDM include: (1) inhibition of cross-bridge force development which may be due to altered cross-bridge kinetics or a prevention of cross-bridge attachment (Backx et al., 1994; Gwathmey et al., 1991; Hajjar et al., 1994; Perreault et al., 1992; Watkins et al., 1992), (2) a reduction in the Ca^{2+}-sensitivity of the myofilaments (Backx et al., 1994; Gwathmey et al., 1991; Perreault et al., 1992; West and Stephenson, 1989) and (3) a decrease in free $[Ca^{2+}]_i$ as shown by a decrease in the amplitude of the Ca^{2+} transient (Backx et al., 1994; Gwathmey et al., 1991; Perreault et al., 1992). Whatever the mechanism of action, the use of BDM in dissecting solutions has been shown to prevent contracture in cardiac muscle (Hajjar et al., 1994; Perreault et al., 1992). The effects of BDM on both cardiac and skeletal muscles have been summarised by Sellin and McArdle (1994).

Several studies have reported that the effects of BDM on cardiac muscle are reversible (Kotsanas et al., 1993; Mulieri et al., 1989; Watkins et al., 1992; West and Stephenson, 1989), even after long periods of storage in a BDM solution (Mulieri et al., 1992). Of particular importance in the context of this thesis is the finding of Kiriazis and Gibbs (1995) that the use of BDM during dissection affects neither the mechanical nor energetic properties of rat papillary muscles once the BDM has been washed out. Inclusion of BDM in the dissecting solution thus allowed functional preparations of small cross-sectional area (CSA) to be obtained even when substantial trimming of the papillary muscle was necessary (Mulieri et al., 1989). For the experiments reported in this thesis, the heart

remained immersed in the oxygenated BDM-Krebs-Henseleit solution throughout the dissection period.

2.4 Preparation oxygenation

The muscle preparations used in this study were continuously supplied with oxygen throughout dissection and experiments. Papillary muscles were either immersed in oxygenated Krebs-Henseleit solution or, during recordings of energy output, enclosed in a humidified, oxygenated chamber (see Section 2.5).

A previous study from this laboratory used a mathematical model, based on work by Loiselle (1982; 1985a), to assess the adequacy of diffusive O_2 supply to isolated papillary muscles (Baxi et al., 2000). That analysis indicated that for the muscles used in that study (CSA ~1 mm^2) O_2 diffusion would have only just been adequate to meet the metabolic demands at contraction rates of 2-4 Hz. To improve O_2 supply, smaller preparations were used in the current study (range of mean CSA ~0.5-0.7 mm^2) but in some experiments a higher temperature was used (30°C versus 27°C used by Baxi et al., 2000). This latter factor would not favour O_2 supply since the active metabolic rate is more sensitive to temperature (Q_{10}=1.56, calculated from Buckberg et al., 1977) than the diffusivity of O_2 in muscle (Q_{10}=1.04, Mahler et al., 1985). Therefore, the analysis was repeated for the conditions and muscles used in the current study.

Details of the analysis are given by Baxi et al. (2000) and Loiselle (1982, 1985a) and are described only briefly here. The profile of the partial pressure of oxygen (Po_2) through the cross-section of a cylindrical muscle was estimated by solving the differential diffusion equation:

$$\frac{d^2 Po_2}{dr^2} + \frac{1}{r} \times \frac{dPo_2}{dr} - \frac{m(Po_2)}{K} = 0$$

where r is the radius of the muscle (cm)

$m(Po_2)$ is a function describing the dependence of mitochondrial oxygen consumption on Po_2

K is the diffusivity of O_2 through muscle

The assumptions underlying this model are (Baxi et al., 2000; Loiselle, 1985a): (1) the papillary muscle preparations were cylindrical and of uniform radius, (2) oxygen diffusion through the ends of the preparation was negligible (CSA of the ends of a cylinder with

muscle dimensions would be <10 % of the area of the sides of the cylinder) and (3) the metabolic rate was constant over time and through the muscle. The boundary conditions used in solving the equation were that Po_2 at the muscle surface was 0.95 atm, corresponding to the fraction of O_2 in the carbogen gas mixture (95 % O_2 - 5 % CO_2), and that the rate of change of Po_2 with radial distance into the muscle was zero at the muscle's centre. The values of the other variables used in the equation are shown in Table 2.1.

Table 2.1 Values used to solve O_2 diffusivity equation

	Published value	Temperature of reported value (°C)	Q_{10}	Value adjusted to 27°C	Value adjusted to 30°C
Basal heat rate (mW g^{-1})	4.4 [a]	27	1.31 [b]		4.644
Active heat rate (mW g^{-1})	12.06 [c]	27	-		
	9.66 [d]	30			
Diffusivity of O_2 (cm^2 atm^{-1} min^{-1})	2.39×10^{-5} [e]	25	1.04 [e]	2.409×10^{-5}	2.437×10^{-5}

[a] Baxi et al. (2000); [b] Loiselle (1985b); [c] value obtained from high frequency afterloaded isotonic contractions at 2 Hz; [d] value obtained from realistic contractions at 2.2 Hz; [e] Mahler et al. (1985). Note that the active Vo_2 values were obtained using different protocols and so a Q_{10} value has not been calculated. The rate of oxygen consumption was calculated from the heat rate using an energetic equivalent of 21 J ml^{-1} O_2.

The maximum rate of O_2 consumption (active Vo_2) in the protocols used was calculated from the rate of enthalpy output averaged over 3 complete, steady-state cycles near the end of the contraction protocol described in Chapter 3. When muscles are in an energetic steady-state, an amount of phosphocreatine (PCr) equal to the amount split in each contraction is resynthesised in each cycle so that there is no net breakdown of PCr over a full cycle (Paul, 1983). In this case, the average rate of enthalpy output can be assumed to reflect the rate of mitochondrial O_2 consumption. This method of calculation of the maximum rate of O_2 consumption differs from that used by Baxi et al. (2000). They estimated the rate from the slope of the enthalpy versus time record after the last cycle of a contraction series had finished. However, at that time there would be a net resynthesis of PCr and that process absorbs energy. The rate of enthalpy output would, therefore, underestimate the rate of mitochondrial heat production and thus the rate of oxygen consumption. Consistent with this reasoning, data from the muscles used in the current

analysis showed that the steady-state rate of enthalpy output was up to twice as great as that recorded at the start of the recovery period. The analysis described here used the steady-state rate of enthalpy output to estimate V_{O_2} and was performed using the appropriate range of CSA of the muscles used in this study.

The rate of oxygen consumption was calculated from the enthalpy output assuming an energetic equivalent of 21 J ml^{-1} O_2. Basal metabolism is not affected by changes in extracellular $[Ca^{2+}]$ (Chapman, 1976; Wendt and Loiselle, 1981), therefore, no correction was made for the lower $[Ca^{2+}]_o$ used in the current study (1.6 mM compared with 2.54 mM in Baxi *et al.*, 2000). The results of these analyses are shown in Figure 2.1.
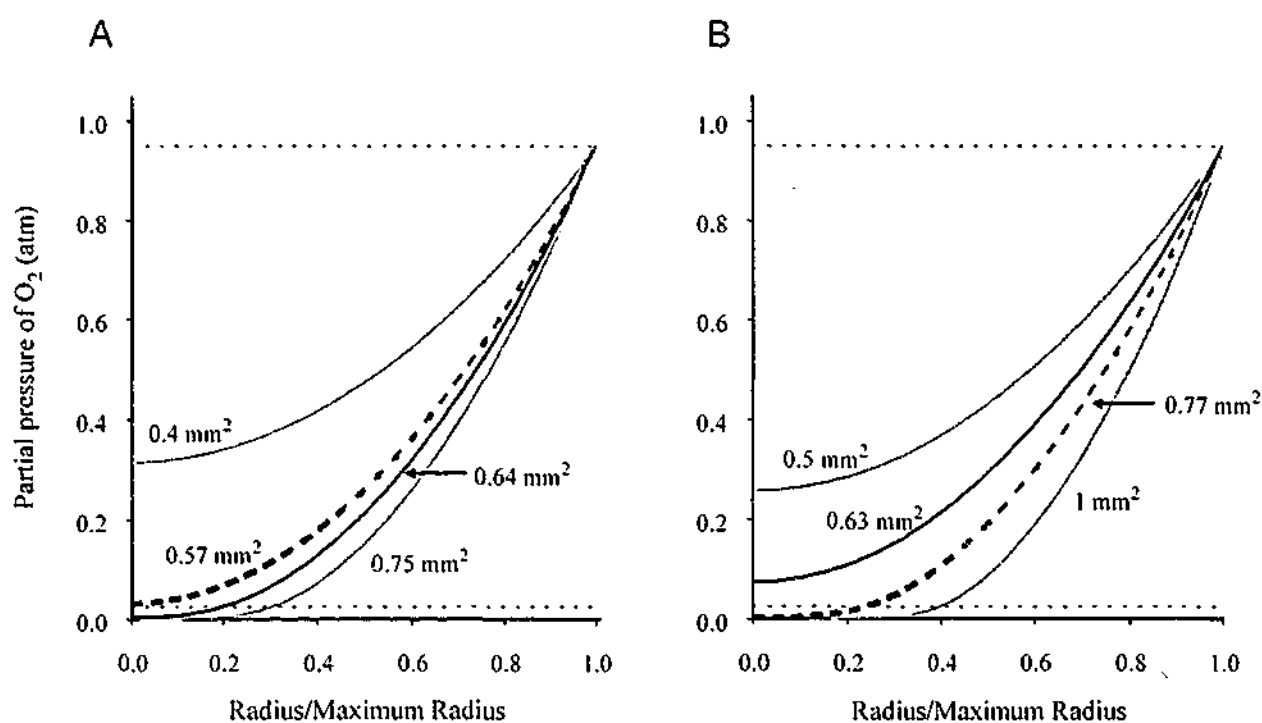
Figure 2.1 Results of diffusive O_2 supply modelling

Predicted O_2 profiles for a representative muscle at 27°C in an energetic steady-state performing afterloaded isotonic contractions at 2 Hz (**A**) and another at 30°C performing realistic contractions at 2.2 Hz (**B**). In each example, the solid black line represents the actual CSA of the muscle used in the model, the dashed black line represents the mean CSA of the group of muscles performing each contraction protocol and the solid grey lines represent the outer limits of CSA used in the respective protocols (see Chapters 3 and 5 for details).

This analysis suggests that the rate of diffusive O_2 supply into papillary muscles would have been just adequate to meet the metabolic requirements of the average papillary muscle. However, it also indicates that the largest muscles used may have had a compromised oxygen supply. Overall, the analysis indicates that the metabolic

requirements of the muscles used in the current study most likely could be met by diffusive O_2 supply. However, the analysis also emphasises the importance of using small diameter preparations when such high stimulation rates are used. This would be particularly important if steady-state activity was to be studied over longer periods of time than those used in the current study.

An assumption that has a considerable effect on the results of the analysis is that the rate of oxygen consumption was equal to the steady-state value throughout the protocol. This is clearly not the case in the protocols used in this study which encompass the transition from rest to steady-state activity. If it is assumed that (1) the basal rate of oxygen consumption is constant during the protocol and (2) the active V_{O_2} increases exponentially towards the steady-state value with a time-constant of 5 s, then it can be estimated that the average V_{O_2} during the contraction protocols would have been about 80 % of the steady-state value. If this rate of oxygen consumption is used in the analysis, even the largest preparations would have had adequate O_2 supply.

Two factors that would have favoured O_2 diffusion into muscles in the current experiments compared with those of Baxi *et al.* (2000) were the smaller CSA of preparations (~0.5-0.77 mm^2 range of mean CSA used in the current experiments compared to ~1 mm^2 in Baxi *et al.*, 2000) and the lower $[Ca^{2+}]_o$ (1.6 mM compared to 2.54 mM in Baxi *et al.*, 2000) which resulted in lower work and enthalpy outputs.

It is important to provide some comment on the validity of the assumptions used in this analysis. Firstly, some O_2 would be expected to diffuse through the ends of the muscle, although the surface area of the ends is much smaller than that of the length of the muscle and the ends are effectively clamped. Also, not all muscles were perfectly cylindrical in shape. Some preparations were wider and flatter than others. In this case, the maximum radius would be less which would favour O_2 supply. Thus the assumptions are reasonable and any errors resulting from them would be small relative to the estimated safety margin (Figure 2.1).

2.5   Experimental apparatus

2.5.1   The horizontal thermopile

Muscle preparations were mounted between a semi-conductor force transducer (see Section 2.6.1) and a servo-controlled lever (see Section 2.7.1). Rods constructed of fine tungsten wire (140 μm diameter) provided low compliance links between the preparation

and the recording apparatus (Figure 2.2). The rods were made by hanging a 50 g weight from one end of the rod and passing current (8 A) through the tungsten wire to heat it and make it rigid. The ends of the tungsten rods closest to the preparation were bent into hooks. The platinum loops attached to the ends of the muscle were placed over these hooks to allow attachment of the muscle to the recording apparatus. The use of platinum loops in preference to silk thread loops further reduced compliance of the force recording system (see Section 2.6.4). The thermopile was positioned between the force transducer and the lever so that the mounted papillary muscle rested along the central region of the thermopile (see Section 2.8.1).
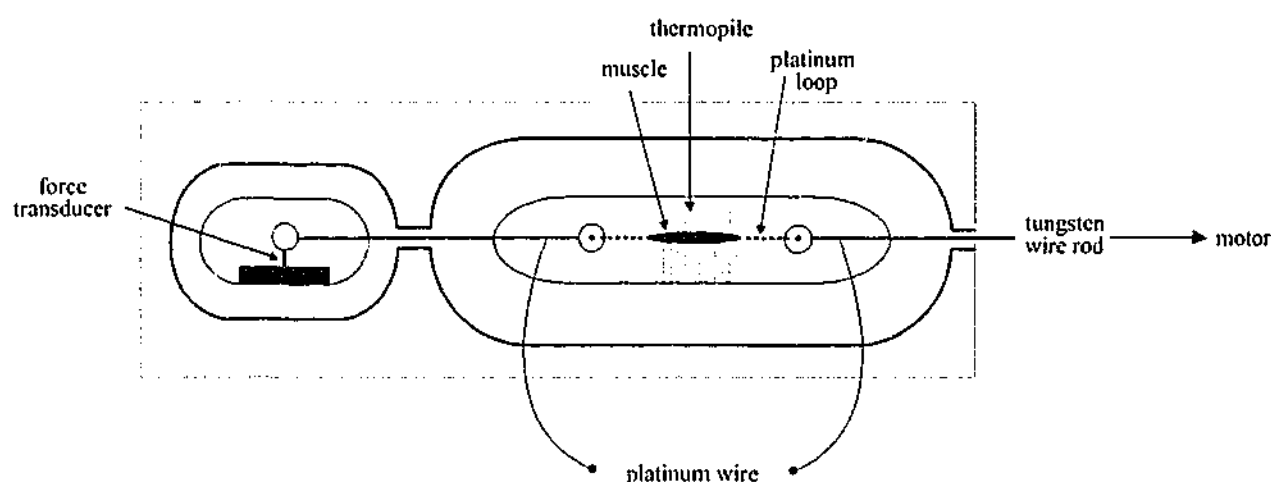
Figure 2.2 Diagram of arrangement of a muscle on the recording apparatus

The preparation lay along the central region of the thermopile, over the active thermocouples. Tungsten wire rods provided low compliance links between the preparation and the recording apparatus. At each end of the preparation, one end of a platinum wire loop was bound to the muscle and the other end of the loop was placed over a hook in the end of the tungsten rod. The muscle was stimulated via two fine platinum wire electrodes soldered to the tungsten rods.

The experiments reported in this thesis were performed using a horizontal thermopile arrangement. The horizontal thermopile holds several advantages over the traditional, vertical arrangement. (1) It was easier to position preparations accurately along the active thermocouples. (2) It was also easier to reduce the total heat capacity by removing excess solution from around the muscle prior to recording heat output. This was important for enabling the small temperature changes that occurred in the small papillary muscle preparations used in this study, particularly in protocols using low twitch frequencies, to

be recorded. In fact, the preparations used in the present experiments are amongst the smallest papillary muscles used for heat recordings (~0.5 mm^2; compared with Kiriazis and Gibbs, 1995; Mast and Elzinga, 1988; Mulieri *et al.*, 1989). (3) The thermal stability of this arrangement was also found to be superior to the vertical arrangements used previously in this laboratory, presumably due to the greater thermal sink for the reference junctions. There must also have been less thermal fluctuation around the active junctions, although the reasons for this are unclear. (4) The output of the thermopile equilibrated more quickly following removal of the solution from the thermopile chamber prior to recording heat output. Muscle preparations were immersed in oxygenated Krebs-Henseleit solution during non-recording periods and when recordings were made, the lid of the thermopile box was closed which kept the preparation in a humidified, oxygen-saturated environment. It was found that the temperature stabilised more quickly (~2-8 min) following the lid being opened and closed than an equivalent disturbance in the vertical arrangement where stabilisation could take as long as 20 min.

The thermopile was mounted in an aluminium frame (Figure 2.3). The thermopile frame was a large (~12 × 10.5 × 4 cm; 504 cm^3) aluminium block and as such had a large heat capacity. Heat transferred to the frame along the thermocouples was therefore quickly dispersed minimising temperature changes at the reference junctions (Woledge *et al.*, 1985). The temperature of the frame was controlled by pumping water, from a 40 l reservoir, through channels in the frame. The temperature of the water in the reservoir was maintained at the required temperature by a thermostatically-controlled heater (F10-HC, Haake Circulators, Karlsruhe, Germany) connected in series with a cooler (K11, Julabo Circulators, Schwarzwald, Germany). This arrangement was designed to minimise temperature oscillations inherent in thermostatically-controlled systems.

The aluminium frame was held in a custom-made box (designed by C. J. Barclay and P. D. Arnold, manufactured by P. D. Arnold; Figure 2.4). A cavity accessible from the side of the box allowed small containers (~20 ml) of solution to be positioned below the muscle chamber. Solution was forced out of the container and into the chamber by partially depressing a plunger into a syringe. Partially withdrawing the plunger drained the solution from the chamber back into the container. Solution was removed from and returned to the chamber as appropriate over the course of the experiments. A photograph of the experimental apparatus is shown in Figure 2.5.

Figure 2.4 Photograph of exterior of insulated thermopile box

This photograph shows the main features of the horizontal thermopile box. All connecting tubes and cables have been disconnected to allow better visualisation. The black knob visible on the right-hand side of the thermopile box is the point at which containers of solution were inserted into the box.
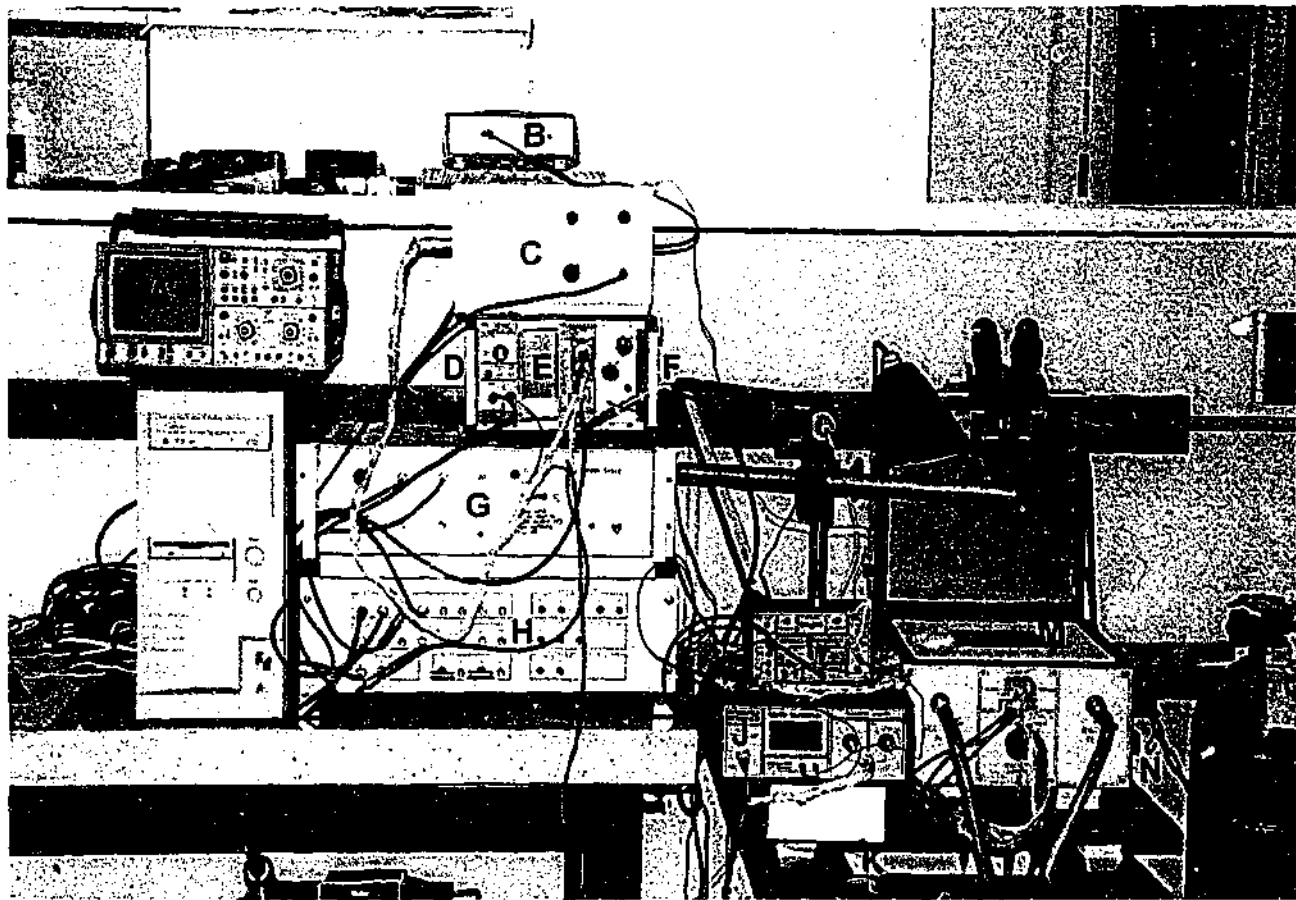
Figure 2.5 Photograph of experimental apparatus

This photograph shows the main features of the experimental apparatus including the oscilloscope (**A**), the power supply (**B**) for the thermopile amplifier (**C**), the force transducer amplifier (**D**), the Peltier current unit (**E**), the stimulator (**F**), the servo-controller for the motor (**G**), the A-D converter interface panel (**H**), the stimulus reverser (**I**), the thermopile interface panel with facility to vary the number of thermocouples recorded from (**J**), the syringe for removing and returning solution (**K**), the thermopile box (**L**), the thermopile frame (**M**) and the entry point for the containers of solution (**N**). The heating and cooling units (not shown) were located below the thermopile box arrangement.

2.5.2   Stimulation of muscle preparations

The method used for stimulating muscle preparations was constantly modified and improved over the course of the experiments reported in this thesis. Muscles were stimulated via two platinum wire electrodes attached to the tungsten connecting rods at either end of the muscle, as depicted in Figure 2.2. In the experiments reported in Chapters 3 and 4, the electrodes were attached to the tungsten rods using a silver-loaded epoxy resin (CircuitWorks, Chemtronics, USA). A fine coating of the epoxy resin was continued along the tungsten wire to the tip of the hook (Figure 2.6A). The platinum loops, attached to the ends of the muscle, were placed over the hooks at the ends of the tungsten rods, forming an electrical circuit. The apparatus was further modified for the experiments reported in Chapter 5 as a result of an apparent reaction between the epoxy resin and the surrounding solution that resulted in increased electrical resistance across the stimulation path. For the experiments reported in Chapter 5, the fine platinum wire was wound around the tungsten rods up to the tip of the hook (Figure 2.6B), removing the need to use the epoxy resin along the tungsten rod. Standard hot soldering techniques were used for this arrangement.

A   B

epoxy resin   solder
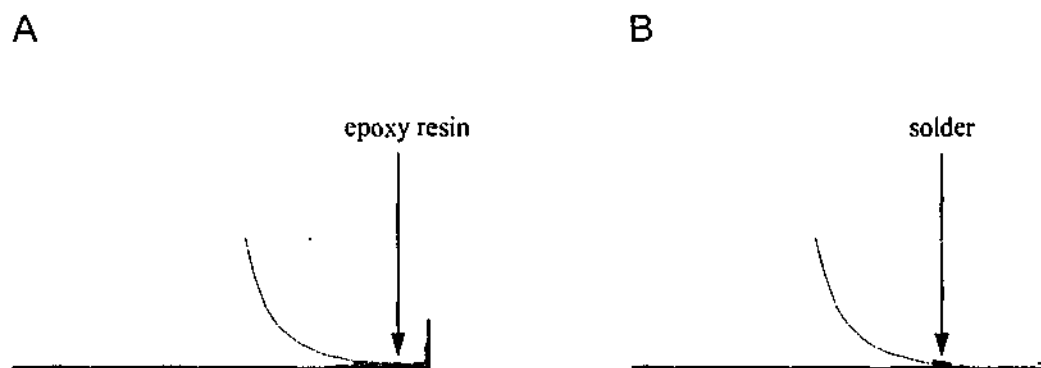
Figure 2.6 Arrangement of stimulating electrodes

Diagram of the stimulating arrangements used in Chapters 3-4 (**A**) and Chapter 5 (**B**). In **A**, conductive epoxy resin was used to attach the stimulating electrode to the tungsten rod. A fine coating of the resin was continued to the hook so that the platinum loop (not shown) was in contact with the resin. In **B**, the platinum wire was wound around the tungsten rod up to the hook so that the platinum loop (not shown) was in direct contact with the platinum wire.

The diameter of the platinum wire electrode at the force transducer end was 15 μm. This very fine wire did not provide resistance to movement of the connecting rod. The same (Chapter 3) or slightly thicker platinum wire (25 μm; Chapters 4-5) was used at the lever end, where the air inlet was situated. Air bubbles frequently collected around the wire at the air-solution interface and it was found that the thicker wire resisted force from the air
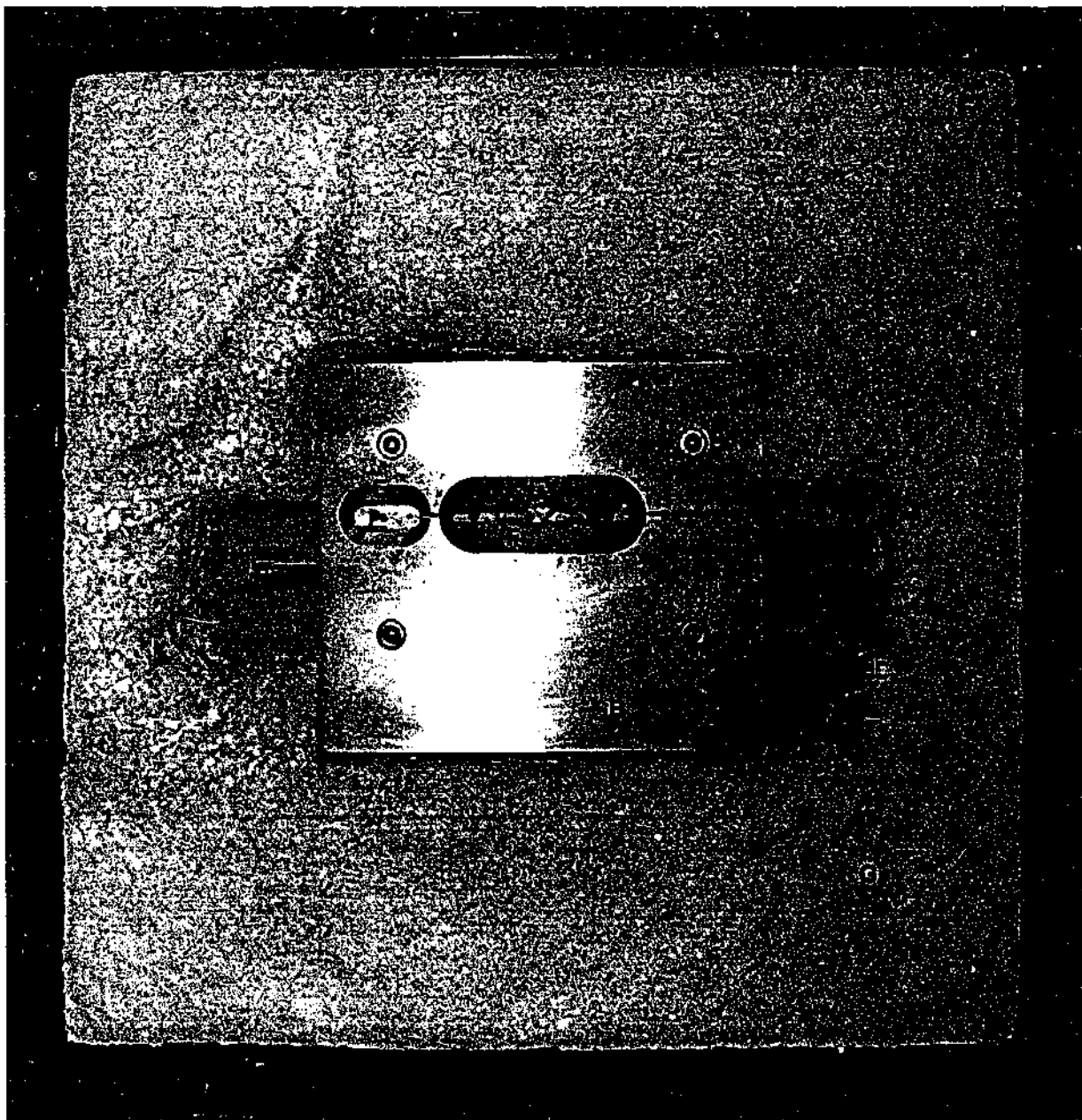
Figure 2.3 Photograph of thermopile arrangement

This photograph shows the horizontal thermopile arrangement (compare with Figure 2.2). The thermopile (**A**) was mounted in an aluminium frame (**B**). Tungsten rods (**C**) connected the muscle (not shown) to the recording apparatus. The motor (**D**) for controlling and measuring muscle length was positioned on the right-hand side of the thermopile and the force transducer (**E**) was positioned on the left. Platinum wire stimulating electrodes (**F**) protruded from the frame and were soldered to the tungsten wire connecting rods. The thermopile frame was insulated with polystyrene foam (**G**). Figure is ~50 % of actual size.

bubbles more effectively than the finer wire. The wire was still fine enough that movement of the connecting rod at the lever end was not affected by the electrode.

Stimulating muscles via the connecting rods was an improvement to the pre-existing cantilevered electrode arrangement used in this laboratory. That arrangement involved the electrodes being in direct contact with the sides or upper surface of the muscle and it was difficult to position the electrodes so that they didn't interfere with the movement of the muscle when it shortened. This was particularly important for the current study in which complex patterns of length changes and relatively high contraction frequencies were used.

Papillary muscles were stimulated using rectangular, electrical pulses of alternating polarity. At the beginning of each experiment, pulse width and amplitude were adjusted to elicit a twitch response with the solution drained from the chamber. Stimulus pulses were typically of 1-2 ms duration with an amplitude of 5-7 V. Stimulus pulse amplitude and/or duration were necessarily varied in some preparations. Stimulus heat was always less than 2 % of the total heat recorded (see Section 2.9.3).

2.6   Measurement of force production

2.6.1   Force transducer

Force produced by muscle preparations was measured using a semi-conductor force transducer (AE801, SensoNor, Norway). A stainless steel pin was glued to the face of the transducer using a fast-setting adhesive (Prism 406, Loctite, Welwyn Garden City, UK) and the connecting rod to which the muscle was attached was placed over the pin and held in place with a small drop of wax. The force transducer chamber was covered with reflective foil as it was found to be quite sensitive to light.

This type of force transducer provided a stable, low noise signal and operated over a range of 0-120 mN. The greatest forces measured in this study were the passive forces produced when muscles were exposed to low temperatures (Chapter 5). Under these conditions the passive force reached ~70 mN. Typical twitch forces at 27-30°C were 10-20 mN.

2.6.2   Calibration of force transducer

The force transducer was calibrated using a series of accurately weighed masses, spanning the range of expected muscle force outputs. The transducer was removed from its horizontal cavity and positioned vertically. Each mass was hung from the connecting pin of the force transducer so that force was exerted on the transducer in the same direction as

the generation of force by muscle preparations during experiments. The change in force transducer output for each load was displayed on an oscilloscope (HM 205-3, Hameg Instruments, Frankfurt, Germany) and measured. The relation between force transducer output and force exerted by the calibration masses is shown in Figure 2.7. The data were fitted with a straight line using least squares regression. For the transducer used in this thesis, the slope of the line was 0.59 mV mN^{-1}.
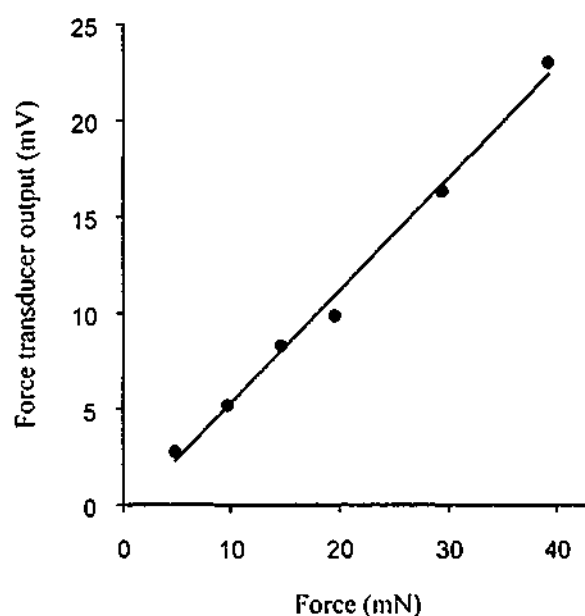
Figure 2.7 Calibration of force transducer

Relation between force exerted on the force transducer pin (mN) and force transducer output (mV). Force exerted on the pin was calculated as the product of the added mass (mg) and the acceleration due to gravity (9.8 m s^{-2}). Each data point represents the mean value of 3-6 measurements. The output of the force transducer used in this study was 0.59 mV mN^{-1}.

Transducer output was amplified by a factor of 100-500 (amplifier designed and constructed by W. Brenton, Department of Physiology, Monash University). Force output was calculated as follows:

$$\text{Force output (mN)} = \frac{\text{signal amplitude (V)}}{\text{calibration factor (V mN}^{-1}) \times \text{amplifier gain}}$$

The frequency response of the transducer/amplifier system was limited by the amplifier bandwidth. The amplifier's cut-off frequency was ~150 Hz. In comparison, the quoted resonant frequency of the transducer was 12 kHz.

2.6.3 Frequency spectrum of force signals

An example of the frequency spectrum of a force record is shown in Figure 2.8A. The force signal, taken from a sinusoidal protocol, was separated into its frequency components (Figure 2.8A) using a fast Fourier transform. This transformation was performed using a programme designed by C. J. Barclay using Testpoint (Capital Equipment Corporation, Burlington, MA, USA).
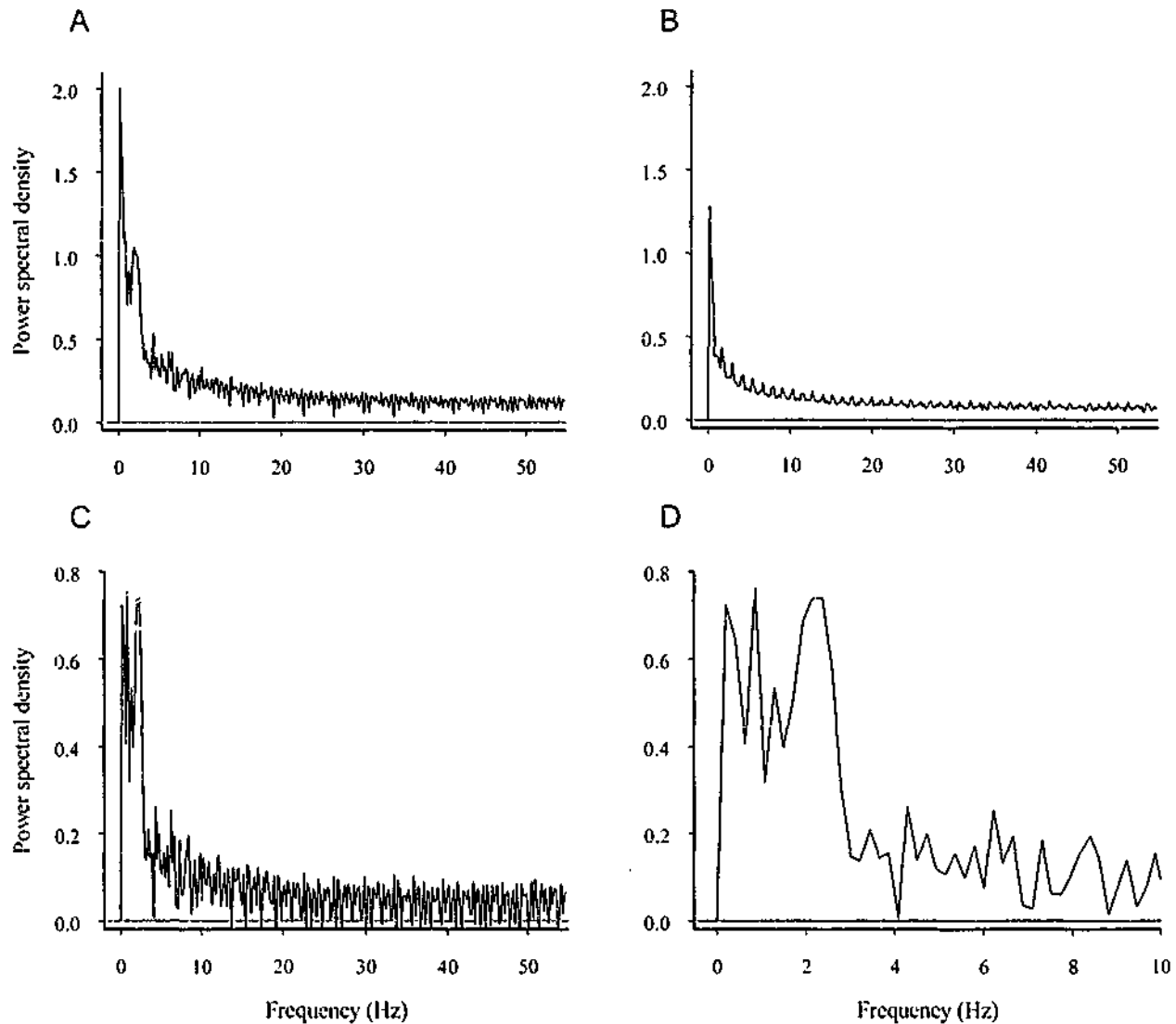
Figure 2.8 Example of frequency spectrum of a force signal

The spectra used in this example are taken from the fast Fourier transform of a 2 s section of a record of sinusoidal contractions at 2 Hz. The spectrum shown in **A** includes both signal and noise components while **B** shows just the noise component. The noise spectrum was subtracted from the signal + noise spectrum (*i.e.* **A-B**) to give the spectrum of just the signal (**C**). The power spectral density for the lower range of frequencies (1-10 Hz) is shown on an expanded scale in **D**. (Sampling rate, 110 Hz).

The majority of the signal spectrum was below 10 Hz. Of note is the peak at 2 Hz (Figure 2.8C), which corresponds to the stimulus frequency used in this example.

2.6.4   Compliance of force recording system

The compliance of the force recording system was the sum of the compliances of the force transducer and the tungsten rod arrangement including the wax drop. This latter compliance was determined by gluing a pin to the underside of a metal bench and attaching a connecting rod with a drop of wax. A 500 mN load was hung from the hook of the connecting rod and the change in length of the pin and rod arrangement measured. Using this method, the length of the rod increased by 29 µm per 1 mm unit length. Thus, the compliance of the tungsten rod arrangement was ~0.06 µm mN^{-1} and the compliance of the entire force recording system including the force transducer was ~0.64 µm mN^{-1}.

In an isometric twitch producing forces in the higher range, the transducer strain amounted to ~13 µm (0.64 µm mN^{-1} × 20mN) or ~0.26 % of the preparation length. This is small not only relative to preparation length but also in relation to the change in length of the series elastic elements in these muscles (see Chapter 4).

2.7   Measurement of muscle length changes

2.7.1   Servo-controlled lever

Changes in muscle length were controlled and measured simultaneously by a servo-controlled lever (300H, Cambridge Technology, Inc., Watertown, MA, USA). The motor was positioned ~5 cm from the thermopile and was insulated with foam so that heat produced by the motor was not detected by the thermopile (Woledge, 1998).

2.7.2   Calibration of lever

The characteristics of the lever's feedback circuit were adjusted according to the manufacturer's instructions except, rather than optimising the lever's response to a square wave input, the best match between a sinusoidal input signal generated by a function generator (3310A, Hewlett Packard, CA, USA) and lever movement was obtained. The reason for this was that sinusoidal and ramp changes in length were used during the experiments and the initial calibration of the lever in which the lever's response was optimised to square wave signals resulted in a poor match between input and output signals for the waveforms used in the current experiments.

2.7.3 Frequency spectrum of length signals

Using the same data and method as that used in Section 2.6.3, the length change signal from the realistic protocol was separated into its frequency components (Figure 2.9) using a fast Fourier transform. The spectrum of the length signal spanned ~0-30 Hz and again there is a peak at 2 Hz corresponding to the stimulus frequency (Figure 2.9D).
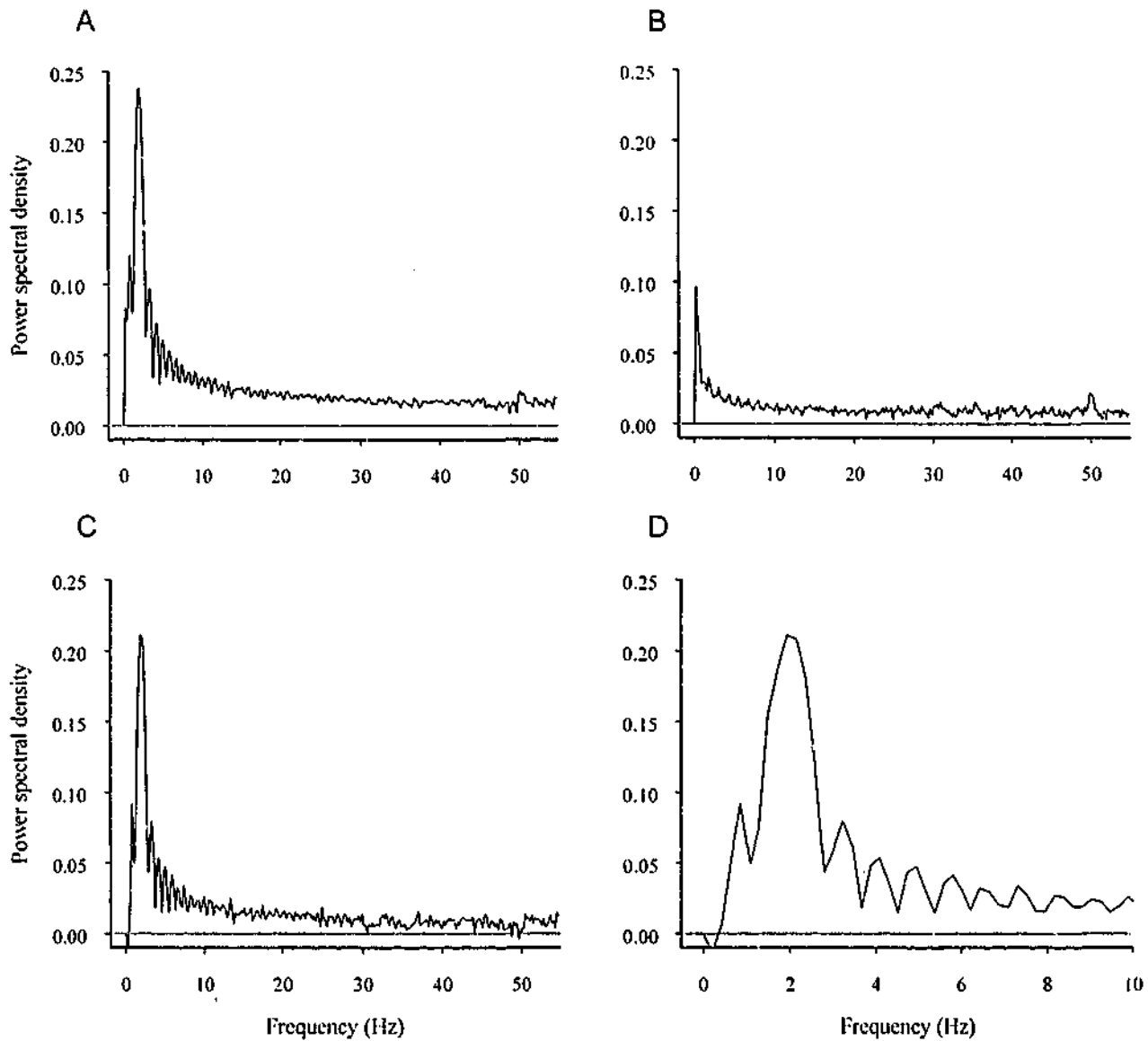
Figure 2.9 Example of frequency spectrum for a length change record

The spectra used in this example are taken from the fast Fourier transform of a 2 s section of a record of sinusoidal contractions at 2 Hz. The spectrum shown in **A** includes both signal and noise components while **B** shows just the noise component. The noise spectrum was subtracted from the signal + noise spectrum (*i.e.* **A-B**) to give the spectrum of just the signal (**C**). The power spectral density for the lower range of frequencies (1-10 Hz) is shown on an expanded scale in **D**. The sampling rate for the length record was 110 Hz. Note the peak at 50 Hz in **B** corresponding to mains frequency.

2.7.4   Frequency response of the lever

The frequency response of the servo-controlled lever system was determined by driving the lever with sinusoidal signals of known amplitude and frequency. These input signals were compared to the measured time-course of the position of the lever. The amplitude ratio (output voltage/input voltage) and the phase lag were determined over a frequency range of 10-300 Hz. Examples of the recordings are displayed in Figure 2.10.
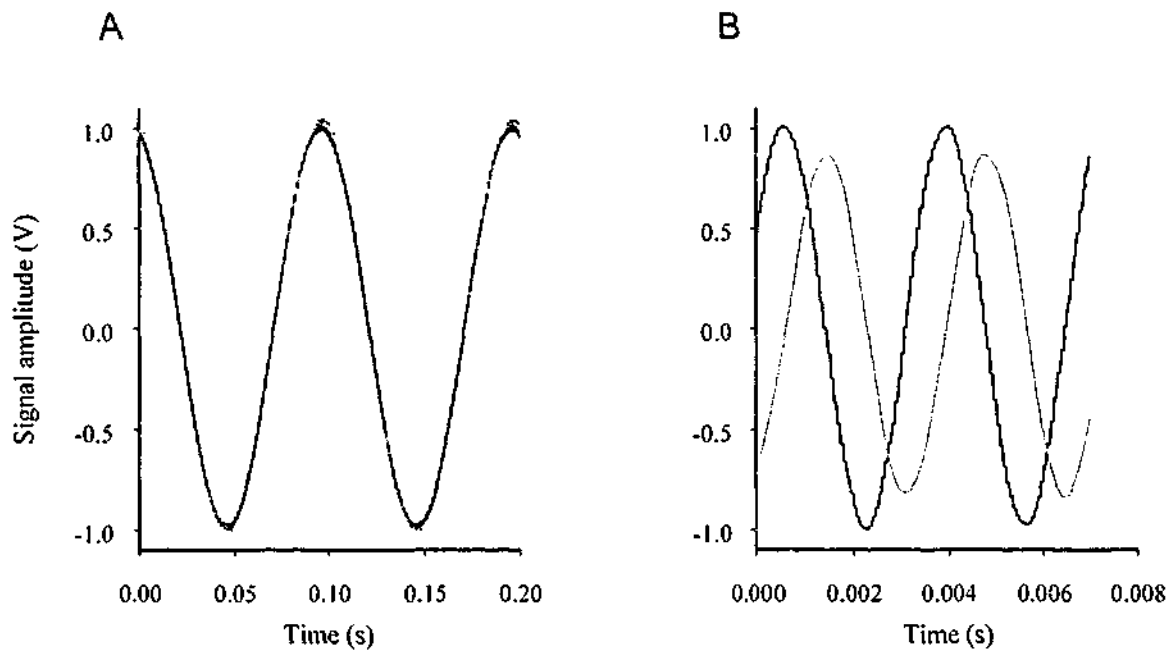
Figure 2.10 Input and output signals of the lever

An example of the input to the lever (black) and output from the lever (grey) for input signal frequencies of 10 Hz (**A**) and 300 Hz (**B**). The amplitude ratio decreases and the phase lag increases as frequency increases. Sampling rate was 25000 Hz for the 10 Hz input signal frequency and 45000 Hz for the 300 Hz input signal frequency.

The phase lag was measured from the records and converted to degrees using the following equation (Geddes and Baker, 1968):

$$\phi = 360° \, tf$$

where ϕ is phase lag (°)

   t is phase lag (s)

   f is frequency (Hz)

Over this entire range of frequencies, the measured frequency of the lever was the same as the input frequency. The amplitude ratio was constant for frequencies below 30 Hz and

then decreased over the remaining range of frequencies investigated (Figure 2.11). The phase lag varied linearly over the 0-30 Hz range of frequencies. These characteristics meet the requirements of the current experiments in which the length cycle frequencies were only 2-2.5 Hz in both the cyclic contractions and in the afterloaded isotonic contractions.
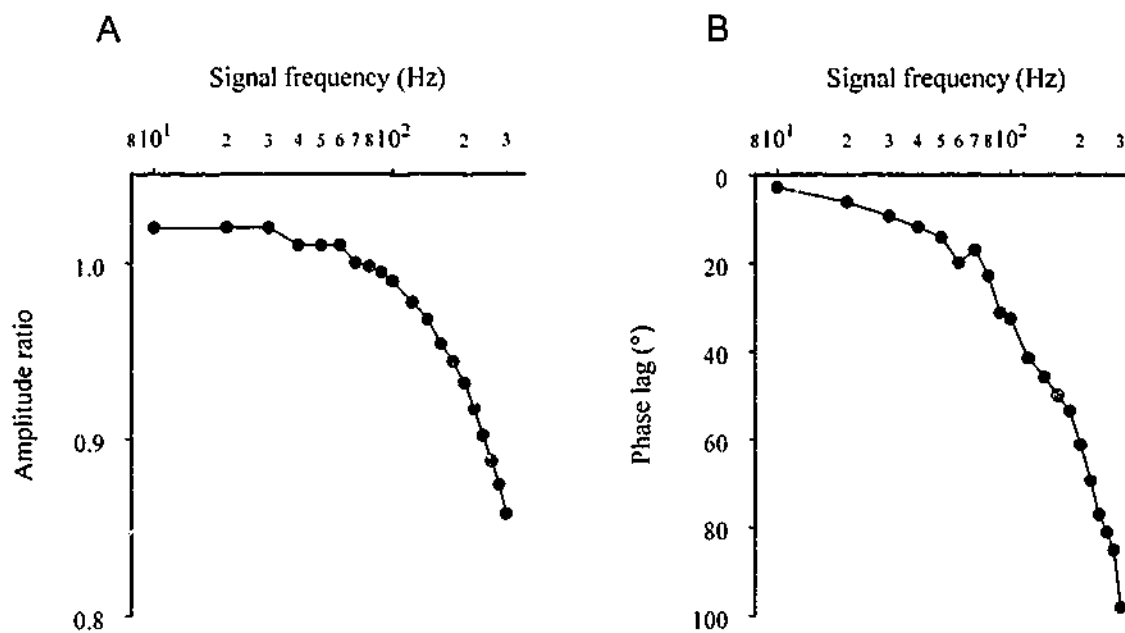
Figure 2.11 Determination of frequency response of lever

Amplitude ratio (A) and phase lag (B) in response to a range of input signal frequencies of 10-300 Hz. The amplitude ratio decreased as signal frequency was increased. The phase lag increased with increasing signal frequencies. The sampling rate was 25000–45000 Hz

2.8 Measurement of muscle heat production

The method used to determine the heat produced by papillary muscles took advantage of the relationship between the heat produced by the muscle and the change in muscle temperature:

$$\Delta Q = \Delta T \, m \, C$$

where ΔQ is the heat produced by the muscle (μJ)

ΔT is the change in muscle temperature (mK)

m is the mass of the preparation (mg)

C is the specific heat capacity of the muscle ($\mu J \, mK^{-1} \, mg^{-1}$)

2.8.1   Measurement of temperature change using a thermopile

For the experiments reported in this thesis, changes in muscle temperature were measured using a thermopile. The basic unit of a thermopile is a thermocouple, which is formed by a junction between two metals. Figure 2.12 is a diagram of a thermopile for measuring temperature changes in isolated muscle preparations. A series of thermocouples is arranged so that every second thermocouple lies along the centre of the thermopile (active thermocouples) and the alternate thermocouples are on the edges (reference thermocouples). The edges of the thermopile are clamped under the aluminium frame so that the reference thermocouples are maintained at the same temperature as the aluminium frame. The muscle preparation lies along the active thermocouples and so the temperature of the active region is regulated by muscle temperature.
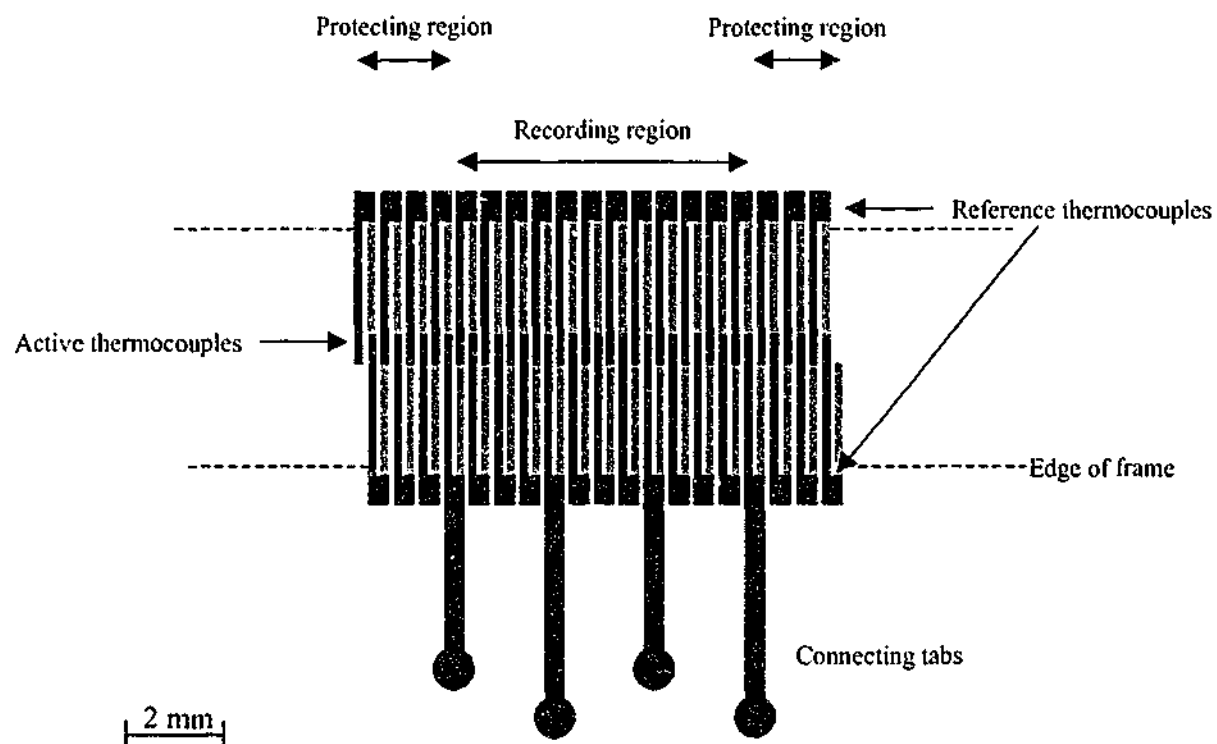
Figure 2.12 Schematic diagram of a vacuum deposited thermopile

This diagram illustrates the alternate arrangement of thermocouples made from antimony (dark grey) and bismuth (light grey) metals to form a thermopile. This arrangement results in every second thermocouple being kept at a reference temperature due to close thermal contact with the frame. The alternate thermocouples are in the centre of the thermopile (active thermocouples) and the temperature of these junctions reflects the muscle temperature. The thermopiles used in these experiments consisted of 4 thermocouples per mm. In this example, there are 8 thermocouples between successive tab positions, resulting in a total recording region of 6 mm. The positions of the connecting tabs allowed muscle temperature change to be measured along different regions of the thermopile.

During and after a contraction protocol, muscle temperature increases which causes the temperature of the active thermocouples to increase. The difference in temperature between the active and reference thermocouples results in a difference in potential (thermoelectric electromotive force, V) between the two sets of junctions. The magnitude of this potential difference is proportional to the difference between the temperatures of the frame and the muscle.

2.8.2   Procedures involved in the construction of antimony-bismuth thermopiles

The thermopiles used in the experiments reported in this thesis were constructed by Mr Peter Arnold according to well-established procedures developed in our laboratory (Barclay *et al.*, 1995), based on those pioneered by Mulieri *et al.* (1977). Each thermopile was constructed by vacuum depositing thin films of antimony and bismuth metals onto a polyethylene terephthalate film (Melinex; DuPont, Wilmington, DE, USA). These metals have high Seebeck coefficients and are suitable for evaporation. The underside of a second layer of Melinex was coated with adhesive (Prism 406, Loctite, Welwyn Garden City, UK) and placed over the metals. The thermopile was clamped until the adhesive had set resulting in a durable, watertight thermopile.

Some materials used previously to insulate thermopiles have been brittle (*e.g.* Mica), rendering the thermopiles extremely fragile (Woledge *et al.*, 1985). Melinex was found to be the ideal insulating material for the thermopile due to its strength, durability and flexibility. Melinex is very thin (~8 μm) so when combined with the small quantity of deposited metals, the total thickness of the thermopile was ~30 μm. Further, the plastic has a reasonable thermal conductivity (0.13-0.15 W m^{-1} K^{-1}) and is impermeable to water.

The thermopiles used in this study differed slightly from those described previously (Barclay *et al.*, 1995) in that the tabs connecting the thermopile to the recording circuitry were constructed of antimony rather than copper. Antimony evaporates at a lower temperature than copper which allowed the tabs to be vacuum deposited onto the Melinex substrate with less likelihood of thermal damage to the polymer. Leads were attached to the antimony tabs with conductive epoxy resin.

2.8.3   Additional features of the thermopile

During a contraction protocol, the heat produced by the muscle is shared with adhering solution, the insulating materials and the metals of the thermocouples (Woledge, 1998; Woledge *et al.*, 1985). To maximise the temperature change, the amount of solution

adhering to the muscle must be minimised and the heat capacity of the materials used to construct the thermopile must be small relative to the heat capacity of the muscle itself to allow rapid transfer of heat from the muscle to the active junctions of the thermopile. The small heat capacity of the thermopiles used in the present studies made them suitable for use with the small papillary muscle preparations. In the current experiments, the heat capacity of the muscles was ~7-15 mJ $°C^{-1}$ and the heat capacity of the thermopile used in Chapters 2 and 3 was 0.409 mJ K^{-1} (see Table 2.2). The temporal resolution of these thermopiles was very fast as shown in Figures 2.15 and 3.3.

It was important that the muscle completely covered the recording region of the thermopile with the ends of the muscle protruding into the protective regions. The protective regions are thermocouples that are not connected to the recording circuit. The rate of heat loss from the muscle to the frame is therefore uniform along the length of the muscle. Most of the protocols used in the current experiments involved reducing muscle length which resulted in parts of the muscle moving onto the recording thermocouples that were not previously in contact with this region. Since the portion of the muscle that moves from the protective to the recording region has the same rate of heat loss, a temperature gradient is not generated along the length of the muscle (Hill, 1937). Temperature change was typically measured across 16 thermocouples (4 mm) and muscle length was typically ~5 mm. The maximum shortening was ~15 % of muscle length so it was of critical importance to position the muscle carefully.

2.8.4 Calibration of thermopiles using the Peltier effect

During an experiment, the thermopile senses temperature changes resulting from heat produced by the muscle and generates a corresponding voltage (see Section 2.8.1). To relate the output of the thermopile to actual muscle temperature changes, it was first necessary to calibrate the thermopile. This was performed according to the methods described by Kretzschmar and Wilkie (1972, 1975) and Woledge et al. (1985). The procedure determined the Seebeck coefficient (α; μV $°C^{-1}$ thermocouple^{-1}) which allowed thermopile output to be converted to temperature units.

The calibration procedure involved placing a series of silver blocks of known mass (12-61 mg; heat capacity = 0.234 mJ K^{-1} mg^{-1}) on the thermopile. A small, known mass of glycerol (<0.4 mg; 89 % glycerol, 11 % water; heat capacity = 2.59 mJ K^{-1} mg^{-1}) was placed on the underside of the silver block prior to placement on the thermopile. This provided good thermal contact between the silver block and the thermopile by preventing

air gaps between the two. A constant current (either 100 or 116 µA) was passed through the thermopile, generating heat at the active junctions (Peltier heating) and heating the silver block until a steady temperature was attained. The current was then switched off and the time-course of cooling of the silver block recorded (Figure 2.13).

A   B
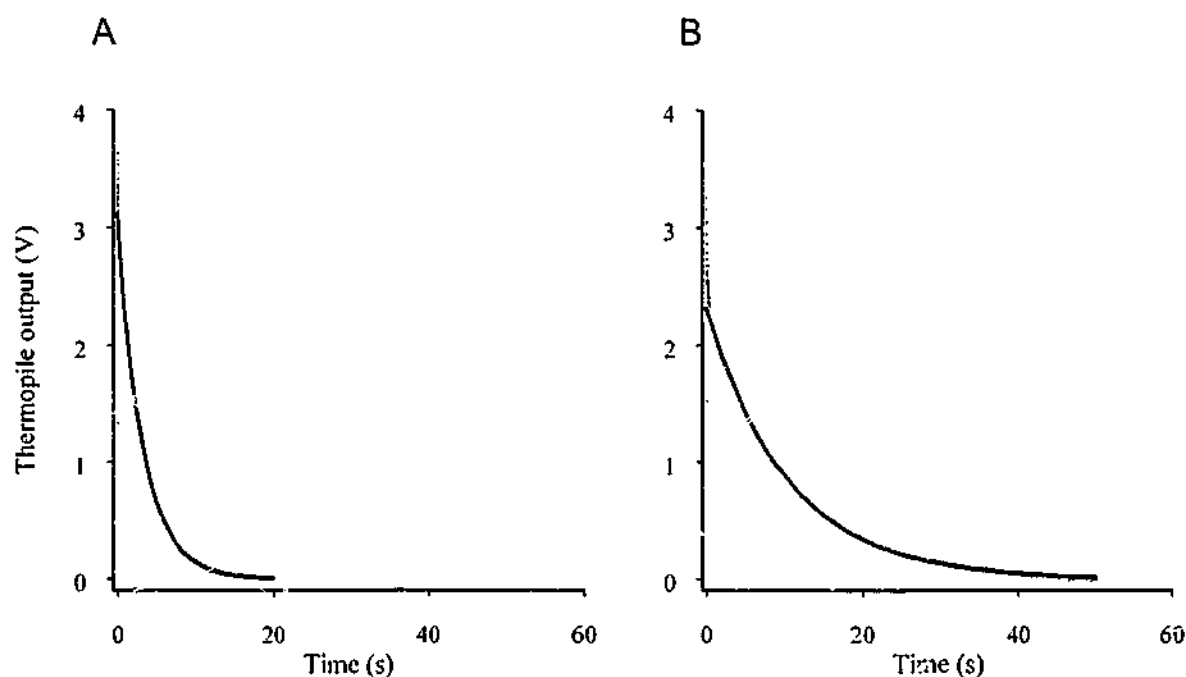
Figure 2.13 Time-course of cooling of silver blocks

Time-course of cooling of a 12 mg silver block (A) and a 61 mg silver block (B) following 20 and 50 s periods of Peltier heating, respectively. The cool-off data after the first 1 s were fitted with exponential curves. These had rate-constants of 0.309 s^{-1} (A) and 0.096 s^{-1} (B). The initial ~1 s of the measured cool-off is due to the rapid temperature change of the reference junctions. The sampling rates were 100 Hz in A and 50 Hz in B.

The majority of the time-course of cooling was well described by a single exponential function from which a time-constant for heat loss could be obtained. Note that the first 1 s of cooling was not included in the fitting as it was not well described by the exponential. The rapid drop during this time most likely reflects the relatively quick change in temperature of the reference junctions. Consistent with this idea was the observation that the initial, rapid drop in temperature was independent of the heat capacity added to the active junctions. The relation between the rate of cooling and the added thermal capacity of each silver block and glycerol is described by the following formula:

$$\frac{dV_o}{dt} = \frac{ITn^2\alpha^2}{(C_{tpile} + C_{silver})}$$

where dV_o/dt is the rate of cooling

I is the current passed though the thermocouples (A)

T is the absolute temperature (K)

n is the number of thermocouples that the current was passed through

α is the Seebeck coefficient (μV K^{-1} couple^{-1})

C_{tpile} is the heat capacity of the thermopile under the silver block (J K^{-1})

C_{silver} is the heat capacity of the silver (J K^{-1})

The equation was transformed into linear form:

$$\frac{1}{(dV_o/dt)} = \frac{1}{ITn^2\alpha^2} \cdot (C_{tpile} + C_{silver})$$

and represented graphically (Figure 2.14). The heat capacity of the thermopile was determined from the intercept of the extrapolated line of best fit and the abscissa. The Seebeck coefficient, α, was determined by the gradient of the line. Values for the Seebeck coefficient and the heat capacity were determined for each thermopile used in this study and are presented in Table 2.2.
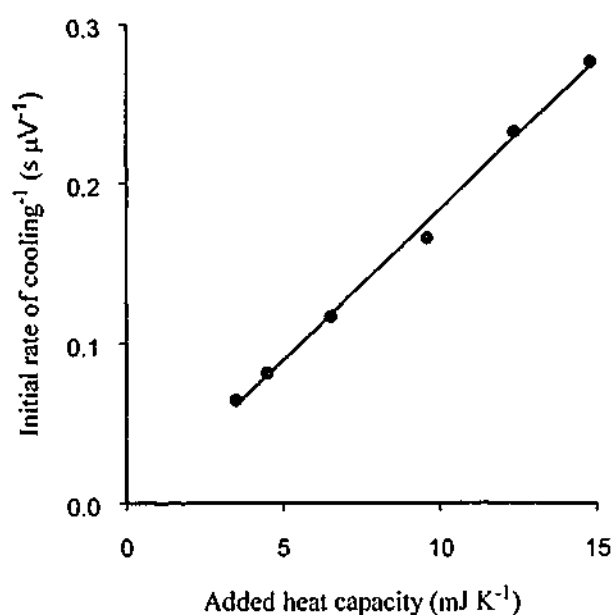
Figure 2.14 Determination of thermopile characteristics

The Seebeck coefficient (α) and the heat capacity of the thermopile were determined for each thermopile using the method described above. Data points represent mean values of the three measurements made for each silver block. Details of the characteristics of each thermopile are shown in Table 2.2. The data shown in this figure were measured using Thermopile 1 in the table.

Thermocouples constructed of antimony and bismuth have a theoretical α value of 122 $\mu V\,°C^{-1}$ couple^{-1} at 0°C (Kaye and Laby, 1973). However, the very thin thermocouples used in thermopiles typically have α values ~60 % of the maximum theoretical value (Mulieri et al., 1977).

The method used to determine the heat capacity of the thermopile and of the muscle and thermopile made use of the Peltier effect. When small currents are used for Peltier heating, the Joule effect is negligible (Woledge et al., 1985). To ensure that the measurements reflected the Peltier effect rather than an effect of Joule heating, the rates of heating due to both effects were calculated. Power dissipated as a result of Peltier effect is given by:

$$Power\,(W) = ITn\alpha$$

and for the Joule effect:

$$Power(W) = I^2 R$$

where R is the resistance across the thermopile (Ω).

The Peltier effect and the Joule effect calculated for each thermopile used in the current experiments are shown in Table 2.2. The Peltier effect was ~10× greater than the Joule effect in all thermopiles.

What effect would Joule heating have on measured muscle heat output? If Joule heating contributed an additional 10 % heating during calibration of the thermopile, dV_o/dt would have been 10 % higher than that due to Peltier heating alone and thus α^2 would have had the same relative error. α would then have been ~2 % greater than the true value. This relative error would have been reproduced in the calculated temperature changes (they would be underestimated by ~2 %) but would have had a negligible effect on calculated muscle heat capacities as, although the numerator in the heat capacity formula would be 2 % too great, the measured rate of cooling (denominator) would have also been overestimated. Thus, the Joule heating would have had only a very small influence (~1.8 % at maximum efficiency) on calculated enthalpy outputs.

The heat capacities calculated for two of the thermopiles have negative values (Table 2.2). While a negative heat capacity is nonsensical, these values give an indication of just how small the heat capacities of these thermopiles were. The heat capacity is determined by the intercept of the extrapolated line of best fit and the abscissa. A value that does not lie on the line of best fit may not significantly alter the gradient and, therefore, the Seebeck

coefficien... ...ver, since the heat capacity of the thermopile is close to zero, even a small alteration to the gradient of the line caused by an outlier may affect the intercept of the extrapolated line of best fit.

Table 2.2 Thermopile characteristics

Thermopile	1	2	3
Active region (mm)	5	4	4
I (A)	116×10^{-6}	116×10^{-6}	100×10^{-6}
n	20	16	16
T (K)	300.4	300.4	300.4
α (μV K^{-1} couple^{-1})	61.862	67.896	50.736
R (Ω)	*	287	220
C_{tpile} (mJ K^{-1})	-0.219	0.409	-1.479
Output (mV °C^{-1})	1.237	1.086	0.812
Peltier effect (W)	4.31×10^{-5}	3.78×10^{-5}	2.43×10^{-5}
Joule effect (W)	*	3.8×10^{-6}	2.2×10^{-6}

* Resistance was not recorded for Thermopile 1, therefore the Joule effect could not be calculated. Thermopiles 1 and 2 were used for the experiments reported in Chapter 3, Thermopile 2 was used for those reported in Chapter 4 and Thermopile 3 was used for the experiments reported in Chapter 5. Note that the number of thermocouples (n) used to record muscle temperature change was sometimes less than the total active region. This simply reflects recording from different regions of the thermopile by recording from leads attached to different tab positions.

2.8.5 Determination of the impulse response of the thermopile

During experiments, heat produced by the muscle preparation must first diffuse through the insulating layer of the thermopile (Melinex) before it reaches the active junctions. A difference in temperature between the active and reference junctions develops and a potential difference between the ends of the thermopile can be measured. This process distorts the recorded signal. Every effort was made to minimise this delay. Firstly, thin layers of metal were used to minimise the heat capacity of the thermopile. Secondly, Melinex was selected as the insulating material because it is very thin (~8 μm). Finally, thin muscle preparations were used to minimise heat conduction distances (Woledge et al., 1985).

The temporal characteristics of the thermopile can be summarised by its response to a brief burst of heating – its impulse response. The thermopile was heated using an infra red diode (2-3235 gallium aluminium arsenide infra red diode, Dick Smith Electronics, Australia; radiant power 28 mW cm^{-2}; output rise time 200 ns). The application of the 1 ms trigger pulse and the resulting thermopile output are plotted against time in Figure 2.15.
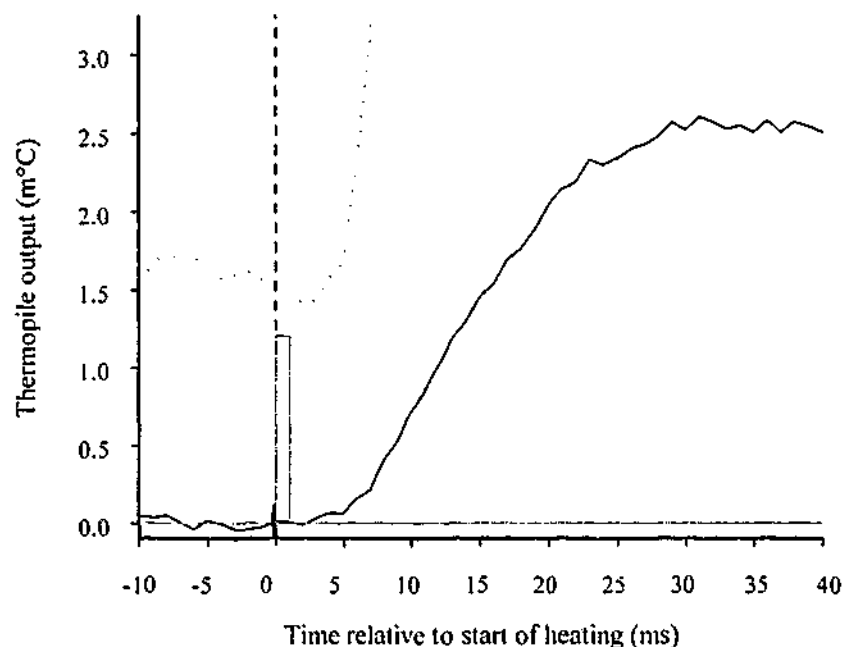
Figure 2.15 Determination of thermopile lag

The thermopile was heated for 1 ms using an infra red diode. The short pulse shown in grey indicates the duration that current flowed through the diode. The thermopile response is shown by the solid black line (average of 4 trials). The response of the amplifier alone to a step input is also shown (dashed line). The dotted line illustrates the method used to determine the time at which the thermopile first responded to the applied heating (Close, 1981). It represents the standard error of the estimate of a straight line fitted through progressively more points of the thermopile output. The standard error of the estimate decreases in magnitude as more points on a straight line are included but increases when the signal deviates from a straight line. The delay between the start of heating and the first response of the thermopile was ~3 ms and the peak response occurred in ~25 ms. The response then decayed back to pre-heating values with an exponential time-course of 700 ms.

The thermopile response consisted of a brief delay of ~3 ms, an increase in output that reached its peak value in 24 ms (half peak reached in ~14.2 ms) followed by an exponential decline back to its pre-heating value with a time-constant of 700 ms. The thermopile amplifier did not significantly contribute to this lag (Figure 2.15), thus the measured lag between the application of the current and the generation of a thermopile signal could be attributed to the thermopile itself. These characteristics can be interpreted

as follows: (1) the initial delay reflects the time taken for heat to diffuse through the Melinex to the active junctions; (2) the rise in temperature reflects the increase in temperature of the thermocouples and the cooling reflects the rate of transfer of heat from the active junctions to the thermopile frame and (3) the heat loss correction used in this study compensates for the latter process (along with heat diffusion out of the muscle) but makes no correction for the short delay in response. This was appropriate as this study was not concerned with the fine detail of the time-course of heat output.

2.8.6 Determination of muscle heat capacity

Muscle heat capacity (C; mJ °C^{-1}) was determined from the time-course of cooling following a period of Peltier heating (Kretzschmar and Wilkie, 1972; 1975). This involved passing a small constant current through the active junctions of the thermopile to heat the muscle. The following relation was used to calculate heat capacity:

$$C_{muscle} = \frac{ITn\alpha}{(dT_o/dt)}$$

where I, T, n and α are as defined previously

dT_o/dt is the initial rate of temperature change following removal of the current.

This thermopile output (μV) was converted to units of temperature change (°C) using:

$$\Delta T = \frac{\Delta V}{n\alpha}$$

Finally, the change in temperature was converted to units of heat (mJ) using:

$$\Delta Q = \Delta T \times C_{muscle}$$

It should be noted that some of the heat that the muscle produces goes to heating the thermopile under the preparation and any solution surrounding the muscle. The Peltier calibration method takes account of this, giving the effective heat capacity of all contributing factors.

2.8.7 Frequency response of the thermopile amplifier

The thermopile amplifier used in this study (ANCOM CM 1251; described in Dijkema *et al.*, 1985) possessed filter cut-off settings ranging from 1 to 100 Hz. The effects of setting the cut-off frequency to 10, 33 or 100 Hz were tested to determine whether signals were reproduced accurately. At each filter setting, input signals of known amplitude and

frequency were fed to the amplifier and the output was measured using an oscilloscope. Both the amplitude ratio and the phase lag (°) were determined. The relations between signal frequency and phase lag at the different filter settings are displayed in Figure 2.16.

In light of these results, the filter cut-off was set to either 33 or 100 Hz to ensure that signals were reproduced accurately prior to amplification.
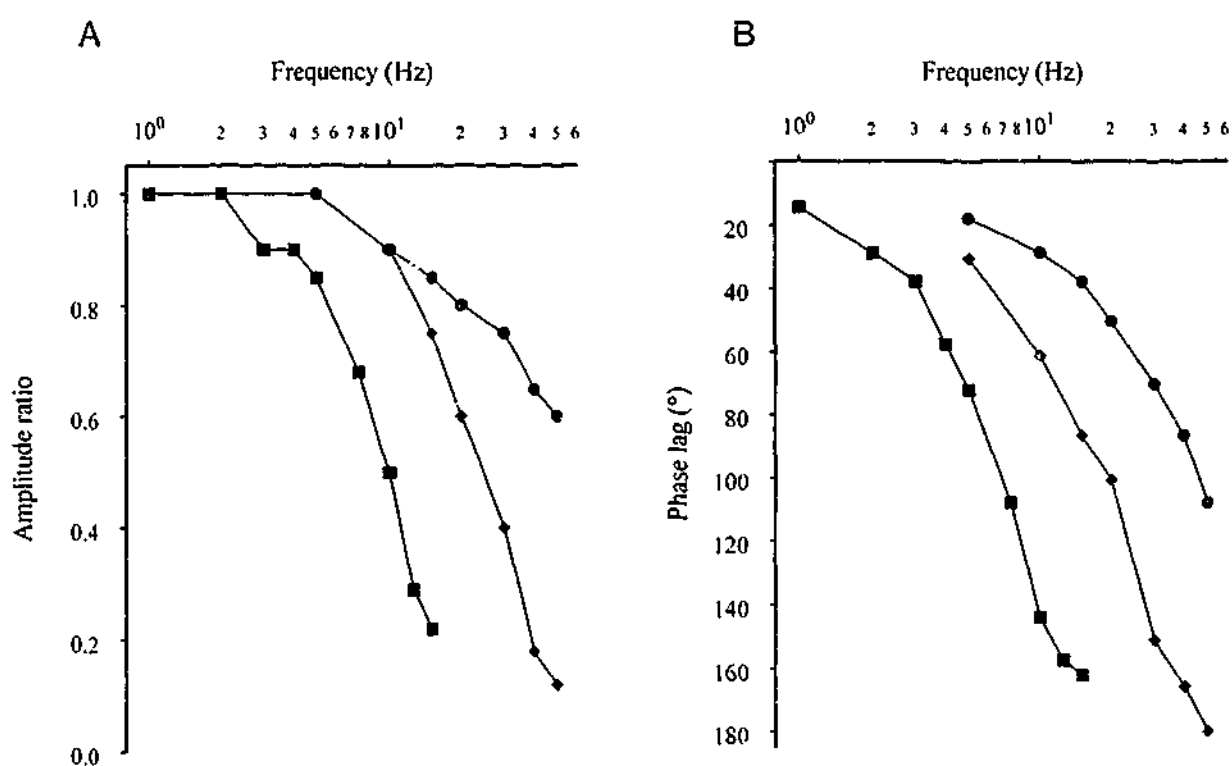
Figure 2.16 Frequency analysis of thermopile amplifier

The thermopile amplifier used in these experiments possessed filter cut-off settings in the range 1-100 Hz. The effects of setting the cut-off to 10 (■), 33 (♦) and 100 (●) Hz on the amplitude ratio and phase lag are displayed in this figure. The amplitude ratio is the amplitude of the output signal expressed as a proportion of the amplitude of the input signal.

2.8.8 Frequency spectrum of temperature signal

Signal output from the thermopile was passed through a low-pass filter with a cut-off frequency set to 33 or 100 Hz, depending on the magnitude of 50 Hz mains frequency noise. The signal was then amplified by a factor of 1×10^5 using a low noise amplifier (Dijkema *et al.*, 1985) where the resistance of the input was well matched to that of the thermopile (Woledge, 1998).

To ensure that signal information was not lost due to over-filtering, the temperature signal was separated into its frequency components (Figure 2.17) using the method described in

Section 2.6.3. The example shown in Figure 2.17 is taken from a realistic contraction protocol (Chapter 5) where the contraction rate was 2.2 Hz.
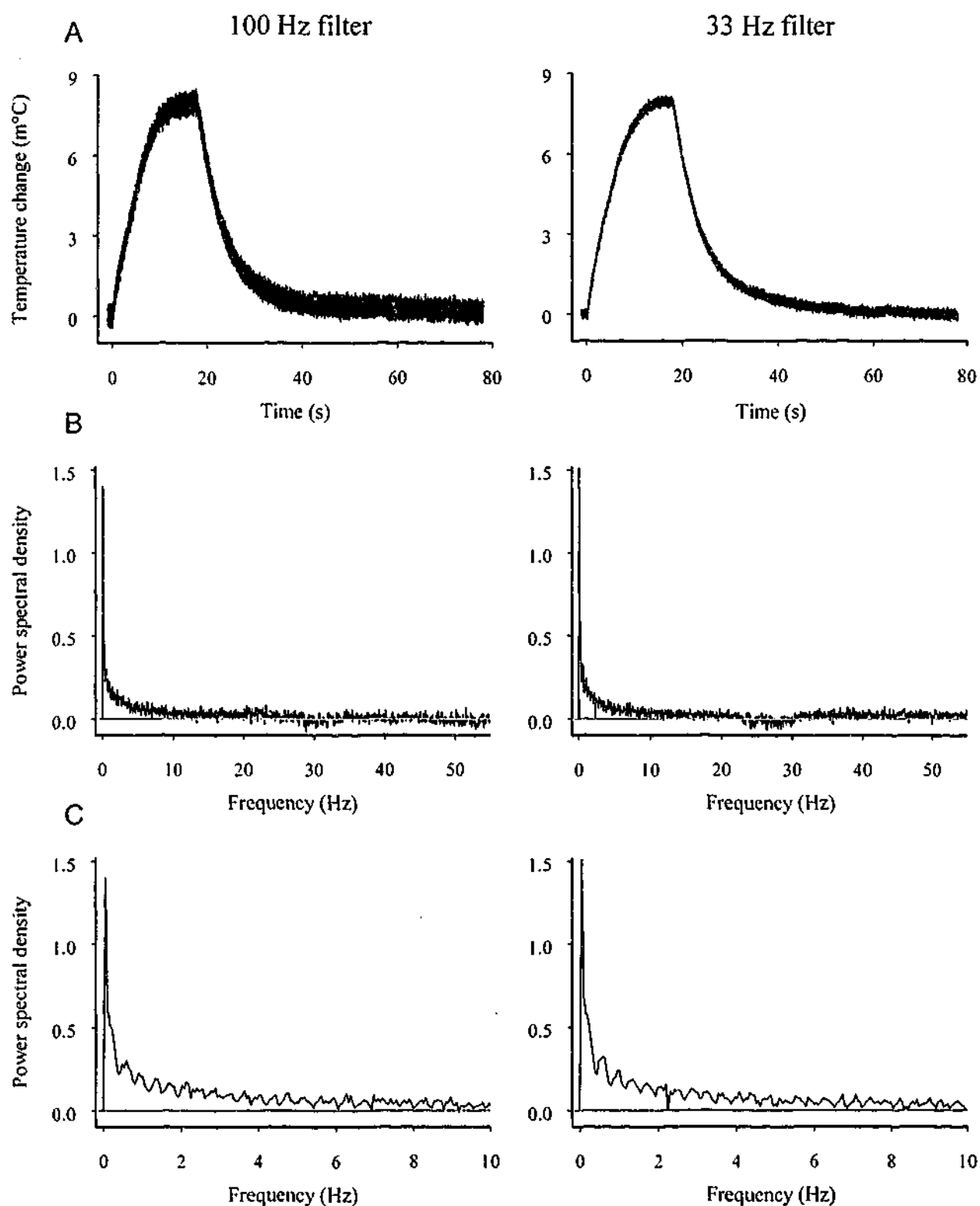
Figure 2.17 Frequency spectrum of temperature signal

Two original temperature records (A) from a muscle performing 40 twitches at 2.2 Hz with a filter cut-off frequency of 100 Hz (left panel) or 33 Hz (right panel). The frequency spectra (B) were obtained using fast Fourier transformation analysis. Note that the noise has already been subtracted from the signal, therefore, there is no peak at 50 Hz. The power spectral densities for the lower range of frequencies (1-10 Hz) are shown on expanded scales in C.

Note the fast Fourier transforms shown are the signal components only; the noise has already been subtracted as for Figures 2.8 and 2.9. When the filter cut-off was set to 100 Hz (left panels, Figure 2.17), the range of peaks was <10 Hz. A second recording, using the same protocol as before, is displayed in Figure 2.17 (right panels), only this time the filter cut-off was set to 33 Hz. The spectral peaks over the lower range of frequencies were not affected by the lower filter setting.

The cut-off frequency used to filter thermopile output prior to amplification must be greater than the highest frequency component of the signal. The highest signal frequency component was <10 Hz, thus, the cut-off frequencies of 33 and 100 Hz used in this thesis were sufficiently high to ensure faithful reproduction of the temperature signals (Figure 2.16).

2.9   Analysis of thermal signals

2.9.1   Determination of heat output

During analysis of the records, thermopile output was filtered using a low pass, digital filter (cut-off frequency 10 Hz; pp. 558-559, Press et al., 1992; Figure 2.18).
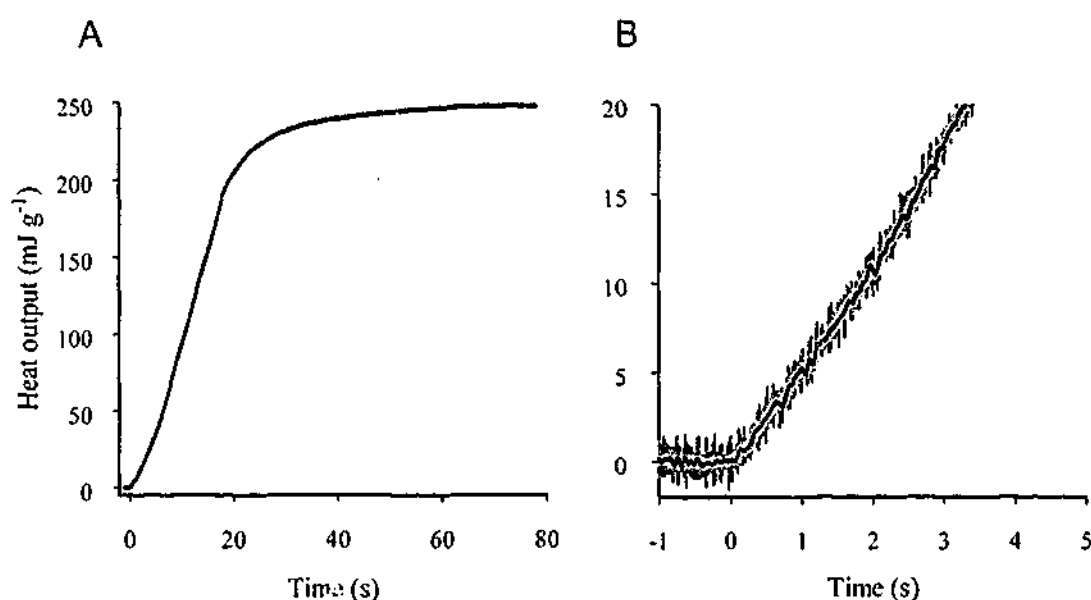
Figure 2.18 Effects of filtering heat signal with a digital filter with a cut-off frequency set to 10 Hz

This figure shows an original heat signal that was recorded with the thermopile amplifier filter set to 100 Hz (grey line; A and B). The signal was later digitally filtered during analysis with a cut-off frequency set to 10 Hz. The signal filtered at 10 Hz (black line; A) lies within the original heat signal, indicating that signal characteristics were not significantly altered by the additional filtering. Of note is the close fit of the filtered record to the original record during rapid changes (B). Any rounding effects of filtering would be most evident here.

The record was then corrected for heat lost from the muscle during recording and multiplied by the muscle heat capacity to give heat output. Heat loss (see Section 2.9.2) and muscle heat capacity (see Section 2.8.4) were determined from the time-course of cooling and the steady-state temperature reached after a period of Peltier heating.

The thermopile output sometimes exhibited a steady drift during recordings that was not related to muscle heat output. An adjustment was made to records that were affected by this baseline drift using Testpoint software written by C. J. Barclay. To correct for the drift, it was assumed that there was a constant rate of drift so that a linear correction could be made. Where the drift was clearly non-linear (e.g. step or transient change in the heat record), the recording was discarded.

2.9.2 Determination of rate-constant for muscle heat loss

Heat loss from the muscle was characterised just prior to a set of recordings, with the solution drained (see Section 2.11), using the Peltier effect as described in Section 2.8.4. The path of heat loss is primarily via the thermocouples. For the muscles used in this study, the rate-constant for heat loss was usually between 0.2 and 0.4 s^{-1}. An example of the time-course of heat loss from a muscle is shown in Figure 2.19.
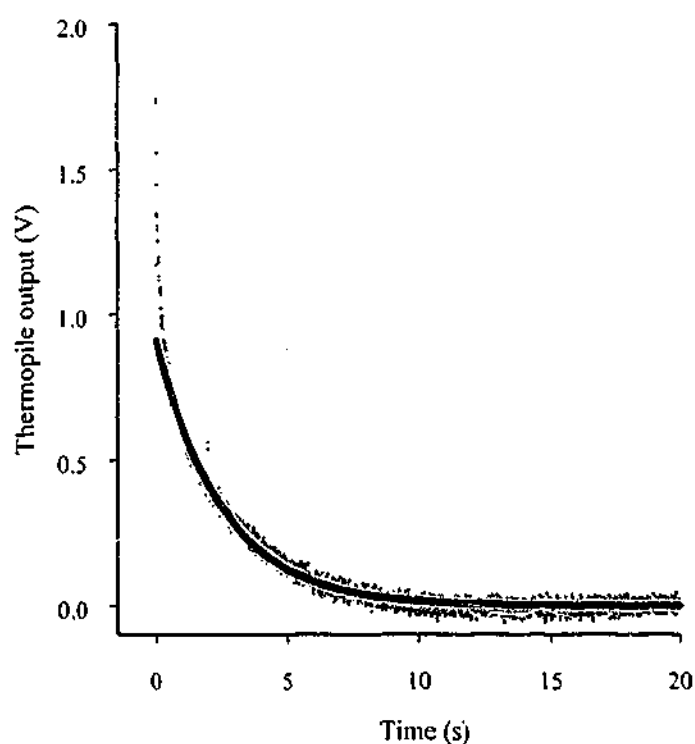
Figure 2.19 Time-course of heat loss from a muscle

Example of a recording of thermopile output following a period of Peltier heating. A rate-constant of cooling was obtained from a single exponential function that was fitted to the data. Heat loss recordings were sampled at 100 Hz.

As discussed in Section 2.8.4, the majority of the time-course of cooling was well described by a single exponential from which a rate-constant for heat loss could be obtained. Again, the first 1 s of cooling was not included in the fitting as it was not well described by the exponential. An example of a record of muscle temperature change that has been corrected for heat loss is shown in Figure 2.20.
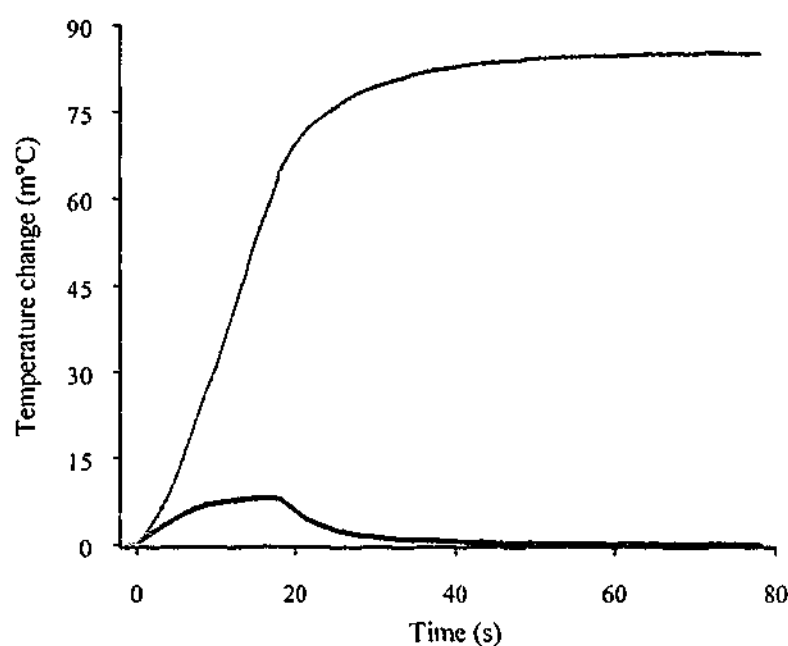
Figure 2.20 Example of heat loss correction

An original recording of muscle temperature change for a contraction protocol consisting of 40 twitches at 2.2 Hz (black trace). Muscle temperature increases during the contraction protocol and then decreases back to its original temperature due to heat loss. The grey trace shows the temperature change following correction for heat loss.

2.9.3   Determination of stimulus heat

When a current flows through a resistance, heat is dissipated in the resistor. Similarly, the stimulus current passing through the muscle can give rise to heat which would be recorded along with the metabolic heat from the muscle.

To determine the proportion of the total measured heat output that was due to stimulus heat, several muscles were rendered inexcitable with 20 mM Procaine. Each muscle was then stimulated 20, 40 or 60 times at 1-2 Hz and the resulting temperature change measured. Stimulus heat per pulse (μJ) was calculated for a range of stimulus amplitudes and durations, encompassing those used during recordings of muscle heat output. This procedure was repeated for each of the stimulating electrode arrangements described in Section 2.5.2. For pulses with a duration of 1 ms and an amplitude of 7 V, heat arising

from stimulation was ~0.2 μJ pulse^{-1} using the stimulating arrangement shown in Figure 2.6A and ~0.04 μJ pulse^{-1} when using the arrangement shown in Figure 2.6B. Estimates of the amount of stimulus heat based on these measurements indicated that it was always <2 % of the total heat recorded and, consequently, no correction for stimulus heat was made. Examples of the contribution of stimulus heat to total heat output are shown in Table 2.3.

Table 2.3 Stimulus heat

Stimulating arrangement	Stimulus heat (μJ pulse^{-1})	Total stimulus heat (mJ (40 pulses)$^{-1}$)	Total heat output (mJ g^{-1})	Stimulus heat as % of total heat output
Figure 2.6A	0.4	0.016	293	~1.8
Figure 2.6B	0.08	0.0032	134	~0.8

Stimulus pulses were 2 ms 7V in both examples. In the first example, the muscle performed 40 afterloaded isotonic twitches at 2 Hz (27°C). In the second example, the muscle performed 40 realistic contractions at 2.2 Hz (30°C). A muscle producing a low total heat output was chosen deliberately for the second example to show that stimulus heat was very small using the second arrangement.

2.10   Determination of energetic variables

2.10.1   Net mechanical efficiency

Efficiency is the term used to quantify the transformation of energy between two forms. One measure of efficiency of muscular contraction is the thermodynamic efficiency which is calculated as work output for a given free energy change (ΔG). In other words, this is the efficiency with which muscles can convert chemical energy from ATP hydrolysis into work, or mechanical energy. Thermodynamic efficiency is difficult to measure experimentally due to the difficulty in determining the molar free enthalpy change of ATP splitting.

Another common measure of efficiency in muscle, and one that can be measured experimentally, is the mechanical efficiency. Mechanical efficiency is the ratio of work output to enthalpy output and enthalpy output is, under suitable experimental conditions, proportional to the amount of ATP used. One of the principle techniques used for determining mechanical efficiency in striated muscle is to make simultaneous measurements of work and heat outputs. The work and heat outputs can be summed to give the enthalpy output. Under conditions in which muscles have an adequate supply of

O_2 and metabolic substrate and activity levels that do not lead to contractile failure (*i.e.* extreme fatigue), enthalpy output arises predominantly from the net breakdown of PCr.

In the current experiments, net mechanical efficiency was calculated. Net mechanical efficiency (ε_{Net}) was defined as the percentage of the total, suprabasal enthalpy output (H_{Total}) that appeared as external, mechanical work:

$$\varepsilon_{Net} = \frac{W_{Total}}{H_{Total}} \times 100$$

where H_{Total} included all the enthalpy, in excess of the basal enthalpy output, produced during and after a series of contractions and thus included both initial and recovery metabolisms. Initial and recovery metabolisms were measured together due to the tight temporal coupling of these processes in cardiac muscle. Note that over a complete contraction and recovery protocol there is no net breakdown of PCr. All PCr is resynthesised so that the net enthalpy output reflects the mitochondrial activity required to regenerate all the high energy phosphates used. Thus, the enthalpy output is the energetic equivalent of the oxygen consumed. W_{Total} was the sum of the work output produced in each contraction in the series. Including basal metabolism would decrease the efficiency values (see Chapter 3, Section 3.4.4 for an estimation of the contribution of basal metabolism to total enthalpy output).

This method is based on the conservation of energy principle. The muscle and thermopile are effectively a closed system since there is no exchange of energy with the external environment and so all the energy produced by the muscle appears as either work or heat.

2.10.2 Work output

Determination of work output was dependent on contraction type. Three types of contraction protocols were used in this study: afterloaded isotonic (Chapter 3), sinusoidal (Chapter 3) and realistic contraction protocols (Chapters 4 and 5).

Work output in isotonic contractions was defined as the product of the total force (*i.e.* active force + passive force) and shortening amplitude. Work output, as defined, is the work output during just the shortening phase of the isotonic contraction since there is no net work output over the complete cycle as shortening and relengthening take place against the afterload. The assumptions used in calculating work output in afterloaded isotonic contractions are discussed in detail in Chapter 3, Section 3.2.3.

For the sinusoidal and realistic protocols, net work output was determined by integrating force with respect to muscle length change, which is equivalent to calculating the area enclosed by the 'work loop' formed when force is plotted as a function of change in muscle length. Net work output is the difference between the work done by the muscle during shortening and that done on the muscle to relengthen it.

2.10.3 Enthalpy output

Enthalpy output (ΔH) is the total energy released by the muscle. In this study, H_{Total} included all the enthalpy, in excess of the basal enthalpy output, produced during and after the series of contractions and thus included both initial and recovery metabolisms. Determination of enthalpy output was also dependent on the type of contraction under investigation. During the sinusoidal and realistic protocols, energy was liberated from the muscle as both heat and work and the enthalpy output was the sum of the total heat produced and total work (net) performed (*i.e.* $\Delta H = \Delta W + \Delta Q$). In isotonic contractions, it was assumed that an amount of heat equivalent to the work done during shortening was liberated in the muscle as a consequence of doing work on the muscle to relengthen it (Gibbs *et al.*, 1967; Hill, 1949). Therefore, the total enthalpy output was equivalent to the total heat output (*i.e.* $\Delta H = \Delta Q$; *i.e.* the heat output included a component equivalent in magnitude to the work done). Again, a more detailed discussion of this aspect of isotonic contractions is presented in Chapter 3, Section 3.2.4.

2.11 Experimental protocols

Following dissection, papillary muscle preparations were mounted on the experimental apparatus (see Section 2.5.1) and performed isometric contractions for a period of 1.5 hr at a rate of 0.2 Hz to allow mechanical performance to stabilise (Figure 2.21).

equilibration period, 0.2 Hz, under solution

| 45 min - 1 hr | 1.5 hr | 30 min |

heart removed | dissection complete | determination of L_{mus}/L_{opt} | experiment start | muscle removed
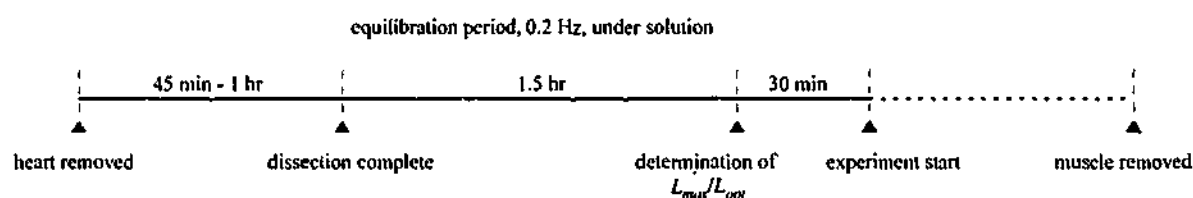
Figure 2.21 Schematic diagram of general experimental protocol

This diagram illustrates the initial experimental methods common to all the experiments reported in this thesis.

Experimental recordings of force output, changes in muscle length and muscle temperature change were made with the solution drained from the thermopile chamber. Stimulation of the muscle ceased prior to drainage to allow any heat generated by the muscle during stimulation to dissipate into the solution. Following drainage, any remaining droplets of solution on the thermopile were carefully blotted using a small piece of tissue. This minimised added heat capacity due to water, which can alter the time-course and magnitude of the recorded temperature change signal (Holroyd and Gibbs, 1992). The preparation remained unstimulated for ~8 min prior to the start of the experimental protocols, allowing thermopile output to stabilise.

2.11.1 Data acquisition

Data were recorded using a laboratory computer and a multi-function data acquisition board (DAS1802AO, Keithley Instruments, Cleveland, OH, USA) using software developed by C. J. Barclay using TestPoint.

Force, length and temperature signals were sampled at 110 Hz, digitised using an analogue to digital (A-D) converter and stored on disk. A sampling rate of 110 Hz was selected so as not to be a multiple of the mains frequency (50 Hz) and also to be of a high enough frequency to reproduce signals adequately according to the Nyquist rule. This rule states that the sampling rate must be twice the highest frequency component of the sampled data. The frequency components of the force, length and heat signals were determined and the highest component was found for the length change signal and was <30 Hz. Thus, the sampling rate of 110 Hz used in this study was high enough to reproduce signals accurately.

For these experiments, a 12-bit A-D converter (DAS1802AO, Keithley Instruments, Taunton, MA, USA), with an input range of ± 10 V, was used to convert the recorded analogue signals to digital signals for display and storage. A-D converters transform a continuous analogue signal to discrete numbers. The error introduced into a signal by dividing it into discrete steps is the quantisation error. The A-D converter in this study operated over a range of ± 10 V (*i.e.* 20 V). One quantum thus corresponded to $20/2^{12} = 4.88$ mV. Therefore, as long as the input signal was greater than 1 V, the quantisation error would be <0.5 %.

It should be noted that much care was taken in grounding the equipment to keep raw temperature signals as free from noise as possible and to avoid the creation of ground loops. It was found that twisting the cables and shielding them with aluminium foil was

very effective in reducing the amplitude of the noise by a factor of 20. Appropriate grounding of the equipment was accomplished using a trial and error approach.

2.11.2 Determination of experimental muscle length

The lengths at which active isometric force (L_{max}; Chapters 3-5) and sinusoidal work output (L_{opt}; Chapter 3) were maximal were determined as appropriate (Figure 2.22) with the muscle under solution.
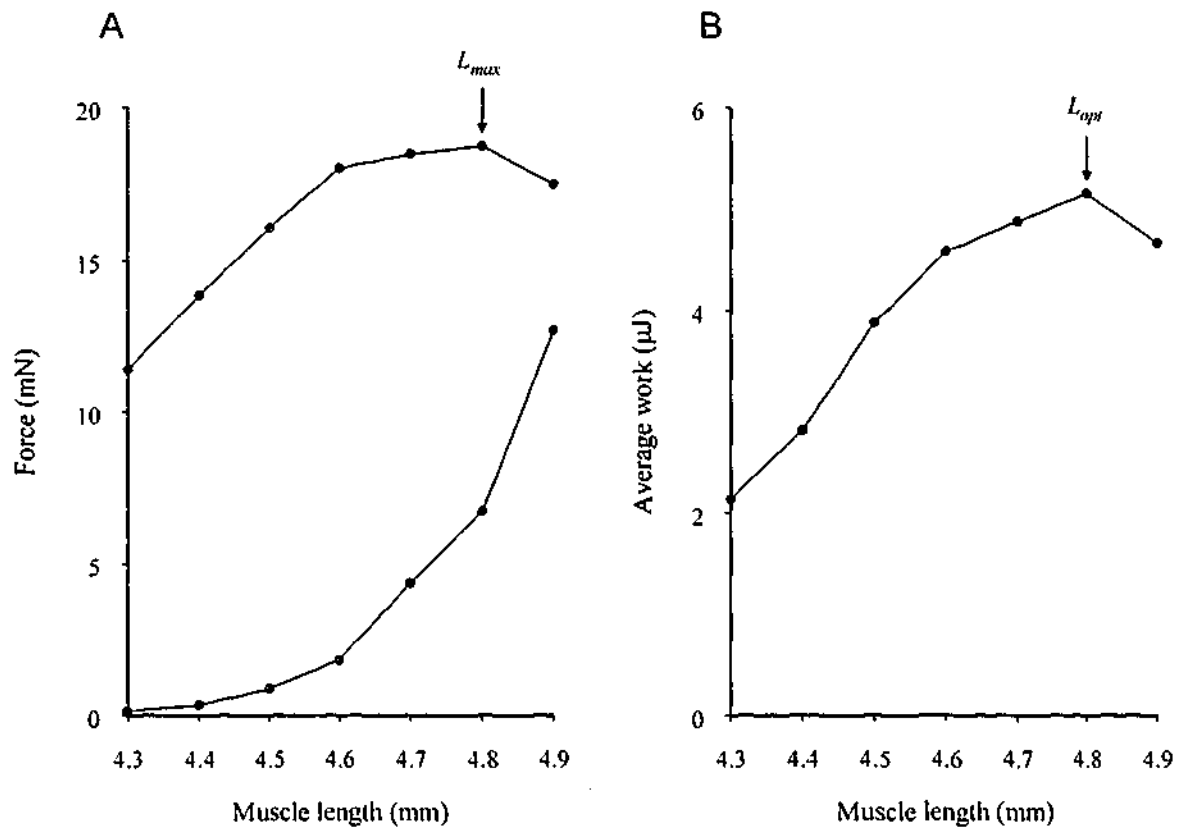
Figure 2.22 Length-force and length-work relationships

Example of passive (lower line) and active (upper line) force (**A**) and average work (**B**) plotted against muscle length. The procedure used to determine these relationships is described in the text. Note that L_{max} and L_{opt} are the same length.

The isometric length-force relation was determined by setting the muscle to perform 10 twitches at 0.2 Hz at each length. The average maximum active force in the last five twitches was calculated. Sinusoidal work output was determined using a series of 10 twitches at 2 Hz during which length was altered in a sinusoidal pattern, also at 2 Hz, *i.e.* the muscle performed one contraction in each length cycle. The amplitude and stimulus phase used were ±5 % initial length and -10° respectively. Stimulus phase was defined as the deviation (in degrees) from the maximum length point in each cycle. In these

experiments, this deviation corresponded to 14 ms prior to the maximum length. The average work performed in the last five contractions at each length was calculated. Muscle length was altered in increments of 0.1 mm and was measured using fine calipers (505-633-50, Mitutoyo, Japan) while viewed under a microscope ($\times 100$; Nikon, Japan).

2.11.3 Post-experimental procedure

At the conclusion of each experiment, the preparation was removed from the experimental apparatus and the ends of the muscle beyond the ties removed. The muscle was lightly blotted using filter paper and its mass determined (to the nearest 0.01 mg) using an electronic balance (Cahn 25, Cahn Instruments, Cerritos, CA, USA). The average CSA of each muscle was calculated using the following equation:

$$CSA = \frac{mass}{(length \times density)}$$

assuming a density of 1.06 g cm^{-3} (Hill, 1931). All forces were normalised by CSA.

2.12 Data presentation and statistical analysis

Data were analysed using a Microsoft Windows-compatible statistical package (SPSS 10.0.5, Statistical Packages for the Social Sciences, SPSS Inc., Chicago, IL, USA). Data were tested for homogeneity of variances prior to analysis. Inhomogeneous data were transformed using square root or logarithmic transformations. Data were analysed using analysis of variance (ANOVA) with repeated measures. Where an ANOVA revealed a significant difference between groups, *post hoc* testing to uncover differences between mean values was performed using the Least Significant Difference (LSD) test. Values were included in the analysis only when all relevant protocols were successfully completed on the one preparation. All decisions concerning statistical significance were made at the 95 % confidence level. Original, untransformed data are presented as the mean $\pm$ 1 s.e.m. (standard error of the mean).

Chapter 3: Efficiency of rat papillary muscles during afterloaded isotonic and sinusoidal length change contractions

3.1 Introduction

3.1.1 Contraction protocols for use with isolated papillary muscles

Many investigations of ventricular energetics have used isolated papillary muscles as a model of ventricular muscle. The most common contraction protocols used *in vitro* have involved either isometric or afterloaded isotonic contractions and, more recently, sinusoidal protocols. As a model of ventricular function, isometric contraction protocols are less than ideal since, unlike the contracting ventricle, no mechanical work is performed during contraction. However, even afterloaded isotonic contractions are not ideal since they produce no net work because the muscle shortens and lengthens against a constant force (Gibbs *et al.*, 1967). Consequently, the amount of work done on the muscle to lengthen it is the same as that done by the muscle during shortening. Another criticism of the afterloaded isotonic protocol is that the combination of force and length changes is unrealistic. Additionally, very low contraction frequencies (~0.2 Hz; Gibbs and Chapman, 1979a; Kiriazis and Gibbs, 1995) have often been used which further distances these protocols from *in vivo* activity.

In an effort to approach a more realistic pattern of length changes, a number of recent studies have used sinusoidal length change protocols to model cardiac function (Baxi *et al.*, 2000; Layland *et al.*, 1995; Syme, 1994; Syme and Josephson, 1995). The use of this type of protocol in cardiac muscle largely followed its successful application to skeletal muscle (Altringham and Johnston, 1990; Askew and Marsh, 1997; Barclay, 1994; Curtin and Woledge, 1993; Josephson, 1985; Moon *et al.*, 1991). An advantage of using the sinusoidal protocol with ventricular muscle is that with appropriate selection of cycle frequency and timing of stimulation, net work is performed and the force-length diagrams resemble the pressure-volume diagrams of the intact ventricle (Baxi *et al.*, 2000).

3.1.2   Energetics of rat papillary muscles using different contraction protocols

The efficiency of muscular contraction is, in general terms, the ratio of work output to energy cost. In studies using isotonic contractions, work output is defined as the product of shortening force and distance shortened (Gibbs *et al.*, 1967; Hartree and Hill, 1928; Kiriazis and Gibbs, 1995; Sonnenblick, 1962). In other words, the work output during only the shortening phase of the contraction is calculated. Using this definition, previous studies using afterloaded isotonic contraction protocols have reported maximum net mechanical efficiency values between 20 and 25 % (Gibbs and Chapman, 1979a; Kiriazis and Gibbs, 1995), achieved when shortening against a load of ~ 0.3 P_0 (where P_0 is the maximum isometric twitch force, excluding passive force). Twitch frequency in these protocols was typically ~ 0.2 Hz and energy use was measured from a total of 10 to 20 twitches. In a recent study using a sinusoidal length change protocol, a considerably lower maximum efficiency (~ 15 %) was found (Baxi *et al.*, 2000). However, the protocol used in that study involved higher twitch frequencies (1-4 Hz) and more contractions (40) than in the studies that used afterloaded isotonic contractions. An additional variable was that although both the isotonic and sinusoidal experiments were performed in the same laboratory, different heat recording technologies and different calibration techniques were used in the two studies. For example, the thermopile used in the work of Kiriazis and Gibbs (1995) was wire-wound, electroplated silver and constantan while the thermopile used by Baxi *et al.* (2000) was made by vacuum depositing antimony and bismuth. Calculations of muscle heat loss and muscle heat capacity were made differently in the two studies: Kiriazis and Gibbs (1995) passed high frequency current (100 kHz) through the stimulating electrodes to heat the muscle, while Baxi *et al.* (2000) used the more accurate method of Peltier heating. Thus, it is unclear whether the differing efficiencies

reflected (1) the different patterns of length changes, (2) the higher frequency and greater number of contractions used by Baxi *et al.* (2000) or (3) the different experimental apparatus and conditions used in the studies.

Another factor clouding the comparison between results from the two protocols was that different definitions of work output were, necessarily, used in afterloaded isotonic and sinusoidal protocols. In sinusoidal protocols, net work output is calculated by determining the area enclosed by a plot of force output as a function of muscle length. Net work output is the difference between the work done by the muscle during shortening and that done on the muscle to relengthen it. In contrast to the sinusoidal protocol, there is no net work output in an afterloaded isotonic contraction and the work output is taken as the work performed during the shortening phase alone (Gibbs *et al.*, 1967; Hartree and Hill, 1928; Hill, 1949; Sonnenblick, 1962).

3.1.3   Aims of this chapter

The primary aims of the current study were (1) to confirm the different efficiency values in sinusoidal and isotonic contractions by performing both protocols on the same preparation using the same apparatus and (2) to determine if the contraction frequency or number of contractions over which energy output is measured affects efficiency.

In addition, two other factors that can influence estimates of efficiency were assessed: (1) the assumption that, in isotonic contractions, all the work done on the muscle to relengthen it is ultimately converted into heat in the muscle and (2) whether appropriate definitions of work output were used in the two types of contraction protocol.

3.2   Materials and methods

The materials and methods for the experiments reported in this chapter have been described in Chapter 2. Only those methods specific to these experiments will be described here.

3.2.1   Thermopiles

Two thermopiles were used in this study. Muscle temperature changes were recorded over active recording regions 4 or 5 mm in length, containing 16 or 20 antimony-bismuth thermocouples that produced 1.09 mV $°C^{-1}$ and 1.24 mV $°C^{-1}$, respectively (Table 2.2, Chapter 2).

3.2.2 Experimental protocols

The current study was designed to compare the efficiency of papillary muscles performing isotonic and sinusoidal contractions. Three contraction protocols were selected: the afterloaded isotonic protocol used by Kiriazis and Gibbs (1995) (10 twitches at 0.2 Hz), the sinusoidal length change protocol used by Baxi *et al.* (2000) (40 twitches at 2 Hz) and a protocol that combined isotonic contractions with the higher twitch frequency and greater number of contractions used in the sinusoidal protocol. It should be noted that the loads, stimulus timing and length changes used were those shown previously to be required to produce maximum efficiency in the respective protocol (Table 3.1).

Table 3.1 Parameters selected for contraction types to give maximum efficiency

	Stimulus frequency (Hz)	Number of contractions	Starting length	Afterload $(\times P_0)$	Stimulus phase (°)
Afterloaded isotonic	0.2	10	L_{max}	0.3	
Sinusoid	2	40	L_{opt}		-14

The afterload for the isotonic contractions was 0.3 P_0. The pattern of length changes required to generate the isotonic contractions was determined using an adaptive force control algorithm (Peterson *et al.*, 1989) that was adapted to our recording apparatus by C. J. Barclay using Testpoint. Briefly, the pattern of length changes required to produce the desired isotonic contraction was determined in a series of contractions performed before the recording run. To determine the correct pattern of length changes, force output during a twitch was compared to the desired time-course of force output and the difference between the two was used to modify the applied muscle length changes. The desired time-course of force output consisted of the muscle contracting isometrically until the force reached 0.3 P_0, then maintaining this force while the muscle shortened and then relengthened to the initial length, and finally relaxing isometrically (Figure 3.1). Between five and ten twitches were sufficient to refine the length changes so that an isotonic force record was produced. The main difference between the application of this technique and a conventional isotonic lever or ergometer was that the current method produced isotonic contractions in which the *relative* afterload was constant but the absolute afterload varied between contractions in a series of twitches, reflecting the changes in the active force

generating capacity of the muscle. In other words, the afterload in each twitch was 0.3×
the isometric force that could be developed at that time in the contraction series.

3.2.3   Calculation of work output

It should be noted that work output was calculated differently in the isotonic and
sinusoidal protocols. Following the example of Kiriazis and Gibbs (1995), work output in
isotonic contractions was defined as the product of the total force (*i.e.* active force +
passive force) and shortening amplitude. For the sinusoidal protocol, net work output was
determined by integrating force with respect to muscle length change, which is equivalent
to the area enclosed by the 'work loop' formed when force is plotted as a function of
change in muscle length. Note that in an isotonic contraction there is no net work output
over the complete cycle as shortening and relengthening take place against the afterload
(Figure 3.1). Instead, the work output as defined is the work output during just the
shortening phase of the isotonic contraction.
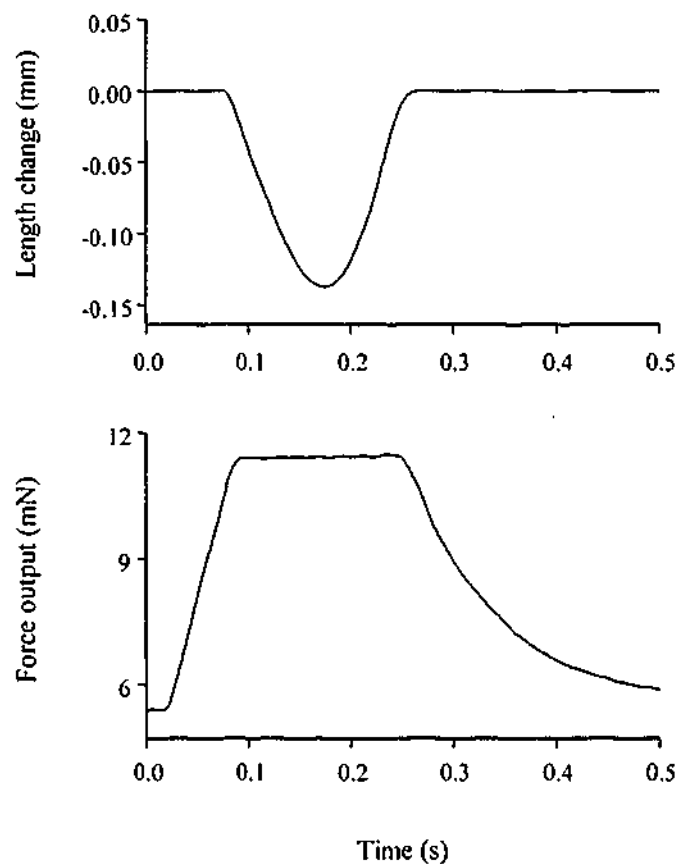
**Figure 3.1 Example of an afterloaded isotonic contraction produced using
the adaptive force control algorithm**

During an isotonic contraction the muscle contracted isometrically until the desired
afterload was reached. The muscle was then shortened and relengthened to hold the
force constant. Once relengthening was complete, the muscle relaxed isometrically.

3.2.4   Calculation of enthalpy output

H_{Total} included all the enthalpy, in excess of the basal enthalpy output, produced during and after the series of contractions and thus included both initial and recovery metabolisms. Enthalpy output was also determined differently in the two protocols. During the sinusoidal length change protocol, energy was liberated from the muscle as both heat and work and the enthalpy output was the sum of the total heat produced and total work (net) performed. In isotonic contractions, it was assumed that an amount of heat equivalent to the work done during shortening was liberated in the muscle as a consequence of doing work on the muscle to relengthen it (Gibbs *et al.*, 1967; Hill, 1949). Therefore, the total enthalpy output was equivalent to the total heat output (*i.e.* the heat output included a component equivalent in magnitude to the work done).

3.2.5   Conversion of mechanical energy into thermal energy

An experiment was designed to determine whether all the work done to relengthen the muscle in an isotonic contraction was dissipated in the muscle as thermal energy.
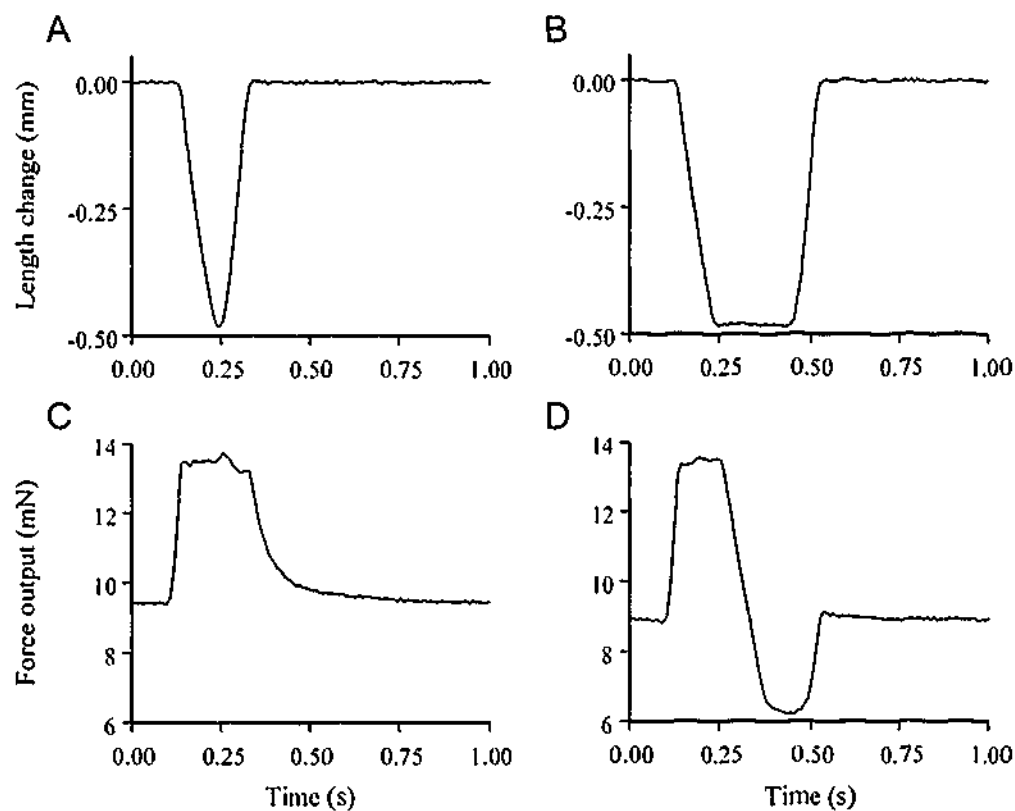
Figure 3.2 Records illustrating the protocol used to check the work and enthalpy outputs during afterloaded isotonic contractions

The left panels show the length change (A) and force output (C) in an isotonic contraction with an afterload of 0.3 P_0. The right panels show a contraction in which muscle length (B) was held at the shortest length until active force generation (D) had ceased. Only then was the muscle returned to the starting length.

Each muscle performed two series of contractions. One consisted of isotonic contractions (20 twitches at a frequency of 1 Hz with an afterload of 0.3 P_0) and the other a similar series in which lengthening was delayed until force had decreased to resting levels (Figure 3.2).

In the latter protocol, the work done during shortening was the same as in the normal isotonic protocol but by delaying lengthening until the force output had decreased to resting levels, there was net work output. Thus, in contrast to the normal isotonic contractions, the heat output did not include a component resulting from relengthening against the afterload. Therefore, the total enthalpy output for this protocol was the sum of the work and heat outputs. Comparison of the total enthalpy output in the two protocols enabled the assumption that all the work done on the muscle during lengthening reappeared as thermal energy in the isotonic protocol to be assessed.

3.3   Results

The primary aim of this study was to compare the efficiency of rat cardiac papillary muscle preparations performing isotonic and sinusoidal contractions. General characteristics of the papillary muscle preparations used in this part of the study are shown in Table 3.2.

Table 3.2 Characteristics of papillary muscle preparations

Wet mass (mg)	3.00 ± 0.32
L_{max} and L_{opt} (mm)	4.95 ± 0.20
Cross-sectional area at L_{max} (mm^2)	0.57 ± 0.06
Passive force at L_{max} (mN)	3.9 ± 0.7
Isometric active force at L_{max} (mN)	16.6 ± 1.2
Active stress at L_{max} (mN mm^{-2})	29.8 ± 2.1
Passive force/active force at L_{max}	0.24 ± 0.04

All values are mean ± 1 s.e.m. (n=6)

For the papillary muscles used in this study, L_{max} and L_{opt} were found to be the same. Harwood et al. (1998) also noted this similarity, however other studies have found that L_{opt} occurred at a slightly shorter length than L_{max} (Baxi et al., 2000; Layland et al., 1995).

3.3.1 Recordings during different contraction protocols

Typical records from all three contraction protocols are illustrated in Figure 3.3. For each protocol, length change, force output, muscle temperature change and muscle heat output are shown. The mechanistic difference between the isotonic and sinusoidal protocols was that, in the former, muscle length was adjusted to give a relatively constant force output, *i.e.* force output was controlled (Figure 3.1), whereas, in the latter, muscle length was controlled (Figure 3.4). A notable difference in the records is that the magnitudes of the temperature change in the two high frequency protocols were substantially greater than in the 0.2 Hz protocol. Small alterations in the temperature baseline (typically with a magnitude of <0.2 m°C) were occasionally observed in the recordings. The high frequency recordings were much less sensitive to these small alterations than the low frequency recordings due to the greater magnitude of temperature change.

Cyclic changes in muscle temperature are particularly clear in the records from the 0.2 Hz twitch frequency protocol (Figure 3.3A). There is an abrupt increase in temperature during each twitch followed by a slow decline in temperature during the interval before the next twitch. The decline in temperature reflects heat being lost from the thermopile into the frame at a greater rate than that at which the muscle produced heat. This is compensated for when the correction for heat loss is made (Figure 3.3, bottom panels; see Chapter 2, Section 2.9.2). In the last half of the low frequency isotonic contraction protocol, the cyclic temperature changes in successive cycles were the same, indicating that the muscle had achieved an energetic steady-state (Paul, 1983). This state was not quite achieved in the two high frequency protocols.

In all three protocols, muscle temperature returned to its pre-stimulation value indicating that all recovery metabolism was complete in less than 1 min after completion of the contractions (Figure 3.3). The decrease in temperature reflects the net effect of heat flowing from the muscle through the metals of the thermocouples to the thermopile frame and the ongoing metabolic heat production that follows a period of activity. Muscle temperature returns to its initial value only when the rate of metabolic heat production is equal to the rate before commencement of the contraction protocol.
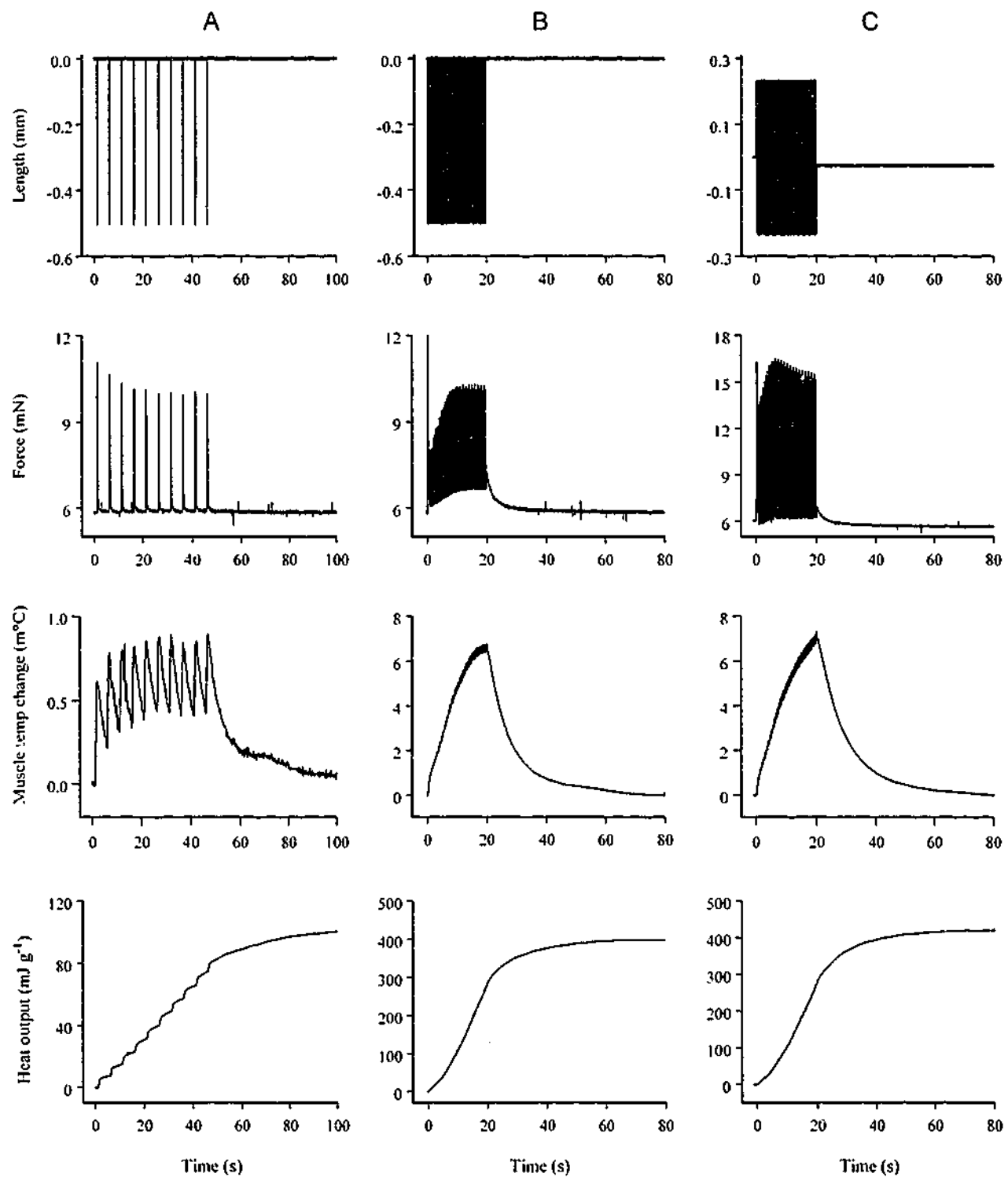
Figure 3.3 Examples of recordings made during the three contraction protocols

Records are shown for low frequency isotonic contractions (A; 10 twitches at 0.2 Hz), high frequency isotonic contractions (B; 40 twitches at 2 Hz) and sinusoidal contractions (C; 40 twitches at 2 Hz). For each protocol records are shown of (from top to bottom) change in muscle length, force output, change in muscle temperature and cumulative heat production. All recordings were made on the same muscle (mass, 2.0 mg; length, 4.6 mm; cross-sectional area, 0.41 mm^2).
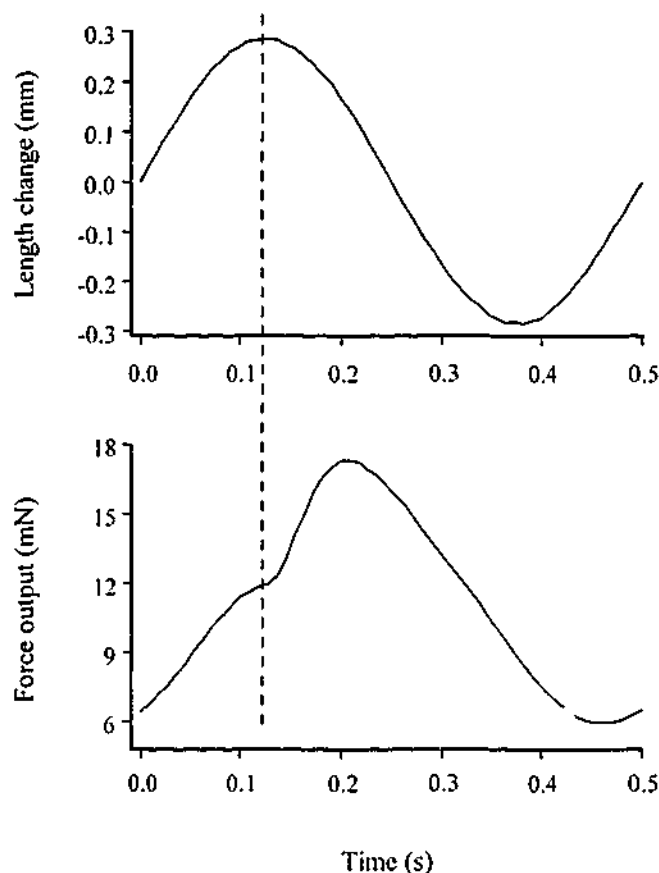
Figure 3.4 Example of length and force changes during one cycle of a sinusoidal length change protocol

During the sinusoidal protocol, muscle length was altered in a sinusoidal pattern at 2 Hz. A stimulus pulse was applied 14 ms prior to the maximum length point in each cycle.

3.3.2   Comparison of low frequency isotonic protocol and sinusoidal length change protocol

The nature of the afterloaded isotonic contraction is such that little or no net work is performed. This is illustrated in Figure 3.5 in which force is plotted as a function of change in muscle length for both types of contraction. In the sinusoidal protocol (Figure 3.5B), the force during shortening was substantially greater than that during the relengthening phase, resulting in a loop, in which time progressed in an anti-clockwise direction, indicating that there was net work output. In contrast, in the isotonic contraction the force was the same during shortening and lengthening so no loop was formed which indicates no net work output (Figure 3.5A). Therefore, work performed in an isotonic contraction is expressed as the work performed during just the shortening phase (*i.e.* total force × shortening amplitude).
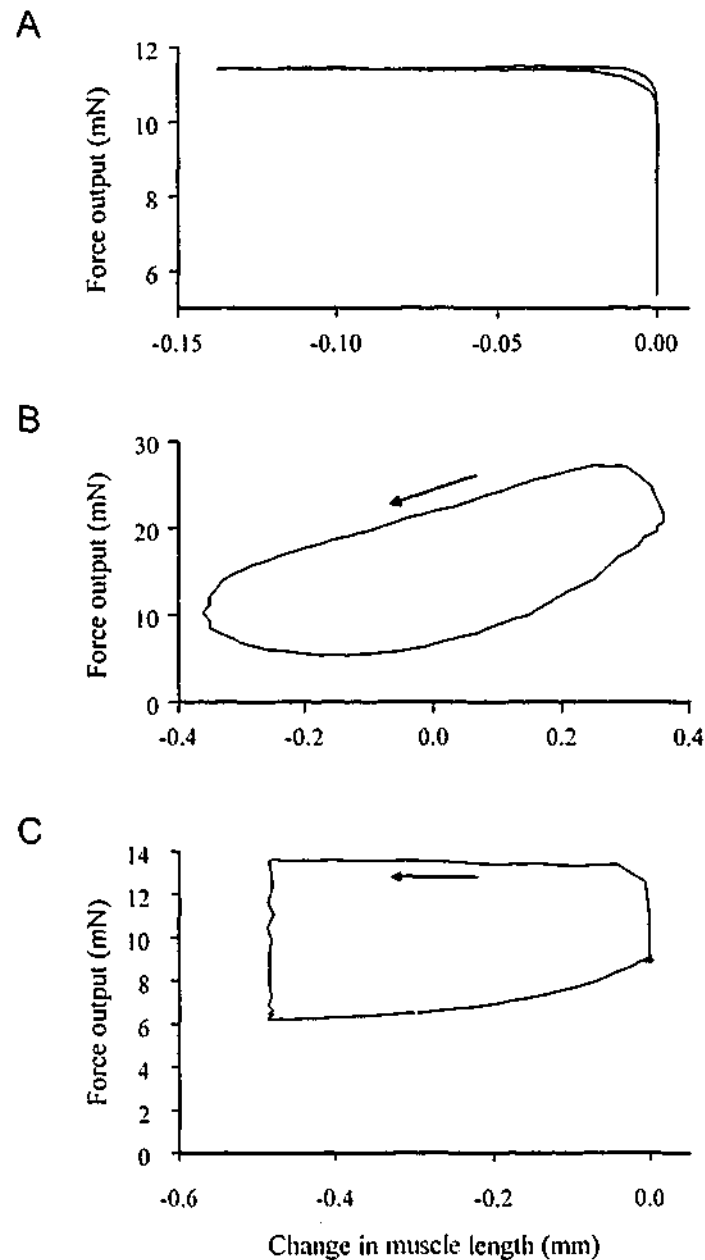
Figure 3.5 Examples of work loops formed during different contraction types

Examples of work loops formed during isotonic (**A**) and sinusoidal (**B**) contractions. Each loop was obtained from a single twitch and was produced by plotting force with respect to muscle length. Contraction rate was 2 Hz for sinusoidal contractions and 0.2 Hz for the isotonic twitch example. Sinusoidal contractions resulted in work loops enclosing a substantial area, indicating net work output. Isotonic contractions did not form work loops, indicating that little or no net work was performed by the muscle. (**C**) An example of the work loop formed when relengthening in an isotonic contraction was delayed until active force production had ceased. The contraction started at the longest length and force increased with no change in muscle length until the force matched the afterload. The muscle then shortened with a constant force output, before being allowed to relax while muscle length was held at the shortest length. The passive muscle was then stretched back to its initial length. Time progressed around the loops in an anti-clockwise direction (arrows, **B** & **C**).

During the contraction protocols used to determine efficiency, the total work output was much greater in the sinusoidal protocol, during which 40 twitches were performed, than during the low frequency isotonic protocol, in which only 10 twitches were performed (Table 3.3). However, more work was performed in each low frequency isotonic twitch than in each twitch with sinusoidal length changes. The total enthalpy output in the sinusoidal protocol (= total heat + total work) was also much greater than that in the low frequency isotonic protocol (where total enthalpy = total heat) but when normalised by the number of contractions, the energy cost per twitch did not differ between the two protocols (Table 3.3). As reported previously, in separate studies, the net mechanical efficiency of the muscles was greater during isotonic contractions than during sinusoidal contractions. In the 0.2 Hz isotonic contractions the mean value of ε_{Net} was 21.1 ± 1.4 % whereas in the sinusoidal protocol ε_{Net} was 13.2 ± 0.7 %.

The third protocol used isotonic contractions combined with the twitch frequency and number of contractions used for the sinusoidal protocol. The notable result was that with this protocol, ε_{Net} was 21.5 ± 1.0 % which did not differ from that in the low frequency isotonic protocol but was significantly greater than that in the sinusoidal protocol. Therefore, the difference in ε_{Net} between the isotonic and sinusoidal contractions was not simply due to either the different contraction frequency or number of twitches.

Table 3.3 Mean values of energetic variables for the three contraction protocols

	Low frequency isotonic	Sinusoid	High frequency isotonic
Contraction frequency (Hz)	0.2	2	2
Number of twitches	10	40	40
Total work output (mJ g^{-1})	19.5 ± 1.6 [a]	51.5 ± 3.1 [b]	60.6 ± 7.8 [b]
Total heat output (mJ g^{-1})	93.0 ± 6.6 [a]	349.1 ± 32.9 [b]	283.6 ± 33.6 [c]
Work per twitch (mJ g^{-1})	1.95 ± 0.16 [a]	1.29 ± 0.08 [b]	1.52 ± 0.20 [b]
Heat per twitch (mJ g^{-1})	-	8.73 ± 0.82	-
Enthalpy per twitch (mJ g^{-1})	9.30 ± 0.66 [a]	10.01 ± 0.89 [a]	7.09 ± 0.84 [b]
Net efficiency (%)	21.1 ± 1.4 [a]	13.2 ± 0.7 [b]	21.5 ± 1.0 [a]

All values are mean $\pm$ 1 s.e.m. (n=6). Letters indicate significant difference (p<0.05). For each variable, values labelled *a* differ from those labelled *b* and *c*, and those labelled *b* differ from that labelled *c*. For isotonic protocols, values for heat output per twitch are not listed since, by definition, heat output per twitch and enthalpy output per twitch are the same.

This study used an adaptive algorithm to control the muscle length changes, giving a constant relative afterload of 0.3 P_0. Comparison of the current results with those of previous studies (Gibbs and Chapman, 1979b; Kiriazis and Gibbs, 1995) indicates that the values of the energetic variables measured from a protocol in which the relative afterload was constant between contractions (current study) were the same as those in which the absolute afterload was constant. The average active force using the current method was only ~5 % greater than that which would have been recorded if the absolute afterload force was constant and equal to 0.3 of the steady-state, isometric twitch force.

3.3.3 Conversion of mechanical energy into thermal energy in isotonic contractions

A series of experiments was performed to determine (1) whether the work output in isotonic contractions was really equivalent to total force × distance shortened and (2) if all the work performed on a muscle during isotonic lengthening (which is equal to the work done during shortening) was dissipated in the muscle as thermal energy. The experiments involved comparing work output calculated in the usual isotonic way with that determined from the area of the work loop formed when relengthening was delayed until force had relaxed to passive values. Mean data for the protocols are displayed in Table 3.4.

Table 3.4 Work and enthalpy outputs for normal and held short isotonic contractions

		Contraction type	
	Calculation	Normal isotonic	Delayed lengthening
Work output (mJ g^{-1} twitch^{-1})	Work = P × ΔL	1.61 ± 0.1 7 [a]	1.48 ± 0.22 [a]
	Work = $\int P dL$	—	0.81 ± 0.15 [b]
Enthalpy output (mJ g^{-1} twitch^{-1})	H = total heat	7.06 ± 1.10 [c]	—
	H = (P × ΔL) + heat	—	8.33 ± 1.15 [d]
	H = $\int P dL$ + heat	—	7.64 ± 1.14 [c]

All values are mean ± 1 s.e.m. (n=5). Letters indicate significant differences using repeated measures comparison: *a* differs from *b* and *c* differs from *d*. P × ΔL = total force × amplitude of shortening. ∫PdL = force integrated with respect to length change = area enclosed by work loop. H = enthalpy output, Enthalpy = heat output for normal isotonics and (heat + work) for isotonics with delayed lengthening.

When work output was calculated as total force × distance shortened, the work output per twitch was, as expected, the same in the two contraction protocols (top row, Table 3.4). However, work output per twitch calculated from the area of the work loops in the delayed relengthening contractions (mean value 0.81 mJ g^{-1} twitch^{-1}) was significantly less than that calculated as total force × shortening amplitude (mean value 1.48 mJ g^{-1} twitch^{-1}). The difference between the two methods for calculating work was that the work loop method took account of the work that had to be done on the muscle to relengthen it; the net work output is the difference between the work performed during shortening and the work required to relengthen the muscle (Figure 3.6).
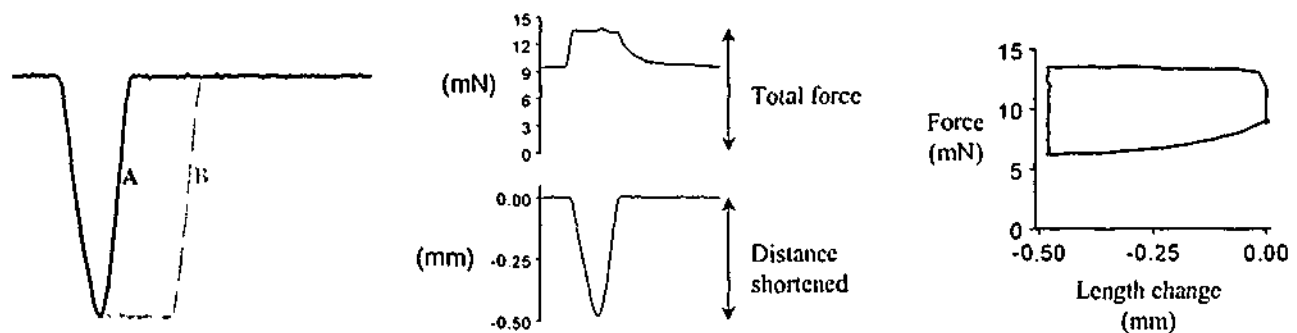
Figure 3.6 Illustration of different methods used to calculate work output

In the left-hand panel of this figure are the length changes associated with a normal isotonic twitch (**A**) and one in which the muscle was held at the short length until the force had relaxed (**B**). In the normal isotonic twitch shown in this figure, work output calculated as total force × distance shortened (centre panel) was ~7 μJ. When the work output was calculated for the twitch in which the muscle was held at the short length, the work output was ~3.25 μJ, calculated from the area of the work loop shown on the right. This may seem to be an extreme example because of the high resting tension. However, when mean work output was calculated for the set of muscles, work output calculated using total force × distance shortened was still twice that measured from a work loop (Table 3.4). It is evident from the work loop shown on the right that the load supported by the passive elements is not included in work output calculated from a work loop.

The comparison of the enthalpy outputs for these two protocols provided a thermodynamic assessment of which method of calculating work was correct. The enthalpy output in response to the normal isotonic protocol was compared to the enthalpy output calculated for the protocol in which lengthening was delayed (Table 3.4). The enthalpy output of the delayed lengthening protocol was equal to the heat + work but work could be calculated two ways: (1) total force × shortening amplitude and (2) area of the

work loop. If work was calculated using the first of these formulae, then the enthalpy output in the delayed lengthening protocol was significantly greater than that in the normal isotonic protocol. However, when the second formula for calculating work (work loop area) was used, there was no significant difference between the enthalpy output in the two protocols (Table 3.4). This is consistent with the idea that the area of the work loop was the accurate index of work output. If this is so, then it can also be concluded that all the work done during relengthening in the normal isotonic contractions was dissipated in the muscle as heat.

3.4   Discussion

The initial set of experiments in this study confirmed that the efficiency, as defined previously, of papillary muscles is different when performing sinusoidal contractions and when performing afterloaded isotonic contractions. The subsequent experiments provided information that can be used to investigate the basis of this difference. Specifically, the final set of experiments indicated that the method of calculating work used in the isotonic contractions overestimated work output and, thus, efficiency in these contractions. Both these issues are addressed in the following discussion.

3.4.1   What is the correct method to calculate work output in isotonic contractions?

Work output calculated as total force × shortening amplitude was substantially greater than that calculated from the area of the work loop in the modified isotonic protocol. The difference between these two estimates of work output is that the former includes work done by elastic elements in parallel with the contractile elements. In contrast, using the area of a work loop to measure work output recognises that work must be done on the muscle to relengthen parallel elastic elements (assuming there is no contractile activity during relengthening), so they contribute no net work output or may even absorb energy (Baxi et al., 2000; Josephson, 1985). It is interesting to note that in early papers on energetics of musc ;s during isotonic contractions, explicit corrections were made for the underlying passive force (Gibbs et al., 1967; Hill, 1949) so that work output was calculated in a manner analogous to the work loop method used with sinusoidal contractions. Using such an analysis yielded maximum efficiency values of between 10 and 15 %.

Support for the idea that the work output during isotonic shortening, excluding parallel elastic work, did correspond to the area of the work loop in the delayed lengthening contractions was provided by observations of the enthalpy output in the two isotonic protocols (*i.e.* normal isotonic twitches and those with delayed relengthening; Figure 3.5). In the delayed relengthening protocol, the heat output was less than that in the normal isotonic protocol. However, when the sum of the heat and net work produced in the delayed relengthening protocol was calculated, it was the same as the total heat produced in the normal isotonic protocol. This is what would be expected if (1) the work output during shortening in the isotonic protocol, excluding work done by parallel elastic elements, was equivalent to the work loop area in the delayed relengthening protocol and (2) all the work required to stretch the muscle in the normal isotonic contractions was dissipated as heat in the muscle (Gibbs *et al.*, 1967; Hill, 1949). If, however, the enthalpy output in the delayed relengthening protocol was calculated using the product of total force and shortening amplitude (the definition used in previous studies), then the calculated enthalpy output was greater than the enthalpy output measured in the normal isotonic protocol.

If calculating work as total force × distance shortened overestimated the actual work output, then efficiency would also have been overestimated. The data in Table 3.4 indicate that, in the preparations used in this study, the values of total force × distance shortened were ~2-fold greater than the work loop area. Correcting for an error of this magnitude reduces the efficiency of isotonic contractions in this study from a mean value of approximately 21 % to 12 %, a value similar to that determined for the sinusoidal contractions. This revised value is also similar to that quoted in an early paper on papillary muscle energetics in which appropriate corrections were made to the work output (Gibbs *et al.*, 1967). In addition, the maximum efficiency of frog ventricular muscle, determined using a work loop technique, was reported to be 13 % (Syme, 1994), again similar to the values in this study if work output is calculated on the basis of active force output alone. Changes in the reported net mechanical efficiency of isolated cardiac muscle are documented in Table 3.5. For each study, the contraction protocol and the method used to calculate work output are indicated.

In a very recent study investigating changes in the energetics of rat papillary muscles with age, Kiriazis and Gibbs (2000) presented data for work output calculated both without and with a correction for changes in passive force during shortening in isotonic contractions. Making an estimate from their data indicates that maximum efficiency was decreased

from ~25 % to 19 % when the total work was replaced by the estimated net work output. The magnitude of the difference between the two methods for calculating work was smaller in that study than ours, which must be due to the passive force at L_{max} being lower in the work of Kiriazis and Gibbs (2000) than in the current study. However, the results of those authors support the idea that the maximum efficiency of papillary muscles is likely to be less than 20 %.

Table 3.5 Efficiency of isolated cardiac muscle

Technique	Muscle preparation	Work calculation	$[Ca^{2+}]$ (mM)	$\sim\varepsilon_{Net}$ (%)	Temp (°C)
Afterloaded isotonic [a]	Rabbit papillary	(Total force × shortening amplitude) – passive force	5	12	20
Sinusoidal [b]	Frog ventricle	Work loop	2	13	21-23
Afterloaded isotonic [c]	Rat papillary	Total force × shortening amplitude	2.54	20-25	27
Sinusoidal [d]	Rat papillary	Work loop	2.54	15	27
Afterloaded isotonic [e]	Rat papillary	(Total force × shortening amplitude) – passive force	2.54	20	27
Afterloaded isotonic [f]	Rat papillary	Total force × shortening amplitude	1.6	21	27
Afterloaded isotonic [f]	Rat papillary	Work loop	1.6	12	27
Sinusoidal [f]	Rat papillary	Work loop	1.6	13.6	27

References corresponding to letters included in the table are: a, Gibbs et al. (1967); b, Syme (1994); c, Kiriazis and Gibbs (1995); d, Baxi et al. (2000); e, Kiriazis and Gibbs (2000) and f, current study.

3.4.2   Comparison with efficiency of whole hearts

There is extensive evidence to indicate that the efficiency of animal (Elzinga and Westerhof, 1980) and human (reviewed by Gibbs and Barclay, 1995) hearts is likely to be at least 20 %. If the efficiency of papillary muscle determined in the current study is an accurate index of the efficiency of ventricular muscle, then for the efficiency of the ventricle to be substantially higher than the net efficiency of the muscles suggests either that some aspect of the *in vivo* environment or operation of cardiac muscle leads to more efficient energy conversion or that some other process contributes to power output of the ventricles, without using metabolic energy from ventricular muscle. The latter idea could occur if, for instance, the energy required to stretch the ventricular muscle during diastole

was ultimately derived from a source other than contraction of cardiac muscle. The former idea could reflect the possibility that neither of the contraction protocols used in the current study could produce efficiency values as high as those for cardiac muscle *in vivo*. To test this possibility, similar experiments were performed using strain patterns that more closely match those occurring *in vivo* (see Chapter 4).

3.4.3 Effects of lower $[Ca^{2+}]_o$ on efficiency

One of the main aims of this thesis was to improve protocols used to measure cardiac energetics by making the conditions and the protocols more similar to those experienced *in vivo*. The superfusing solutions used in this study contained 1.6 mM $[CaCl_2]$. This concentration in solution is within the physiological range of normal ionised $[Ca^{2+}]$ (~1.3 mM in rat plasma, Chambers *et al.*, 1991). An additional advantage of using the lower $[Ca^{2+}]_o$ was that the lower absolute force output resulted in a lower active metabolic rate. In combination with the smaller CSA of preparations used in the current study, the lower $[Ca^{2+}]_o$ ensured that diffusive O_2 supply was adequate under the conditions employed in these experiments (see Section 2.4, Chapter 2).

It is interesting that the efficiency values calculated in the current study for afterloaded isotonic and sinusoidal contractions using 1.6 mM Ca^{2+} were the same as those reported previously using 2.5 mM Ca^{2+} despite the lower $[Ca^{2+}]_o$ and normalised force output. This indicates that the level of activation has little influence on efficiency over this range of $[Ca^{2+}]_o$.

3.4.4 Contribution of basal metabolism to total enthalpy output

The definition of efficiency used in this study excluded basal, or resting, metabolism. Energy consumed for the non-working processes that comprise basal metabolism arise from processes including ion exchange and regulation, protein synthesis and maintenance of the mitochondrial membrane potential. A comprehensive review of cardiac basal metabolism is given by Gibbs and Loiselle (2001). It has been estimated that these processes account for ~20-25 % of the total metabolism of the heart for a human at rest (Gibbs, 1978; Loiselle and Gibbs, 1979).

In isolated rat papillary muscles, the basal metabolic rate decreases progressively over ~4 hr before reaching a plateau (Loiselle, 1985b). Baxi *et al.* (2000) determined that the resting metabolic rate of rat papillary muscle is ~4.4 mW g^{-1} at 27°C. This rate was determined ~2 hr following cardiectomy. It is unclear whether the heart truly has a higher

resting metabolic rate *in vivo* or whether the dissection process causes the resting metabolic rate to increase initially and then decrease to its true value. It has been found previously that the basal metabolic rate is not affected by changes in $[Ca^{2+}]_o$ (Chapman, 1976; Wendt and Loiselle, 1981). It was of interest to determine the contribution of basal metabolic processes to the total energy consumption of the rat papillary muscles used in this study. To do this, the average rate of active enthalpy output ($mW\ g^{-1}$) was determined over 3 twitches at the end of the respective protocols when the muscle was in, or close to, an energetic steady-state (see Section 2.4 in Chapter 2). It was assumed that 4.4 $mW\ g^{-1}$ was an appropriate value for the resting metabolic rate. In the low frequency isotonic protocol, basal metabolism accounted for 72 ± 1.9 % (n=6) of the total metabolism. This figure is much higher than that reported for the human heart due to the very slow contraction frequency (0.2 Hz) used in this protocol. The analysis was repeated for the high frequency and sinusoidal protocols where basal metabolism accounted for 25 ± 2 % (n=6) and 20 ± 2 % (n=6), of the total enthalpy output respectively. At this frequency (2 Hz), the results are similar to those calculated for cardiac muscle of resting humans.

It should be noted that resting heat production is reported to increase with decreasing body size (Loiselle and Gibbs, 1979). Loiselle and Gibbs (1979) found that the enthalpy output per twitch was smaller for the rat than for either cat or guinea pig papillary muscles although different contraction frequencies were used for each species. The work output per twitch was also lower but rat papillary muscles still have a relatively high net mechanical efficiency. When the higher basal metabolism is taken into account, the total mechanical efficiency would be similar across species (Loiselle and Gibbs, 1979). There is no simple relationship between heart weight to body weight between species and the energy cost is also not simply related to heart size (Loiselle and Gibbs, 1979). These factors make it difficult to accurately predict the contribution of cardiac metabolism to whole body metabolism. The ratios of basal metabolism to total myocardial metabolism estimated for the high frequency protocols in the current study are in reasonable agreement with the likely *in vivo* values, providing further confidence that the protocols developed here correspond more closely to the *in vivo* situation than the low frequency protocols used in the past.

3.4.5 Estimation of total mechanical efficiency of rat papillary muscles

It is possible to estimate the total mechanical efficiency of rat papillary muscles using the data obtained from the current experiments and the measurement of resting heat rate in

Baxi *et al.* (2000). Using the sinusoidal data, the average net work output per twitch was 1.29 ± 0.08 mJ g^{-1} and the average enthalpy output per twitch was 10.01 ± 0.89 mJ g^{-1}. If we take the resting metabolic rate of 4.4 mW g^{-1} from Baxi *et al.* (2000) and convert it to enthalpy output per cycle (2.2 mJ g^{-1}), the total energy cost would be 12.21 mJ g^{-1} twitch^{-1}. Note that basal metabolism is very close to 20 % using this method also. Thus, the total mechanical efficiency is now the work output per twitch/total enthalpy output per twitch or ~10.6 %.

3.5   Conclusion

In conclusion, the maximum efficiency of papillary muscles appears likely to be the same in both sinusoidal and afterloaded isotonic contraction protocols, provided that comparable definitions of work output are used. If the definition of work output incorporates the energy cost of relengthening the parallel elastic elements of the muscle, then the maximum net mechanical efficiency of rat papillary muscles in both protocols is between 10 and 15 %.

Chapter 4: The energetics of rat papillary muscles undergoing 'realistic' strain patterns

4.1   Introduction

4.1.1   Papillary muscle dynamics measured *in vivo* compared with strain patterns used *in vitro*

The role of the left ventricular papillary muscles is to provide structural support to the mitral valve during cardiac contraction. The muscles are particularly important for valve closure during systole, ensuring that the valve does not protrude into the atrium (*e.g.* Cronin *et al.*, 1969; Marzilli *et al.*, 1980). Several studies have mapped the strain pattern of papillary muscles *in situ* (Armour and Randall, 1970; Cronin *et al.*, 1969; Gorman *et al.*, 1996; Hirakawa *et al.*, 1977; Marzilli *et al.*, 1985; Rayhill *et al.*, 1994, Semafuko and Bowie, 1975). The typical strain time-course measured in these studies can be separated into three phases: an initial isometric phase that occurs during isovolumic contraction at the start of systole, a shortening phase occurring during ejection (ventricular emptying) and a relengthening phase that coincides with the filling of the relaxed ventricle.

Studies of cardiac energetics *in vitro* have traditionally used the papillary muscle as a model of ventricular muscle. The protocols used in these types of studies have usually involved either isometric or afterloaded isotonic contractions (Gibbs and Chapman, 1979a; Gibbs *et al.*, 1967; Kiriazis and Gibbs, 1995; Kiriazis and Gibbs, 2000). Neither of these

protocols result in a net output of mechanical work and typically the contraction frequency is very low compared to physiological frequencies. These and other interpretative difficulties have been discussed extensively in Chapter 3.

Semafuko and Bowie (1975) highlighted the lack of correspondence between the strain patterns used in traditional *in vitro* studies and those measured from papillary muscles *in situ*. However, there have still been no studies of papillary muscle mechanics or energetics using realistic strain protocols and contraction frequencies. With current technology, it is possible to simulate papillary muscle strain patterns measured *in vivo* using an isolated papillary muscle preparation *in vitro*.

Chapter 3 of this thesis employed a sinusoidal length change protocol, based on that used by Baxi *et al.* (2000), as an approximation of papillary muscle contraction measured *in vivo*. This protocol did produce more realistic patterns of force and length changes, was performed at realistic contraction frequencies and resulted in net work output. However, the sinusoidal strain pattern, although more realistic than isometric or afterloaded isotonic contractions, is still a relatively poor match to strains experienced *in situ*.

4.1.2   Development of a 'realistic' strain pattern for use with isolated preparations

A comprehensive search of the literature describing papillary muscle strain dynamics *in situ* revealed that the muscles undergo cyclic length changes during contraction (Cronin *et al.*, 1969; Marzilli *et al.*, 1985; Rayhill *et al.*, 1994; Semafuko and Bowie, 1975) and shorten by approximately 10 % of their resting length at a fairly constant velocity (Gorman *et al.*, 1996; Hirakawa *et al.*, 1977; Semafuko and Bowie, 1975). Some of these reports identified a brief period of isometric contraction at the start of ventricular systole (Armour and Randall, 1970; Hirakawa *et al.*, 1977; Karas and Elkins, 1970; Rayhill *et al.*, 1994) but the duration of this phase was variable. Other studies have reported that muscle length increased a small amount at the beginning of ventricular systole rather than remaining isometric (Cronin *et al.*, 1969; Marzilli *et al.*, 1985; Semafuko and Bowie, 1975). Both these possibilities were encompassed by the protocols used in this study. Following shortening, re-extension of the muscles to the length recorded at the start of each cycle also occurred at an approximately constant velocity (Figure 4.1).
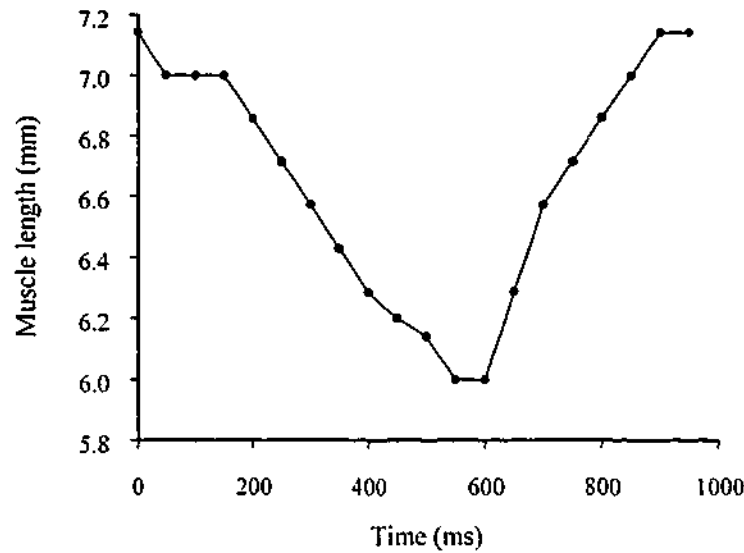
Figure 4.1 Example of papillary muscle dynamics measured *in vivo*

Example of the length changes of an anterior papillary muscle from the left ventricle of a dog. The length changes were estimated from Figure 2 in Hirakawa *et al.* (1977). Values were measured from the recording at 50 ms intervals. In this example, the muscle shortened by ~15 % which is greater than the 10 % average reported for the set of muscles.

4.1.3 Aims of this chapter

The aims of the current study were (1) to determine, from published reports, a typical strain pattern of papillary muscles *in situ*, (2) to incorporate this pattern into a contraction protocol for isolated papillary muscle preparations and (3) to characterise the energetics of rat papillary muscles performing the realistic length change protocol. Due to there being some variation in the fine details of the strain patterns measured *in situ*, the pattern of length changes used in this study was varied to encompass most likely patterns.

4.2 Materials and methods

The materials and methods used for the experiments reported in this chapter have been described in Chapter 2. Only those methods specific to these experiments will be described here.

4.2.1 Thermopile

The thermopile used in this study contained 24 antimony-bismuth thermocouples, had an active recording length of 6 mm and an output of 1.09 mV °C^{-1}.

4.2.2 Experimental protocols

Three experiments were performed. Experiment 1 investigated the effects of varying the strain dynamics, Experiment 2 investigated the effects of varying the shortening duration at constant frequency and Experiment 3 investigated the effects of varying the frequency of contraction while maintaining a constant duration of shortening.

Calculations of work and enthalpy outputs were as described for the sinusoidal contractions in Chapter 3, *i.e.* the work loop method was used to determine work output and the enthalpy output was the sum of the work and heat outputs.

4.2.2.1 Experiment 1: varying strain dynamics

In the first experiment, two aspects of the strain dynamics were investigated. First, the effects of varying the duration of the isometric phase at the start of contraction were studied. The duration was set to either 10, 15 or 20 % of the cycle duration (1 cycle = interval between successive stimuli) (Figure 4.2A). The consequences of incorporating an increase in muscle length (2 or 4 % L_{max}) before the onset of shortening (15 % cycle duration) were also studied (Figure 4.2B). Second, the amplitude of shortening was varied such that it equalled 5, 10 or 15 % L_{max} (Figure 4.2C). Each shortening amplitude was preceded by an isometric contraction accounting for 10, 15 or 20 % of the cycle duration.

4.2.2.2 Experiment 2: varying the shortening duration at constant frequency

A series of experiments was performed to determine whether altering the shortening duration at constant frequency affected the energetic characteristics of the muscle. The pattern of length changes was altered such that the shortening phase accounted for either 20, 30 or 40 % of the inter-contraction interval (Figure 4.2D). Isometric contraction duration was constant at 20 % cycle duration and the duration of the lengthening phase was altered as required to maintain the cycle duration at 500 ms.

4.2.2.3 Experiment 3: varying contraction frequency

A contraction frequency of 2 Hz was selected as the basic frequency for this study. In a recent report on the energetics of rat papillary muscle, this frequency was found to be within the range for maximum work output and maximum net mechanical efficiency at 27°C (Baxi *et al.*, 2000). In addition, a number of experiments were performed at a contraction rate of 3 Hz. This 50 % increase in heart rate is comparable to the range of heart rate increases that occurs between rest and vigorous exercise in rats (Drexler *et al.*, 1985; Mullin *et al.*, 1984). The total durations of the isometric and shortening phases were

kept constant while the duration of the lengthening phase was reduced for the contractions at 3 Hz (Miyazaki *et al.*, 1990). Thus, the *absolute* duration of the combined isometric and shortening phases was the same in the 2 and 3 Hz contraction protocols.
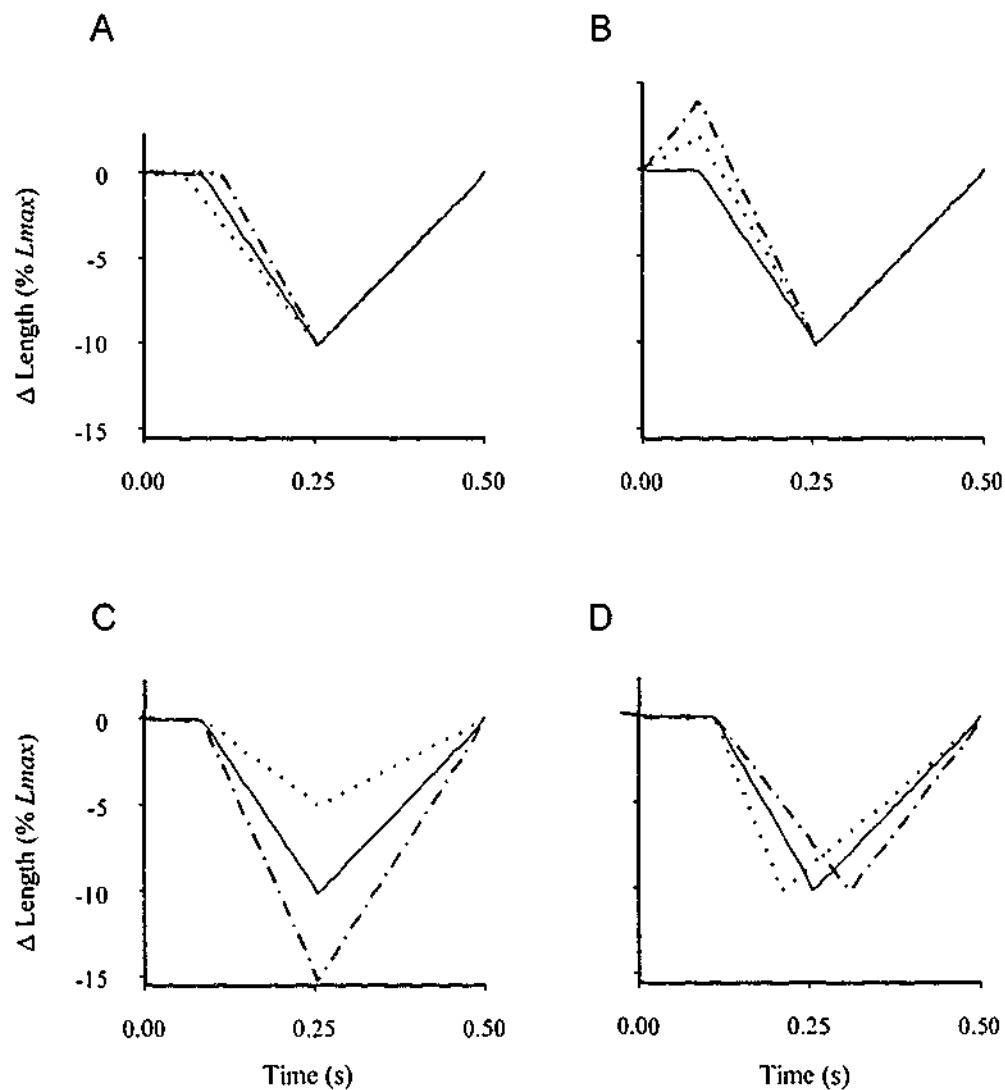
Figure 4.2 Examples of muscle length changes during realistic contraction protocols at 2 Hz

A, B and C show the length change protocols for Experiment 1, and **D** for Experiment 2. In **A**, the duration of the initial isometric contraction was 10, 15 or 20 % of the total inter-stimulus interval (0.5 s; shown for 10% L_{max} shortening only). In **B**, the isometric phase was substituted by a 2 or 4 % L_{max} length increase, accounting for 15 % of the cycle duration. At each isometric duration, the muscle was shortened by 5, 10 or 15 % L_{max} (shown for isometric duration of 15 % of cycle only) (**C**). The duration of the lengthening phase was kept at 50 % of the cycle duration in **A**, **B** and **C**. In **D**, isometric phase duration was 20 % of the cycle duration while shortening was 20, 30 or 40 % of the inter-stimulus interval. Lengthening phase duration was adjusted accordingly. Shortening amplitude was 10 % L_{max} in **B** and **D**. The stimulus pulse was applied at time 0.

4.2.3 Measurement of stiffness of the series elastic component

In Experiment 1, the velocity of shortening of the muscle was varied. To assess the probable effects of these alterations in whole muscle shortening velocity on the contractile component alone, the contractile component velocity was calculated using the following equation (Curtin and Woledge, 1993):

$$V_{CC} = V_L - \left(\frac{1}{S} \times \frac{dP}{dt} \right)$$

where V_{CC} is the shortening velocity of the contractile component (which is a function of force, P), V_L is the shortening velocity of the whole muscle, S is the stiffness of the SEC (also a function of force) and dP/dt is the rate of change in force. V_{CC} was calculated for each sampled value, using appropriate values of V_L, S and dP/dt.
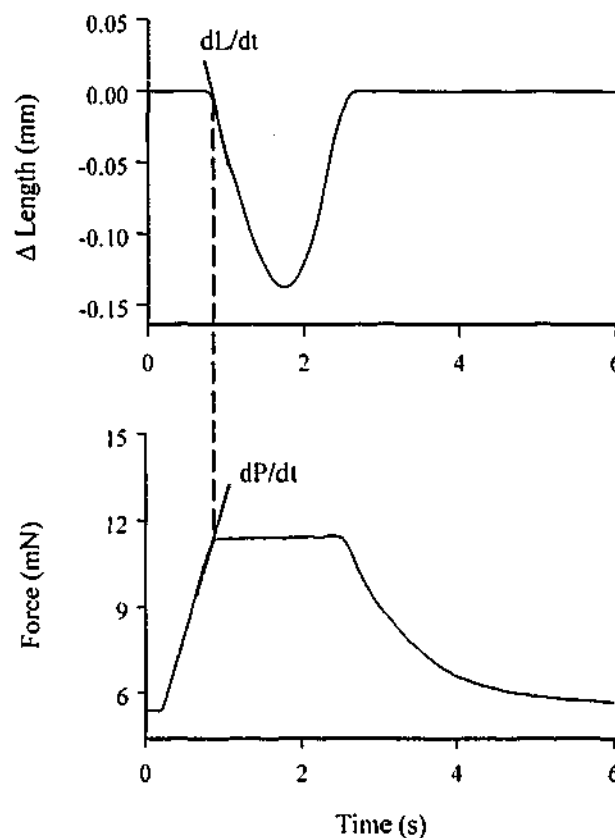
Figure 4.3 Method used to determine stiffness of the SEC

Records of force output (lower trace) and muscle length change (upper trace) during an isotonic contraction. The example shown is from a muscle shortening against a load of 0.6 P_0. The dashed vertical line indicates the time at which shortening started. The solid straight lines were fitted to the muscle length change trace (upper trace) at the start of shortening and to the force trace (lower trace) immediately before shortening started. The slopes of these lines are the initial velocity of shortening (dL/dt) and rate of force development just prior to shortening (dP/dt), respectively. The ratio of dP/dt to dL/dt is the stiffness of the elastic component in series with the contractile element at that load. Sampling rate for these experiments was 1000 Hz.

The stiffness of the series elastic component (SEC) of papillary muscle preparations was measured using the method described by Sonnenblick (1964). Each muscle performed isotonic twitches (10 twitches at 0.2 Hz) against a series of afterloads between 0.2 P_0 and 0.8 P_0. Two runs were performed on each muscle with loads presented alternately in ascending and descending order. The required afterload was achieved using the adaptive force control algorithm described in Chapter 3. For each muscle at each load, stiffness of the SEC (S) was calculated using the following formula (Sonnenblick, 1964):

$$S = dP/dL = \frac{dP/dt}{dL/dt}$$

where dP/dt is the rate of force development immediately prior to the start of shortening and dL/dt the initial velocity of shortening (Figure 4.3).

4.3   Results

The aims of this study were to develop a contraction protocol for use with isolated papillary muscles that mimicked papillary muscle length changes measured *in situ* and to characterise the energetics of rat papillary muscles using this protocol. General characteristics of the papillary muscle preparations are presented in Table 4.1.

Table 4.1 Characteristics of papillary muscle preparations

Wet mass (mg)	2.87 ± 0.27
L_{max} (mm)	4.96 ± 0.19
Cross-sectional area at L_{max} (mm^2)	0.54 ± 0.04
Passive force at L_{max} (mN)	4.6 ± 0.5
Isometric active force at L_{max} (mN)	14.0 ± 1.2
Active stress at L_{max} (mN mm^{-2})	26.9 ± 1.7
Passive force/active force at L_{max}	0.35 ± 0.04
Isometric enthalpy output at L_{max} (mJ g^{-1})	7.5 ± 1.7

All values are mean $\pm$ 1 s.e.m. (n=12, except for isometric enthalpy output where n=4).

Typical records from a realistic contraction protocol are illustrated in Figure 4.4. It can be seen that peak force output varied during the 40 twitches, with the first twitch exhibiting a high peak force output as typically observed in rat cardiac muscle following a period of

quiescence (Ravens, 1992). As described in Chapter 3, the muscle temperature progressively increased throughout the contraction protocol and, once stimulation ceased, decreased back to its initial value in approximately 1 min. The lower panel shows the calculated cumulative work, heat and enthalpy outputs.
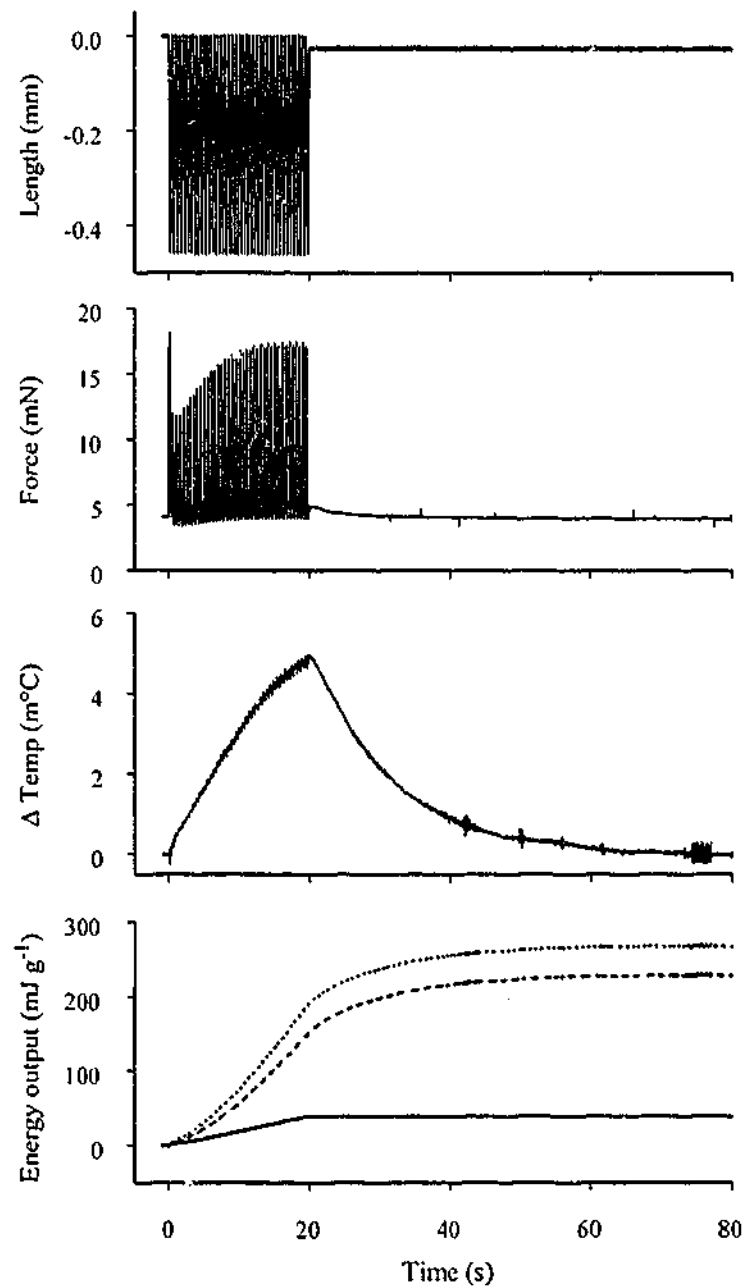
Figure 4.4 Examples of recordings made during a realistic contraction protocol

The records shown are (from top to bottom) change in muscle length, force output, change in muscle temperature and cumulative work (solid line), heat (dashed line) and enthalpy (dotted line) outputs. The enthalpy output is the sum of the work and heat outputs. The muscle returned to its pre-stimulation temperature within 1 min of completion of the contractions, indicating that all recovery metabolism was complete. (Muscle mass, 3.58 mg; length, 4.5 mm, cross-sectional area, 0.75 mm^2).

4.3.1   Experiment 1 - varying strain dynamics

In Experiment 1, the effects of varying the amplitude of muscle shortening and the duration of the initial isometric phase were determined. Examples of work loops for these protocols are shown in Figure 4.5.
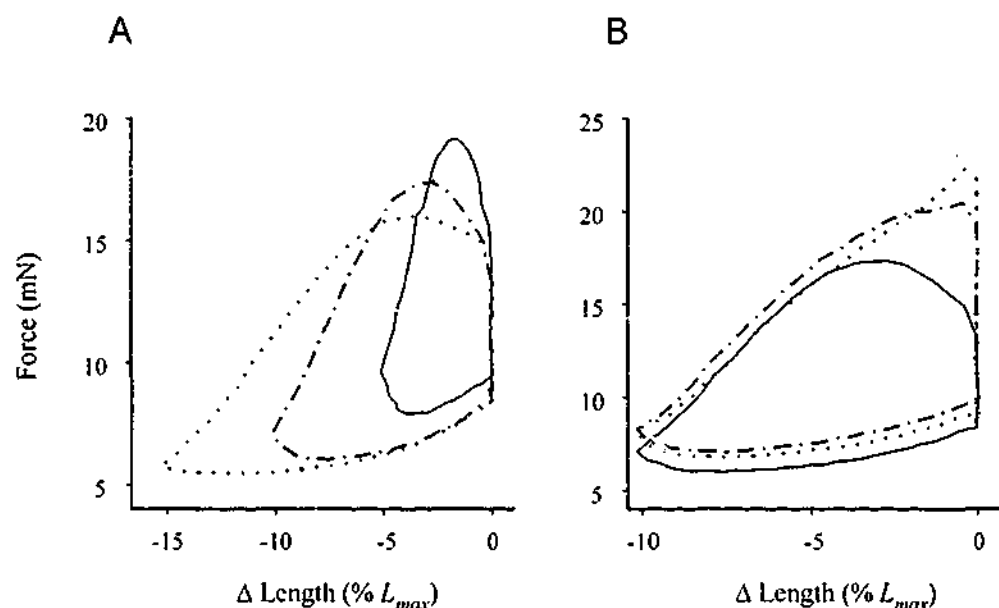
Figure 4.5 Examples of work loops

A. The duration of the initial isometric contraction was 10 % of the cycle duration and the amplitude of shortening was 5 (solid line), 10 (dashed line) or 15 % (dotted line) L_{max}. The duration of the lengthening phase was constant. Therefore, the velocity of shortening increased as amplitude of shortening increased. **B.** Amplitude of shortening was 10 % L_{max} and the duration of the lengthening phase was 50 % of the cycle duration. The duration of the initial isometric phase was 10 (solid line), 15 (dashed line) or 20 % (dotted line) of the cycle duration. Time progressed around the loops in an anti-clockwise direction, indicating that net work was performed.

Increasing the amplitude of shortening increased the work output per twitch as evidenced by the increase in size of the work loops in Figure 4.5A. The enthalpy output per twitch, however, remained constant (Figure 4.6). The consequence of an increase in work output accompanied by little change in enthalpy output was that net mechanical efficiency increased significantly with increased shortening amplitude.

The only energetic consequence of increasing the duration of the isometric phase was that an increase in duration from 10 to 15 % increased work output and enthalpy output when the shortening amplitude was 10 or 15 % L_{max} (Figure 4.6). Extending the isometric phase to 20 % of the cycle duration had no further effect and when shortening was 5 % L_{max}, neither work output nor enthalpy production were affected by the duration of the initial

isometric contraction. There were no significant effects of isometric duration on ε_{Net}. Note that the mean enthalpy output per twitch in Figure 4.6B was similar to the mean enthalpy output measured in an isometric twitch (Table 4.1).
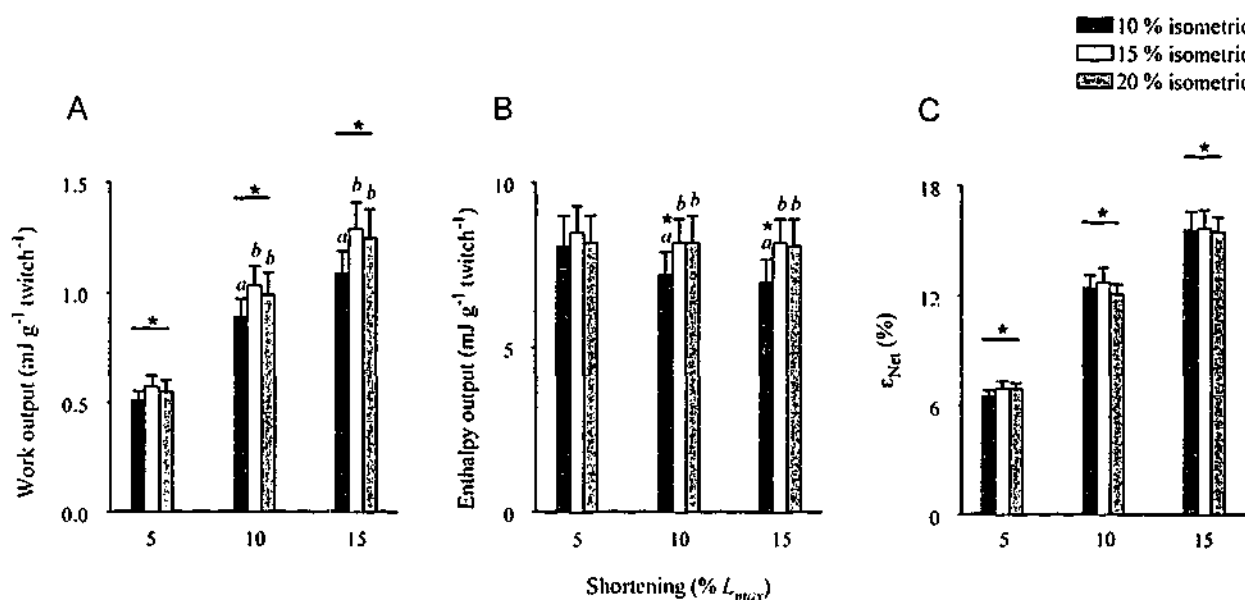
Figure 4.6 Effects of isometric duration and shortening amplitude on energetic variables

Effects of varying shortening amplitude (% L_{max}) and duration of isometric contraction (% cycle duration) on mean work output per cycle (A), enthalpy output per cycle (B) and net mechanical efficiency (C) (n=7). Duration of isometric contraction was 10 % (black columns), 15 % (white columns) or 20 % (grey columns) of the cycle duration. Letters indicate statistically significant differences between variables attributable to the duration of isometric contraction. Asterisks indicate statistical significance, at a particular isometric duration, due to shortening amplitude.

Applying an initial stretch instead of holding the muscle isometric at the beginning of the contraction did not affect enthalpy output (Figure 4.7). The work output per twitch, however, did increase with a greater magnitude of length increase (isometric, 1.04 ± 0.12 mJ g^{-1}; 2 % L_{max} increase, 1.15 ± 0.12 mJ g^{-1}; 4 % L_{max} increase, 1.29 ± 0.14 mJ g^{-1}). There was no significant difference in ε_{Net} between the contractions with an initial isometric phase (12.5 ± 0.6 %) and those with a 2 % L_{max} increase in length (13.0 ± 1.1 %). However, ε_{Net} was significantly greater (14.6 ± 1.2 %) when a 4 % L_{max} increase in length was incorporated into the protocol in place of either 0 or 2 % L_{max} length increases.
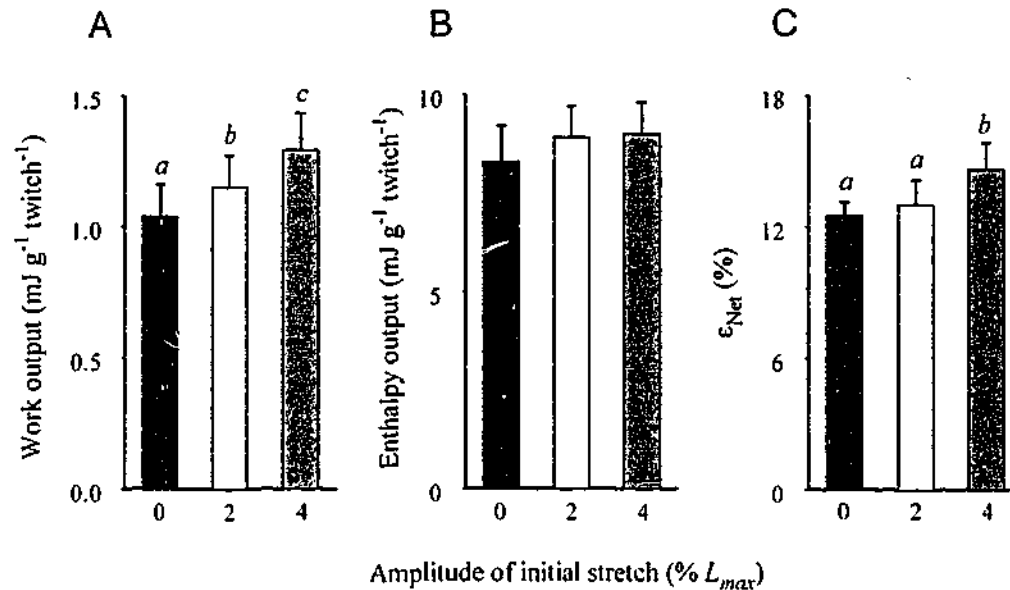
Figure 4.7 Effects of applying an initial stretch on energetic variables

Effects of incorporating an initial stretch in place of the initial isometric period on mean work output per cycle (**A**), enthalpy output per cycle (**B**) and net mechanical efficiency (**C**) (n=6). Duration of the initial stretch or isometric period was 75 ms or 15 % of the cycle duration and shortening was 10 % L_{max}.

4.3.2   Experiment 2 - varying shortening duration at constant frequency

In this experiment, the cycle duration was constant (500 ms = 2 Hz) as was the initial isometric phase (100 ms, 20 % cycle duration). The duration of the shortening phase was either 100, 150 or 200 ms (20, 30 or 40 % cycle duration, respectively) and the duration of the lengthening phase was adjusted accordingly. Thus, the velocity of shortening varied between 0.5 L_{max} s^{-1} and 1.0 L_{max} s^{-1}. The maximum shortening velocity of rat papillary muscle is 6.5 L_{max} s^{-1} at 37°C (Henderson *et al.*, 1970) which would correspond to ~3.25 L_{max} s^{-1} at 27°C, assuming a halving of rate for a 10°C decrease in temperature. Despite this variation in shortening velocity, the enthalpy output, or energetic cost of contraction, was independent of the shortening duration (Figure 4.8). However, less work was performed per twitch when the lowest shortening velocity was used than at either of the other velocities. This was due to the force relaxing to resting levels before shortening was complete, reducing the net work performed. Consequently, ε_{Net} was significantly lower when shortening lasted for 200 ms (11.0 ± 0.7 %) than for 100 ms (13.5 ± 0.7 %) or 150 ms (12.1 ± 0.5 %) shortening.
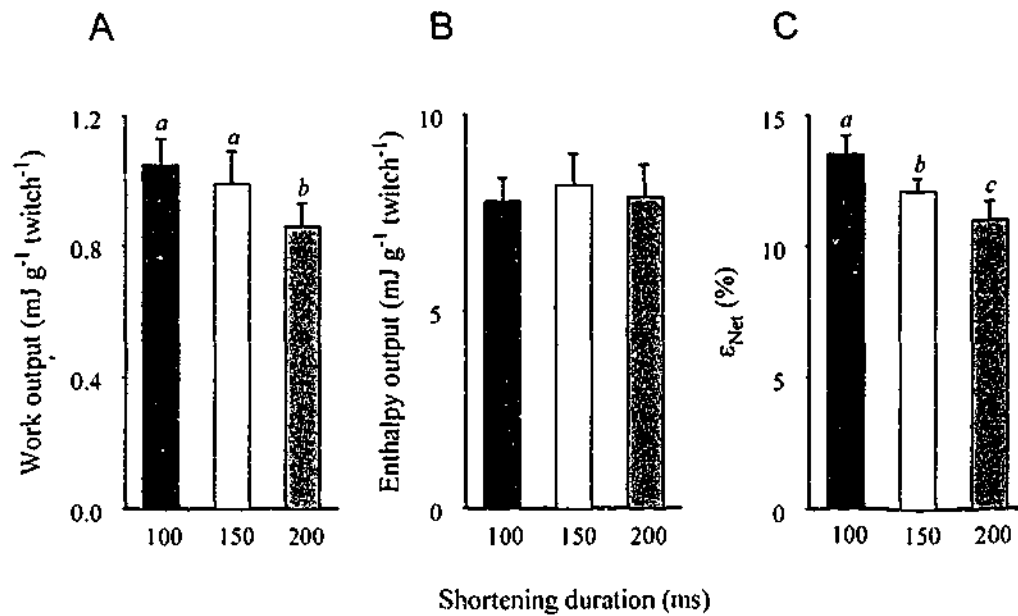
Figure 4.8 Effects of varying the shortening duration on energetic variables

Effects of varying the shortening duration of contractions on mean work output per cycle (A), enthalpy output per cycle (B) and net mechanical efficiency (C) (n=7). Isometric phase duration was 100 ms. Letters indicate statistical significance.

4.3.3 Experiment 3 - varying contraction frequency

Work output per twitch was significantly lower when the contraction frequency was increased from 2 Hz (1.09 ± 0.12 mJ g^{-1}) to 3 Hz (0.89 ± 0.08 mJ g^{-1}) (Figure 4.9).
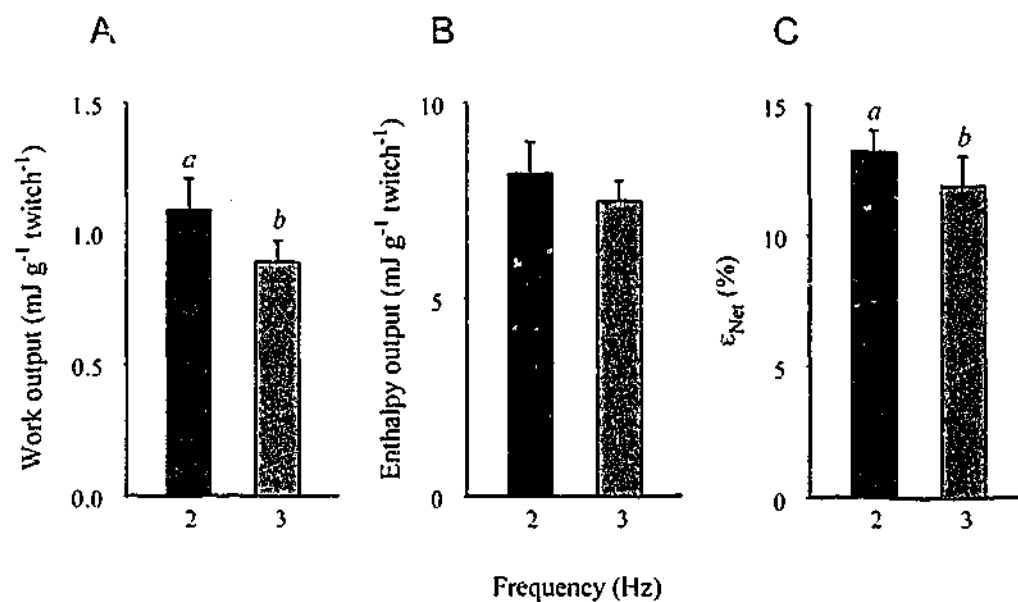
Figure 4.9 Effects of varying contraction frequency on energetic variables

Effects of varying contraction frequency on mean work output per cycle (A), enthalpy output per cycle (B) and net mechanical efficiency (C) (n=6). Duration of the initial stretch or isometric period was 75 ms or 15 % of the cycle duration and shortening was 10 % L_{max}.

Enthalpy output per twitch was also reduced from 8.3 ± 0.8 mJ g^{-1} at 2 Hz to 7.5 ± 0.5 mJ g^{-1} at 3 Hz, however this change was not statistically significant. The overall result was that ε_{Net} was slightly, but significantly, lower at 3 Hz (11.9 ± 1.1 %) compared with 2 Hz (13.2 ± 0.8 %).

4.3.4 Are steady-state and non steady-state energetics comparable?

In vivo, the heart works in an energetic steady-state; that is, ATP is synthesised at a rate sufficient to match ATP use. In the 40 twitch protocol used in the current study, the muscle progressed from rest to steady activity but only reached an energetic steady-state near the end of the protocol. An energetic steady-state can be implied when the pattern of temperature changes repeats in successive cycles (Paul, 1983). To ensure that steady-state energetics were similar to those during the rest to work transition, recordings were made during a protocol consisting of 60 twitches at 2 Hz (Figure 4.10).
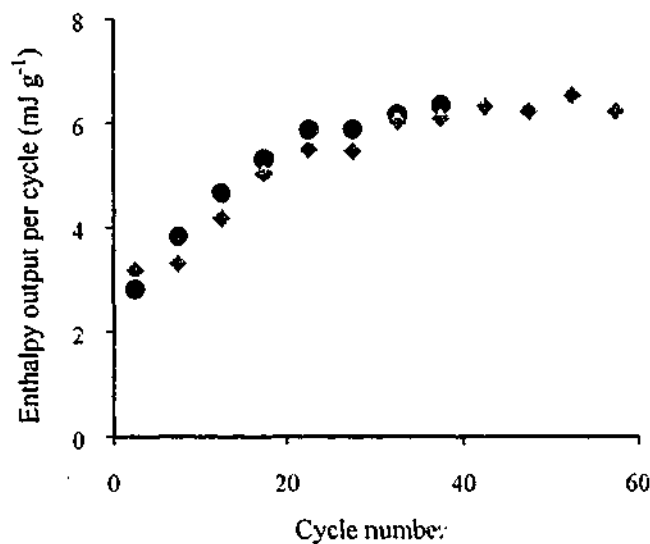
Figure 4.10 Time-course of enthalpy output

Example of the time-course of enthalpy output from a muscle performing 40 (●) and 60 (◆) realistic contractions at 2 Hz. Isometric contraction was 15 % of the cycle duration, while shortening and lengthening phases accounted for 35 % and 50 % of the cycle duration respectively. The shortening amplitude was 10 % L_{max}. Data points represent the average enthalpy output per cycle averaged over 5 successive cycles. The horizontal position of each data point corresponds to the middle of the cycles over which the average values were calculated.

The average work performed per twitch and enthalpy output per twitch were slightly, but significantly, lower in the 60 twitch protocol than in the 40 twitch protocol. There was, however, no effect on ε_{Net} (12.5 ± 0.8 % (60 twitches) compared to 12.7 ± 0.8 % (40 twitches); n=7). Note that in order to compare the steady-state and non steady-state

energetics, it was necessary to record the total enthalpy output (*i.e.* including recovery metabolism) from both 40 and 60 twitch protocols. Consequently, it is inappropriate to just compare the energetics of the first 40 twitches with those of all 60 twitches from a single contraction run.

4.3.5   Using the protocol as a model of ventricular muscle

The shapes of the force-length loops in Figure 4.5 differ from ventricular pressure-volume loops in that the latter generally exhibit a clear isovolumic relaxation phase (for a comprehensive review, see Sagawa *et al.*, 1988). It is unclear, from strain and length change records measured *in situ*, whether papillary muscles remain isometric during the isovolumic relaxation phase with reports indicating varying degrees of shortening (Hirakawa *et al.*, 1977; Marzilli *et al.*, 1985; Semafuko and Bowie, 1975), lengthening (Rayhill *et al.*, 1994) or no significant length change (Hirakawa *et al.*, 1977; Rayhill *et al.*, 1994). Regardless of the disagreement in the literature, if papillary muscles are to be used as a two-dimensional model of ventricular muscle, the addition of an isometric relaxation phase would enhance the realism of the model. To see whether this feature could be incorporated easily into the protocols used in this study, an experiment was carried out in which the muscle length was held constant during part of the relaxation phase. The isometric relaxation phase was incorporated into the length change pattern by selecting a time for shortening to end and holding the length constant until relaxation was complete (Figure 4.11).

The results from these experiments are shown in Table 4.2. As the absolute shortening amplitude was increased, work output per twitch also increased. This result is in agreement with the findings of Experiment 1. Once again, the enthalpy output per twitch varied over only a small range and ε_{Net} thus reflected the variation in work output.
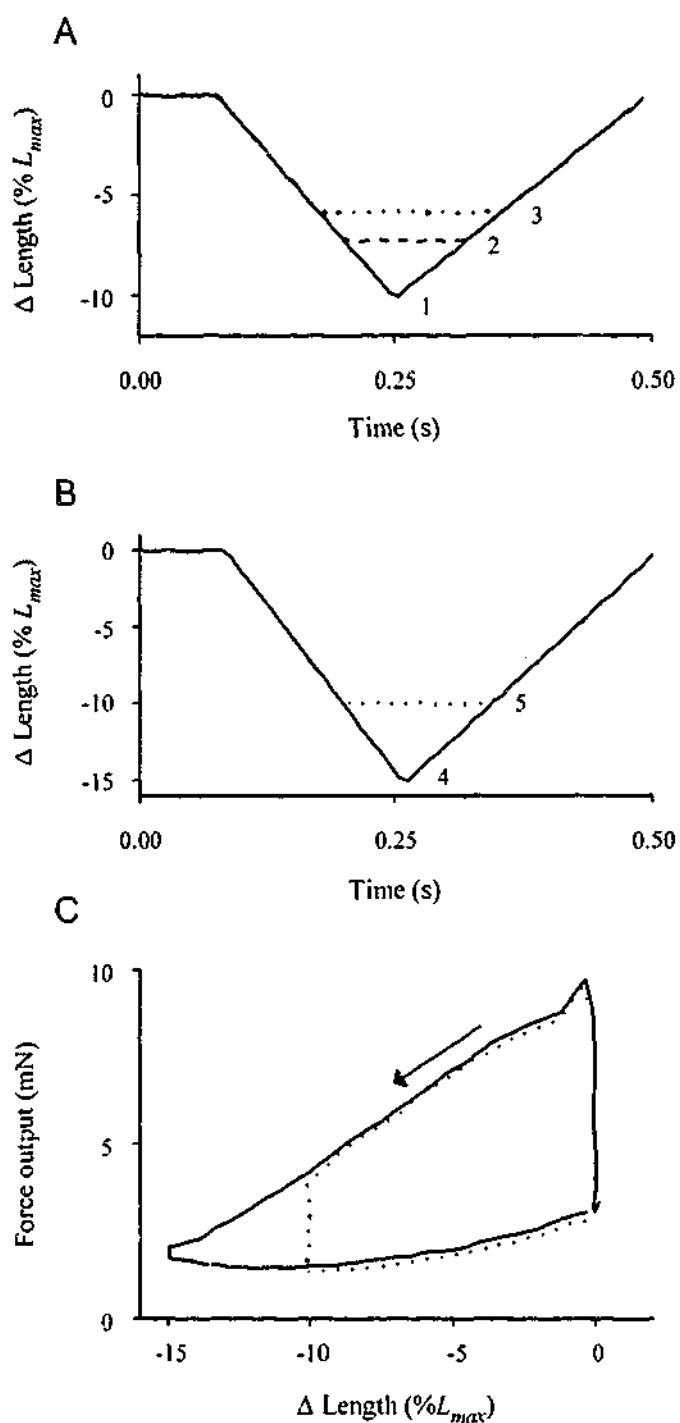
Figure 4.11 Incorporation of isometric relaxation into the realistic contraction protocol

Examples of muscle length changes (**A** and **B**) and work loops (**C**) during realistic contractions with (dotted lines) or without (solid lines) an isometric relaxation period. The length changes shown in **A** are from a muscle shortening by 10 % L_{max} or incorporating an isometric relaxation period such that the absolute amplitude of shortening was less than 10 % L_{max}. The length changes pictured in **B** are similar to those in **A**, except that the maximum amplitude of shortening was 15 % L_{max}. The work loops in **C** correspond to the length changes in **B**. The numbers alongside the traces correspond to the contraction types listed in Table 4.2.

Table 4.2 Effects of incorporating an isometric relaxation period on energetic variables

Contraction type	1	2	3	4	5
Work (mJ g^{-1} twitch^{-1})	1.14 ± 0.11 [a]	1.08 ± 0.13 [a]	0.92 ± 0.09 [b]	1.34 ± 0.14	1.24 ± 0.10
Enthalpy (mJ g^{-1} twitch^{-1})	7.6 ± 1.2	8.0 ± 1.6	8.4 ± 1.9	7.4 ± 1.2	7.9 ± 1.9
ε_{Net} (%)	15.4 ± 1.3 [a]	14.1 ± 1.4 [a]	11.9 ± 1.2 [b]	18.8 ± 1.3 [c]	17.0 ± 2.0 [d]

All values are presented as mean $\pm$ 1 s.e.m. (n=4). Contraction type corresponds to length change patterns illustrated in Figure 4.11. Contraction types: 1. 10 % L_{max} shortening, no isometric relaxation; 2. Isometric relaxation after 7.3 % L_{max} shortening; 3. Isometric relaxation after 5.8 % L_{max} shortening; 4. 15 % L_{max} shortening, no isometric relaxation; 5. Isometric relaxation after 10 % L_{max} shortening. Letters indicate statistical significance (p<0.05) where a is different to b and c is different to d. Note that comparisons were made between groups 1-3 and between 4 and 5.

4.3.6 Stiffness of the series elastic component

Five papillary muscle preparations were used to measure the stiffness of the SEC. SEC stiffness increased linearly with load (Figure 4.12). The slope of the stiffness-load relation was determined for each preparation and the mean value was 3.42 ± 0.17 mm^{-1} (mean muscle length was 6.1 ± 0.3 mm). The linear dependence of stiffness on load implies an exponential dependence of extension of the series elastic component on load, as described previously for papillary muscles by Sonnenblick (1964). The purpose of making these measurements was to enable the velocity of the contractile component during shortening to be calculated and to be compared to the overall velocity of shortening (see Section 4.2.3).

A quantitative assessment was made of the time-course of shortening of the contractile component in realistic contractions. This analysis was performed for applied shortenings of 5, 10 and 15 % L_{max} and tested whether the effect of the series elastic component caused the velocity profiles of the contractile component to be similar for all three shortening magnitudes despite the differences in the velocity profile of the length changes applied to the ends of the muscle. If this was so, then the constancy of the enthalpy output per twitch (*e.g.* Figure 4.6B) might simply reflect the similar pattern of contractile component length changes.
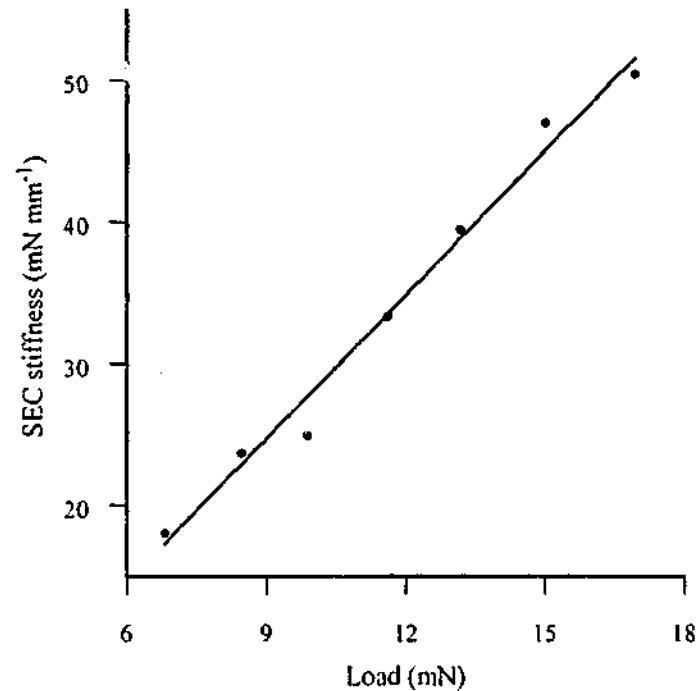
Figure 4.12 Example of relationship between afterload and stiffness of the series elastic component

The range of loads for this preparation (length 6.1 mm) corresponded to 0.2 to 0.8 P_0. The line was fitted through the data using the method of least squares. The method used to calculate stiffness is described in Section 4.2.3 and illustrated in Figure 4.3.

An example of the results of this analysis is shown in Figure 4.13A. The time-course of changes in length of the whole muscle (controlled by the experimenter) is compared to the time-courses of length changes in the contractile component and the series elastic component. The first notable feature is that the contractile component began to shorten and stretch the series elastic component as soon as the contraction started, as reported previously (Brady, 1971; Donald et al., 1980; Wong, 1973). In fact, in this example, in which the initial "isometric" phase lasted 100 ms, the contractile component had shortened by ~5 % L_{max} before the applied shortening even started. During the applied, constant velocity shortening, the velocity of the contractile component was not constant but decreased steadily and reached almost zero by the time the applied shortening ended. During the subsequent relengthening, changes in the length of the contractile component and the whole preparation were quite similar because the rate of change in force was very low during this phase (see Section 4.2.3).

A - Calculated SEC and CC length changes

B - Changes in whole muscle length

C - Calculated CC length changes
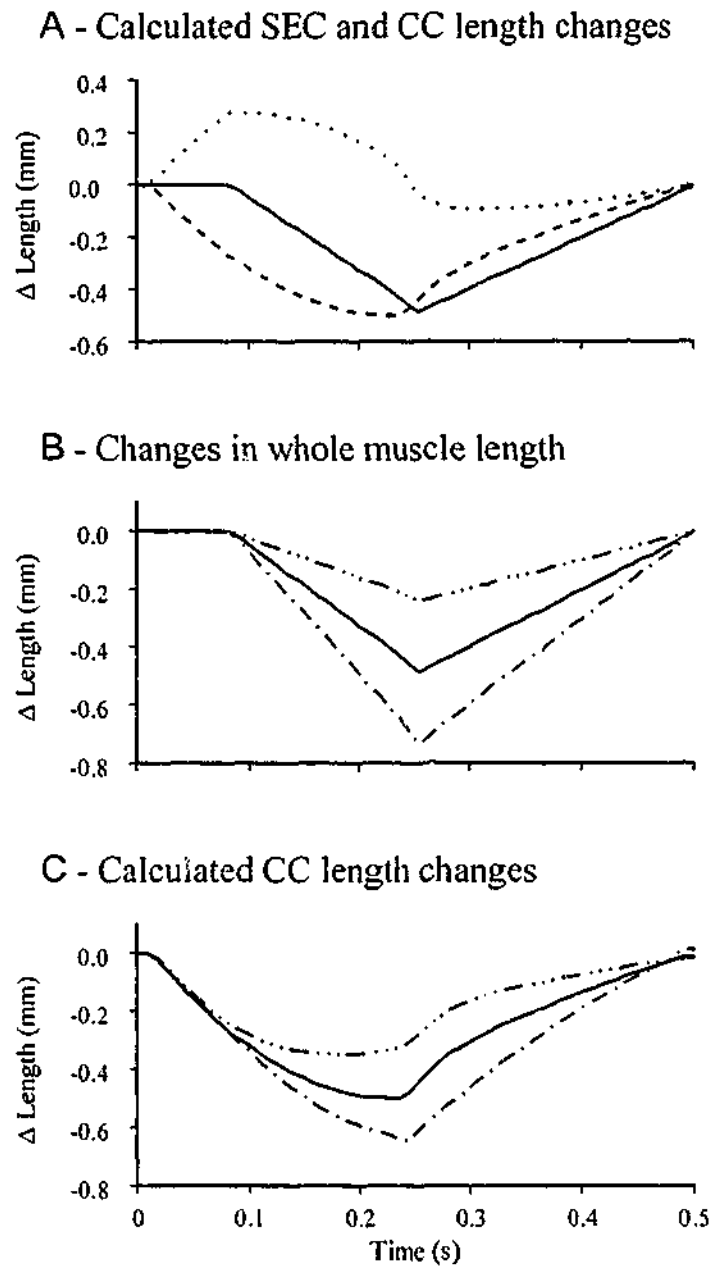
Figure 4.13 Examples of analysis of the time-course of contractile component length changes

Length changes of the whole muscle (solid line) and the calculated changes in length of the contractile component (dashed line) and the series elastic component (dotted line) are shown in **A**. The length changes applied to the whole muscle at shortening amplitudes of 5, 10 and 15 % L_{max} are shown in **B**, while **C** shows the calculated length changes of the contractile component only, at the same shortening amplitudes as in **B**. All recordings were made on the same muscle (L_{max}, 4.8 mm).

In Figure 4.13 (B and C), the time-courses of the applied length changes for the three amplitudes of shortening are compared to the calculated contractile component length changes. Irrespective of the strain pattern, the first 5 % L_{max} shortening of the contractile component had occurred before any change in preparation length. Thus, during this initial

phase, the contractile component shortened at the same velocity and through the same amplitude in all three examples. During the time that muscle length was being decreased, contractile component length continued to decrease at progressively lower velocities. The total amplitude of contractile component shortening was affected by the amplitude of the applied length change but not in a simple way. For instance, when the whole muscle was shortened by 5 % L_{max}, the calculated amplitude of contractile shortening was actually ~7 % L_{max}. When the applied length change had an amplitude of 15 % L_{max}, the calculated contractile component shortening amounted to ~13 % L_{max}. The difference in these length changes is accounted for by changes in the length of the SEC.

It should be noted that the SEC is an integral component of papillary muscles (and all other muscles) and that the purpose of calculating contractile component length change was simply to try to understand the mechanisms underlying the constancy of energy cost.

4.4 Discussion

Isolated papillary muscles have been used extensively as a model of cardiac muscle but in few studies has any attempt been made to use a contraction protocol that matches the strain pattern occurring in either the muscle of the ventricular wall or the papillary muscles themselves. Thus, the purpose of this study was to develop a strain protocol that more closely mimicked the actual strain patterns encountered by papillary muscles *in vivo* and to characterise the energetics of rat papillary muscles using this protocol.

The strain protocol developed was based on published reports of measurements of the actual changes in length of papillary muscles during the cardiac cycle (Armour and Randall, 1970; Cronin *et al.*, 1969; Gorman *et al.*, 1996; Hirakawa *et al.*, 1977; Marzilli *et al.*, 1985; Rayhill *et al.*, 1994; Semafuko and Bowie, 1975). Some aspects of these data varied considerably among studies and so the influence of these variations on the mechanics and energetics of rat papillary muscle were assessed in the present study. The features of the strain patterns that were the least well defined from previous studies were the duration of the isometric phase at the start of systole or whether the length actually increased during this phase and the fraction of the contraction-relaxation cycle that was occupied by shortening. Interestingly, none of these variables had great effects on either the work output or the energy cost per twitch.

Using the current protocol, it was possible to alter the amplitude of shortening (which would occur with stroke volume changes), the duration of the isometric phase at the start

of systole (simulating changes in peak systolic pressure) and the fraction of the cycle occupied by shortening. The latter characteristic enabled contraction frequency to be increased without diminishing power output. The results of the present study clearly indicate that the variable that influenced work output per twitch the most was the amplitude of shortening (Figure 4.6). This variable can be controlled using the realistic protocol whereas in the afterloaded isotonic protocols, the amount of shortening varies inversely with the afterload. No other published contraction protocol allows all the above-mentioned variables to be controlled. Furthermore, incorporating an isometric relaxation phase into the protocol produced force-length loops (Figure 4.5) that closely resemble the pressure-volume loops recorded from intact, beating hearts (Sagawa *et al.*, 1988; Taylor *et al.*, 1993). Therefore, the strain protocol demonstrated in this study has the potential to allow more sophisticated analyses of cardiac muscle function *in vitro* than has been possible with more conventional protocols.

4.4.1   Effects of varying contraction frequency in realistic and sinusoidal protocols

The present study tested the effects of increasing the contraction frequency from 2 Hz to 3 Hz (Experiment 3). In this experiment, the power output (work output × cycle frequency) of the muscle increased by ~20 % and was accompanied by only a small decline in ε_{Net}. This was due to the ability to manipulate the length change protocol so that the durations of the shortening and lengthening periods could be set to allow adequate time for the muscle to complete contracting before being stretched back to its resting length. In sinusoidal protocols, both power output (Baxi *et al.*, 2000; Layland *et al.*, 1995) and ε_{Net} (Baxi *et al.*, 2000) decreased when contraction rate was increased due to the symmetrical s ain pattern of that protocol. As contraction frequency was increased, the time for both shortening and lengthening was reduced (Baxi *et al.*, 2000; Layland *et al.*, 1995) and relaxation was not complete prior to the muscle being stretched back to its resting length (Baxi *et al.*, 2000). Thus, more work was required to stretch the muscle, reducing the net work performed (Baxi *et al.*, 2000; Josephson, 1993).

In the current study, work output per twitch did decrease when contraction frequency was increased but only slightly. The reduction in work output occurred despite there being adequate time for force output to decline to resting levels before the lengthening phase began. How can the decrease in work output and maintenance of enthalpy output per twitch, observed to accompany an increase in contraction frequency, be explained? The

constancy of enthalpy output implies that the total amount of ATP used in each twitch, by both ion pumps and cross-bridges, remained constant. Although the metabolic changes that might be expected with increased contraction frequency (*e.g.* increased intracellular concentrations of inorganic phosphate and hydrogen ions) could have slightly reduced the molar enthalpy output of PCr hydrolysis (Woledge and Reilly, 1988), any such effect would strengthen the argument that the total amount of ATP used did not decrease significantly with the increase in contraction frequency.

In rat cardiac muscle, increasing contraction frequency is sometimes associated with a decrease in the amount of Ca^{2+} released in each twitch (*e.g.* Frampton *et al.*, 1991). This could account for a lower force, and hence work, output but would also be expected to result in a proportional reduction in total energy output. The expected changes in the concentrations of metabolites do have the potential to alter force output without necessarily reducing the total number of ATP-splitting cross-bridge cycles. An increased contraction rate is associated with an increase in inorganic phosphate concentration and acidosis (Elliott *et al.*, 1994), both of which cause a decrease in force output in cardiac muscle (Palmer and Kentish, 1996). It has been suggested that increased concentrations of inorganic phosphate and hydrogen ions alter the equilibrium between the populations of attached but non-force-generating and force-generating cross-bridges, favouring the low force state (Hibberd *et al.*, 1985; Kentish, 1991; Palmer and Kentish, 1996). To be consistent with the current observations, the total number of cross-bridges completing ATP splitting cycles would have had to have remained unaltered, despite any differences in the equilibrium between the attached states.

4.4.2   Efficiency of rat papillary muscle

The maximum net mechanical efficiency of rat papillary muscle using this protocol was ~12 % when the muscle shortened by 10 % L_{max} and ~16 % when shortening was 15 % L_{max}. These values are comparable to those reported for cardiac muscle of frog and rat performing sinusoidal length change protocols (Baxi *et al.*, 2000; Syme, 1994; Chapter 3, this thesis). The values are lower than those reported for rat papillary muscles during isotonic contractions where efficiency was reported to be 20-25 %, (*e.g.* Gibbs and Chapman, 1979; Kiriazis and Gibbs, 1995). However, it was demonstrated in Chapter 3 that the apparently high values can be reconciled with the lower values by correctly taking account of the preload when calculating work output. When this is done, the values of all the studies are consistent, with a maximum efficiency of approximately 15 %.

It was suggested in Chapter 3 that the difference between reported values for the maximum net mechanical efficiency of intact hearts (~20-25 %, *e.g.* Elzinga and Westerhof, 1980; Gibbs *et al.*, 1980) and isolated papillary muscles (~15 %, Baxi *et al.*, 2000; Chapter 3, this thesis) might be reconciled if measurements with isolated muscles were made using a more realistic strain protocol. However, the results of the current study are consistent with the notion that the maximum efficiency of papillary muscles under the conditions used in isolated muscle experiments is indeed ~15 %, regardless of protocol used. The reasons for the difference between the efficiencies of intact hearts and isolated muscles remain unclear.

4.4.3 Why was the energy cost per twitch unaffected by changes in strain pattern?

A striking observation from these experiments was that, at a given frequency, the enthalpy output per twitch varied little, despite the various alterations made to the protocol. As a result, changes in ε_{Net} primarily reflected changes in work output.

In Experiment 1, the applied shortening velocities ranged between 0.25 and 1.0 L_{max} s^{-1}. This is a small range of shortening velocities compared to the complete range of velocities that can be attained *in vitro* using isotonic contractions. However, since the amplitude of shortening and the proportion of the cycle duration occupied by shortening were obtained from measurements made *in situ*, the range of velocities used in this study corresponds to those experienced *in vivo*. As mentioned previously, the maximum shortening velocity (V_{max}) of rat papillary muscle is ~3.25 L_{max} s^{-1} at 27°C. Velocities of 0.25 and 1.0 L_{max} s^{-1} thus correspond to ~0.08 V_{max} and 0.3 V_{max} respectively. It appears likely, therefore, that papillary muscles operate over only a small fraction of the complete range of shortening velocities and any inherent velocity-dependence of enthalpy output would be unlikely to be apparent using this protocol. The calculated time-courses of change in contractile component length indicated that the insensitivity of the enthalpy output per twitch to the pattern of applied length changes was not due to the contractile component undergoing the same pattern of length changes in all cases.

It has been proposed that the energy cost of a cardiac twitch is relatively insensitive to the pattern of mechanical activity during the twitch because cross-bridge kinetics are sufficiently slow that there is only enough time for each cross-bridge to perform a single cycle (Gibbs and Barclay, 1998; Rossmanith *et al.*, 1986). Countering this idea is the observation that energy cost per twitch varies considerably with afterload in isotonic

contractions (Kiriazis and Gibbs, 2000). Furthermore, the energetics of isotonic contractions are difficult to interpret due to the variable time spent in an isometric state at the beginning of the contraction and the variation of shortening amplitude with afterload (see Section 4.4.4).

When contractile filaments slide past one another during shortening, cross-bridges would be expected to detach when they are drawn sufficiently past the position at which their free energy is minimal. If they were then to reattach to another binding site further along the actin filament and split ATP in each cycle, then more ATP would be hydrolysed in each twitch and the enthalpy output would be greater. The current results, and those of earlier investigations (Gibbs and Gibson, 1970; Holroyd and Gibbs, 1992), show that this is not the case; at best, there is only a very modest increase in enthalpy output per twitch between isometric and shortening contractions (compare values in Table 4.1 with Figure 4.6). Thus, if cross-bridges do perform more cycles when a papillary muscle shortens than when it contracts isometrically, the cycles must not be accompanied by ATP splitting. Ideas of this kind have been proposed to account for the decline in rate of enthalpy output with increasing velocity often observed at high shortening velocities in skeletal muscle (Barclay, 1999; Huxley, 1973). An alternative explanation is that cross-bridges in cardiac muscle are unlikely to reattach to another binding site once they have detached. This idea is the basis of most models devised to account for the cardiac muscle phenomenon of shortening deactivation. Briefly, it is envisaged that when a cross-bridge detaches at any time in a twitch other than the first 20 % of twitch duration, the probability of reattachment is low. This is likely to be a consequence of the combination of low intracellular Ca^{2+} levels at these times and the tension-dependence of Ca^{2+}-troponin binding (for a review, see Hunter et al., 1998).

4.4.4 Enthalpy-load relation of muscles performing afterloaded isotonic contractions

The insensitivity of the enthalpy output per twitch to variations in shortening in the current study appears to be inconsistent with the enthalpy-load relation of rat papillary muscles performing afterloaded isotonic contractions (Kiriazis and Gibbs, 2000). To make a direct comparison between values from the current study and isotonic enthalpy-load data, the latter were estimated from Figure 4 in Kiriazis and Gibbs (2000) for loads ranging from 0.1 to 1 P_0. The relative velocity (V/V_{max}) at each load was calculated using the following equation (Woledge et al., 1985):

$$\text{Relative velocity} = \frac{1 - \text{Load}}{(\text{Load} \times G) + 1}$$

where $G = P_0/a$. The value of G at 27°C was 1.96, calculated from equations relating a and P_0 for rat cardiac trabeculae to temperature (Ullrick, 1964). P_0 is simply the active isometric force output and a quantifies the curvature of the force-velocity relation. The calculated relationships between relative velocity and enthalpy output per twitch for the data from Kiriazis and Gibbs (2000) and for the current study are shown in Figure 4.14A.
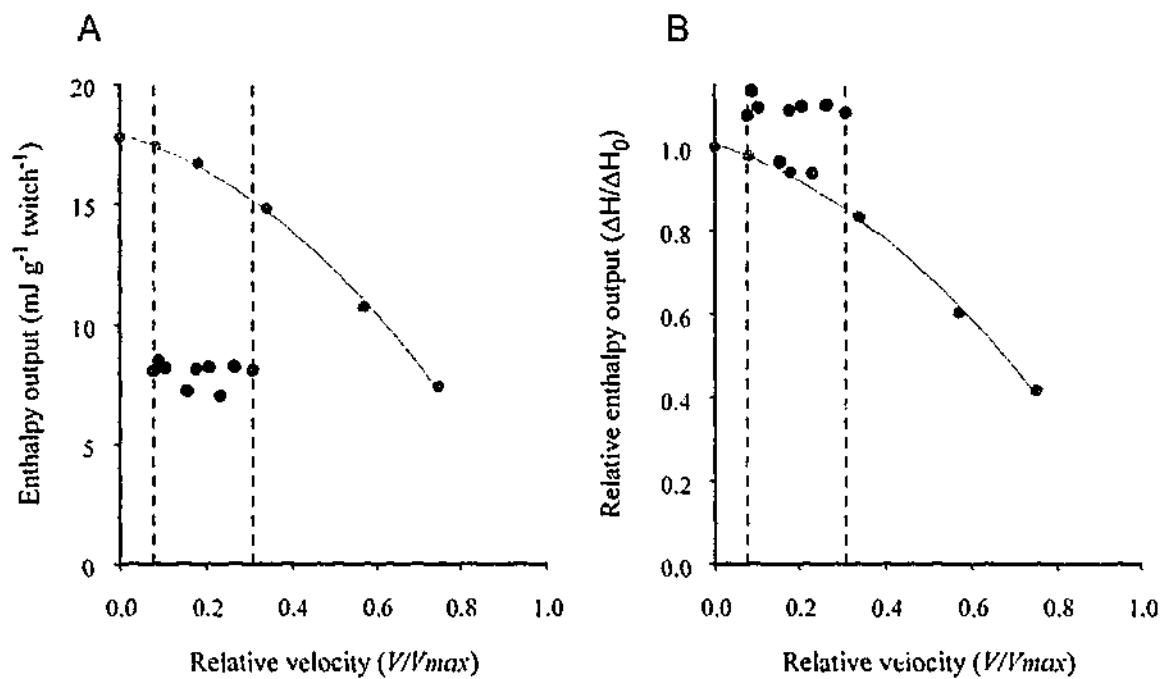
Figure 4.14 Estimate of relationship between relative velocity and enthalpy output

Absolute enthalpy output per twitch is shown as a function of relative velocity in **A**. **B** shows enthalpy output per twitch expressed relative to enthalpy output in an isometric twitch over the same relative velocity range. Data for afterloaded isotonic contractions from Kiriazis and Gibbs (2000) are shown in grey and those from the current study are displayed in black (n=7). The two dashed lines show the range of velocities used in the current study (0.08-0.31 V/V_{max}). As velocity increased over this range, the enthalpy output from afterloaded isotonic contractions decreased by ~15 %. Note that the two lower points from the current study are from contractions where the initial isometric duration was 10 % of the cycle duration and shortening was 10 or 15 % L_{max} (see Figure 4.6). See text for other details.

Based on the data from Kiriazis and Gibbs (2000), increasing shortening velocity from 0.25 to 1.0 L_{max} s^{-1} (0.08 to 0.31 V/V_{max}) would correspond to a drop in enthalpy output per twitch of approximately 15 %. This change in enthalpy output was not observed in the current study. This is shown most clearly in Figure 4.14B where the relative enthalpy output is plotted against relative velocity. Here, the relative enthalpy output remains stable

over the range of velocities tested in the current study (with the exception of two points, see figure legend), but falls away sharply for the experiments of Kiriazis and Gibbs (2000). It is interesting to note that the two points from the current study that were closest to the isotonic data were those with the shortest isometric period before shortening started. This suggests that starting to shorten relatively early in a twitch reduces the energy cost. Perhaps this effect underlies the decrease in energy cost with increasing velocity (decreasing load) in isotonic contractions: the earlier in a twitch that the muscle begins to shorten, the lower the total energy cost. In this scheme, the effects of both shortening velocity and amplitude have less effect on energy cost per twitch than the time at which the muscle begins to shorten. Note that this cannot be the sole determinant of energy cost because the contractions in which the shortening amplitude was 5 % L_{max} and the isometric duration was 10 % cycle duration were not accompanied by the reduced energy cost.

4.4.5   Isometric relaxation

To simulate *in vivo* ventricular muscle length changes, the linear length change protocol was modified to include an isometric relaxation phase. This modification resulted in force-length (work) loops that resemble the pressure-volume loops of the intact ventricle (Sagawa *et al.*, 1988). Initially, it was hypothesised that the force might increase when controlled shortening was stopped abruptly since the muscle was still actively generating force. However, force continued to decline steadily with time despite the abrupt cessation of shortening (Figure 4.11C). This observation is consistent with the shortening-induced deactivation described previously for cardiac muscle. Briefly, once a cross-bridge detaches from the actin filament it is unlikely to reattach to the thin filament. The ability to include an isometric relaxation phase allows the protocol developed in this study to simulate changes in end-systolic volume, which is not achieved easily using conventional protocols.

4.4.6   Comparison with studies of energy use in whole heart

Using an excised, whole heart model, Suga and colleagues have consistently reported a linear relationship between the pressure-volume area (PVA) and the rate of oxygen consumption (*i.e.* energy cost) in the left ventricle of dogs (reviewed by Suga, 1990). It should be noted that the PVA includes not only the work loop, as calculated in the current study, but also a 'potential energy' term that is enclosed by the extrapolation of both the active and passive pressure-volume relationships to zero pressure. For papillary muscles, the two-dimensional analogue of PVA is the force-length area (FLA). There is also a

linear relationship between FLA and the rate of oxygen consumption (Hisano and Cooper, 1987; Mast and Elzinga, 1990). Thus, both PVA and FLA provide indices of the energy cost of a cardiac twitch (Taylor *et al.*, 1993).

The alteration in strain pattern that was likely to have had the greatest effect on FLA in the current study was altering the amplitude of shortening (see Figure 4.5A). An estimate was made of the difference in FLA for contractions with the greatest and smallest amplitude length changes shown in Figure 4.5A. The active and passive isometric force-length relations were plotted to form the boundaries of the FLA diagram for the examples shown in Figure 4.15. This enabled FLA diagrams specific to this particular muscle to be formed. Work loops for this muscle were simply plotted using the same axes as the force-length relations. The remaining area under the lower boundary of the work loop corresponds to Suga's potential energy term.
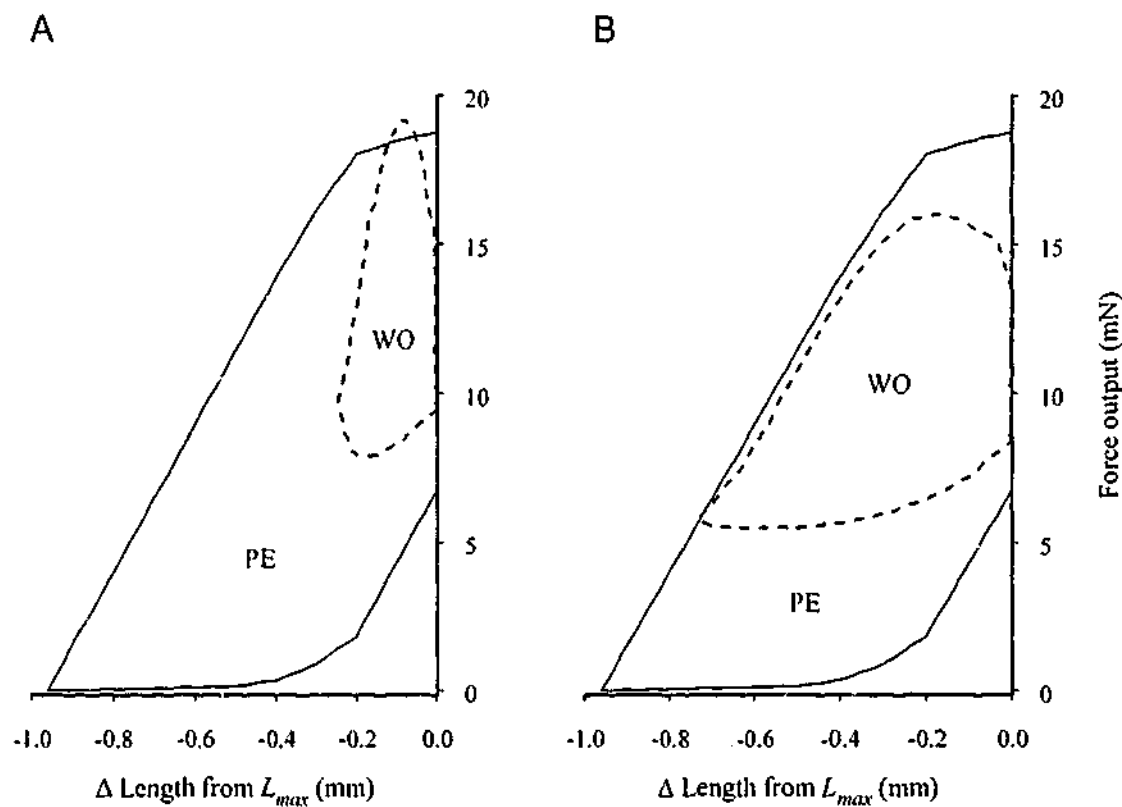
Figure 4.15 Force-length area diagrams for two amplitudes of shortening

Examples of force-length area plotted using single twitches. The passive (lower solid line) and active (upper solid line) length-tension relations were determined from isometric twitches. The FLA for a realistic twitch shortening by 5 % L_{max} is shown in A while the muscle shortened by 15 % L_{max} in B.

It was estimated that FLA for a shortening amplitude of 15 % L_{max} would have been ~90 % of that for the 5 % L_{max} shortening. If it is assumed that the dimensionless slope of

the relationship between enthalpy per beat and FLA is 2.5 and the enthalpy output when extrapolated to FLA of 0 is 4 mJ g^{-1} (Kiriazis and Gibbs, 2000), then the difference in energy cost per beat between shortening amplitudes of 5 and 15 % L_{max} would have been only ~1 %. Such a small difference would be undetectable using our, or any other, energy-measuring technique. Thus, the observed constancy of energy cost per beat in the face of substantial changes in shortening amplitude does not conflict with the idea that FLA, or PVA, provides a good index of energy cost for cardiac muscle.

4.5 Conclusion

Previous studies have made use of measurements made *in vivo* to design contraction protocols for use with preparations *in vitro*. For instance, Marsh (1999) summarises the various 'realistic' contraction protocols for use with isolated skeletal muscle preparations while Harwood *et al.* (1998) used the dynamics of whole fish hearts to design a protocol to make mechanical measurements using ventricular muscle. The current study is the first to adapt strain trajectories of papillary muscles measured *in vivo* to a contraction protocol for use with isolated papillary muscle preparations and the first to measure the energetics of cardiac muscle using such a protocol. This protocol allows more sophisticated analyses of cardiac muscle energetics because it is possible to simulate many of the major characteristics of cardiac function *in vivo*. It is notable that the energy cost per twitch and maximum net mechanical efficiency values were similar to those reported in Chapter 3.

Chapter 5: Effects of hypothermia on the energetics of rat papillary muscles

5.1   Introduction

Cardiac hypothermia, in conjunction with potassium-induced cardiac arrest, has been used extensively during cardiopulmonary bypass surgery as a means of reducing cardiac oxygen consumption to minimise damage to the heart resulting from periods of ischaemia. Ischaemic periods result from the intermittent perfusion that the majority of surgical teams rely on for better visibility of the surface of the heart. Many experimental studies of the effects of cardiac surgery on the heart have incorporated both ischaemic periods of varying duration and hypothermia. Few studies have investigated the effects of just the hypothermic insult on cardiac muscle itself.

Cardiac surgery performed under hypothermic conditions has been used routinely for adult patients since the 1960s (reviewed by Cook, 1999). This practice developed following the important experiments of Bigelow *et al.* (1950b) who reported that whole body oxygen consumption of dogs decreased almost linearly with decreases in body temperature to 20°C. In another paper published later the same year, Bigelow *et al.* (1950a) proposed that whole body hypothermia could be used as a safe platform for cardiac surgery in conjunction with an appropriate anaesthetic to eliminate shivering which would otherwise cause an increase in oxygen consumption. Shortly after the demonstration that whole body

oxygen consumption was decreased by hypothermia, Melrose *et al.* (1955) described a technique for arresting the heart using a high potassium solution. Cardiac surgeons have long believed that the reduction in oxygen consumption caused by the combination of potassium-induced cardiac arrest and hypothermia protects the heart from periods of ischaemia. Damage caused by ischaemia has been well-documented (Hearse, 1990; Hearse and Bolli, 1992; Jennings and Reimer, 1991). Extended ischaemia can cause myocardial necrosis but even relatively brief periods can also lead to some cellular damage. In the latter case, the damage occurs subsequent to reperfusion and is primarily due to Ca^{2+} overload (Allen *et al.*, 1993). Note that most surgery is performed with the heart perfused with low temperature cardioplegia (4-10°C) while the whole body temperature is only mildly hypothermic (28-33°C) (Lichtenstein *et al.*, 1991a; Lichtenstein *et al.*, 1991b; Martin *et al.*, 1994) to protect the brain from neurologic damage (Martin *et al.*, 1994).

Two papers published in the early 1990s advocated a shift to cardiac surgery performed at normothermic temperatures for most patient groups (Lichtenstein *et al.*, 1991a; Lichtenstein *et al.*, 1991b). This was due to concerns over the lasting damage that hypothermia seemed to have on the heart. For instance, it was reported that patients who underwent surgery using the hypothermic technique displayed increased incidences of mortality or lower cardiac output immediately following removal of the cardiopulmonary bypass system and long-term low cardiac output (Lichtenstein *et al.*, 1991a; Lichtenstein *et al.*, 1991b) compared to a similar cohort of patients who underwent surgery with normothermic perfusion. Other negative effects on the heart that have been associated with hypothermia include cell swelling, acidosis, shifts in the oxyhaemoglobin dissociation curve and increased plasma viscosity (Gaillard *et al.*, 2000; Stephenson *et al.*, 2000). A comprehensive review of both cold and warm perfusion techniques is given by Cook (1999).

Although some surgical teams are now routinely using normothermic or 'tepid' (32-34°C) temperatures during cardiac surgery (Cook, 1999; Lichtenstein *et al.*, 1991a; Lichtenstein *et al.*, 1991b; Mauney and Kron, 1995), most cardiac surgery is still performed under hypothermic conditions (Gaillard *et al.*, 2000) in which the heart is intermittently perfused with a potassium-enriched, cold cardioplegic solution. Intermittent perfusion allows for better visualisation of the surgical target but it may be the effects of these ischaemic periods and subsequent reperfusion that account in whole or in part for the negative effects that are attributed to hypothermia, *e.g.* lower post-bypass cardiac output.

5.1.1 Aims of this chapter

Although the clinical advantages and disadvantages of the hypothermic technique have been well publicised, there is little data pertaining to the acute effects of a hypothermic period on cardiac tissue itself following rewarming.

The aim of the experiments described in this chapter was to determine the effect of a period of hypothermia on energetic variables of rat papillary muscles using the realistic strain pattern developed in Chapter 4. The present study investigated the metabolic recovery from hypothermia by measuring energy use, work output and efficiency of isolated papillary muscles over a 2 hr period following rewarming. The effects of both the hypothermic temperature and the duration of hypothermia were investigated. By using an isolated papillary muscle preparation, the effects of hypoxia and ischaemia were avoided so that any observed changes in energetic variables could be attributed to the cold period *per se*. Glucose was provided as the metabolic substrate since the combination of glucose and oxygen has been shown to be beneficial to recovery of rat hearts following hypothermia (Doherty *et al.*, 1992).

5.2 Materials and methods

The materials and methods used for the experiments reported in this chapter are presented in Chapter 2. Only those methods specific to the current experiments will be described here.

5.2.1 Thermopile

Muscle temperature change was measured using a thermopile with an active recording region of 4 mm containing 16 thermocouples. The output of this thermopile was $0.812 \, \text{mV} \, ^\circ\text{C}^{-1}$.

5.2.2 Experimental protocols

In these experiments, muscle temperature was maintained at 30°C during the 1.5 hr equilibration period. The preparation was then set to the length at which active force production was maximum (L_{max}) as described in Section 2.11.2.

The contraction protocol for this study consisted of 40 twitches at a rate of 2.2 Hz. The cyclical strain pattern was based on that developed in Chapter 4 and consisted of three phases: (1) an initial isometric phase that accounted for 10 % of the cycle duration, (2) an isovelocity shortening phase that occupied 40 % of the cycle duration and (3) an

isovelocity relengthening phase that made up the remaining 50 % of the cycle. The amplitude of shortening was 10 % L_{max} (see Figure 4.2 in Chapter 4).

The current study was designed to test whether cooling the papillary muscle preparations affected the energetics of the muscles following rewarming. After the initial stabilisation period at 30°C, 1-3 control recordings of mechanical and thermal energy output were made with the muscle out of solution. The muscle was reimmersed in solution and then cooled over a period of 10 min to either 15°C (Experiment 1) or 8°C (Experiments 2 and 3). The muscle was maintained at the selected temperature for either 1 hr (Experiments 1 and 2) or 2 hr (Experiment 3) (see Table 5.1) and was not stimulated during this time. In all experiments, the muscle was then rewarmed to 30°C over a 10 min period. The first post-rewarming measurement was made 10 min after this to allow time for the thermopile output to stabilise following drainage (see Section 2.11). The muscle was not stimulated until this first recording. Measurements were then made every 20 min for 2 hr, with the muscle being immersed in solution and contracting at 0.2 Hz between recordings (Figure 5.1).

Table 5.1 Experimental protocols

	Experiment 1	Experiment 2	Experiment 3
Initial temperature (°C)	30	30	30
Cold temperature (°C)	15	8	8
Duration of hypothermia (hr)	1	1	2
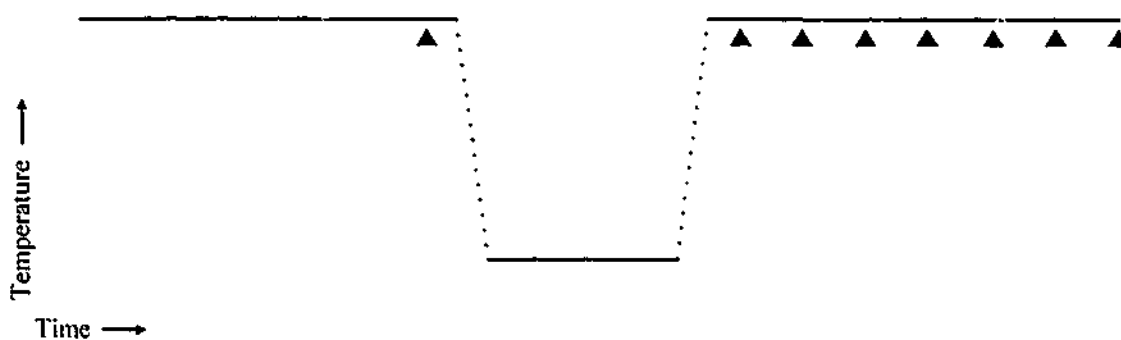
Figure 5.1 Illustration of time-course of experiment

A control recording (left-hand black triangle) was made at the end of the equilibration period. In this example, the muscle was cooled over 10 min (left-hand dotted line) and maintained at the lower temperature for 1 hr. The muscle was then rewarmed over 10 min (right-hand dotted line). Following rewarming, recordings were made every 20 min for 2 hr beginning 10 min after re-establishment of the pre-cooling temperature.

The initial experiments were performed using a hypothermic temperature of 15°C. This temperature was used by Belke *et al.* (1997) and in that study there was a substantial reduction in cardiac output from rat hearts following a 2 hr period of hypothermia. Initially, a 1 hr hypothermic period was used since this is the time that most patients spend on cardiopulmonary bypass during cardiac surgery (Lichtenstein *et al.*, 1991a). Subsequent experiments were conducted at 8°C since many previous studies of the effects of ischaemia and hypothermia used a similar temperature (*e.g.* Ericsson *et al.*, 1999). Finally, the duration of the hypothermic period was extended to 2 hr to determine whether duration of hypothermia had any effect on work output.

It should be noted that the solution was drained from the muscle chamber ~5-8 min prior to making recordings of muscle mechanical and thermal energy outputs. The muscle remained quiescent during this time. Each recording took <2 min to complete so that the maximum amount of time that the muscle was out of solution was 10 min. It has been demonstrated previously that papillary muscles did not suffer any adverse functional effects from periods out of solution for up to 20 min as long as the muscle was supplied with O_2 (Allen *et al.*, 1989). In the current experiments, the chamber was supplied with O_2 saturated with water vapour, even when the solution was drained, providing further confidence that muscle function was not affected adversely by these short periods out of solution.

The temperature of the thermopile frame was controlled by circulating water from a temperature controlled, 40 l reservoir through channels in the frame (see Section 2.5.1). In this study, a second reservoir was maintained at the lower temperature allowing the temperature of the thermopile frame to be altered quickly by interchanging the two reservoirs. The thermopile frame took ~10 min to equilibrate to the new temperature.

5.2.3 Analysis

For each muscle, the post-rewarming values of energetic variables were expressed relative to the control value measured following the stabilisation period to give a within experiment change. These values were then averaged to give mean values expressed as a percentage of the control value. The data were then analysed statistically as described in Section 2.12. Note that the pre-cooling value of 100 % was not included in the ANOVA analysis since this would have artificially decreased the variance. This value was re-included with the remaining data before the LSD test was performed.

5.3 Results

The aim of this study was to determine the effects of a cold period on papillary muscle energetics. General characteristics of the papillary muscles used in this study are presented in Table 5.2. The mean CSA of the preparations was higher in Experiment 1 than in Experiments 2 and 3. This was largely due to the inclusion of 2 preparations of ~1 mm^2 CSA in Experiment 1. The CSA of the remainder of the preparations in this group ranged from 0.56 to 0.75 mm^2. The mean active stress (mN mm^{-2}) in Experiment 1 was lower compared with Experiments 2 and 3 which may reflect the dependence of normalised force on CSA as described previously (Loiselle, 1979; Loiselle and Gibbs, 1979). Note that the mean isometric active force was lower in all experimental groups at 30°C (this chapter) compared to those at 27°C (Chapters 2 and 3). This is due to the well-documented positive inotropic effect of a lower temperature. The lower temperature causes Ca^{2+} to be present in the cytosol for a longer period of time during each twitch which, in turn, allows more cross-bridges to attach. Cross-bridge kinetics are also slowed at lower temperatures resulting in cross-bridges staying attached for longer. Both these effects would tend to increase peak twitch force output.

Table 5.2 Characteristics of papillary muscle preparations

	Experiment 1	Experiment 2	Experiment 3
Number of preparations	8	5	3
Wet mass (mg)	3.91 ± 0.49	1.92 ± 0.19	2.68 ± 0.61
L_{max} (mm)	4.79 ± 0.31	3.92 ± 0.20	5.03 ± 0.88
CSA at L_{max} (mm^2)	0.77 ± 0.07	0.47 ± 0.05	0.53 ± 0.15
Passive stress at L_{max} (mN mm^{-1})	10.9 ± 1.4	11.6 ± 1.5	10.9 ± 1.9
Active stress at L_{max} (mN mm^{-2})	11.2 ± 1.6	14.4 ± 2.6	19.8 ± 2.7
Passive stress/active stress at L_{max}	1.1 ± 0.2	0.9 ± 0.2	0.6 ± 0.1

One muscle was excluded from the 2 hr, 8°C hypothermia data set due to poor mechanical performance. The poor performance was most likely due to over-dissection of this preparation (CSA = 0.29 mm^2). The muscle produced very little force during the initial equilibration period (maximum isometric force output of <3 mN) and failed to respond to

stimulation following the 2 hr hypothermic period. It is interesting to note that none of the muscles used in this study twitched spontaneously (*i.e.* not in synchrony with stimuli) as a result of the cooling period. It has been reported previously that rat papillary muscles and myocytes exhibit spontaneous twitches when cooled to 15°C or below (Liu *et al.*, 1991b; Liu *et al.*, 1990a).

5.3.1 Changes in passive tension during cooling and rewarming

The passive tension produced by the papillary muscles was observed to vary considerably during the cooling and rewarming periods (Figure 5.2).
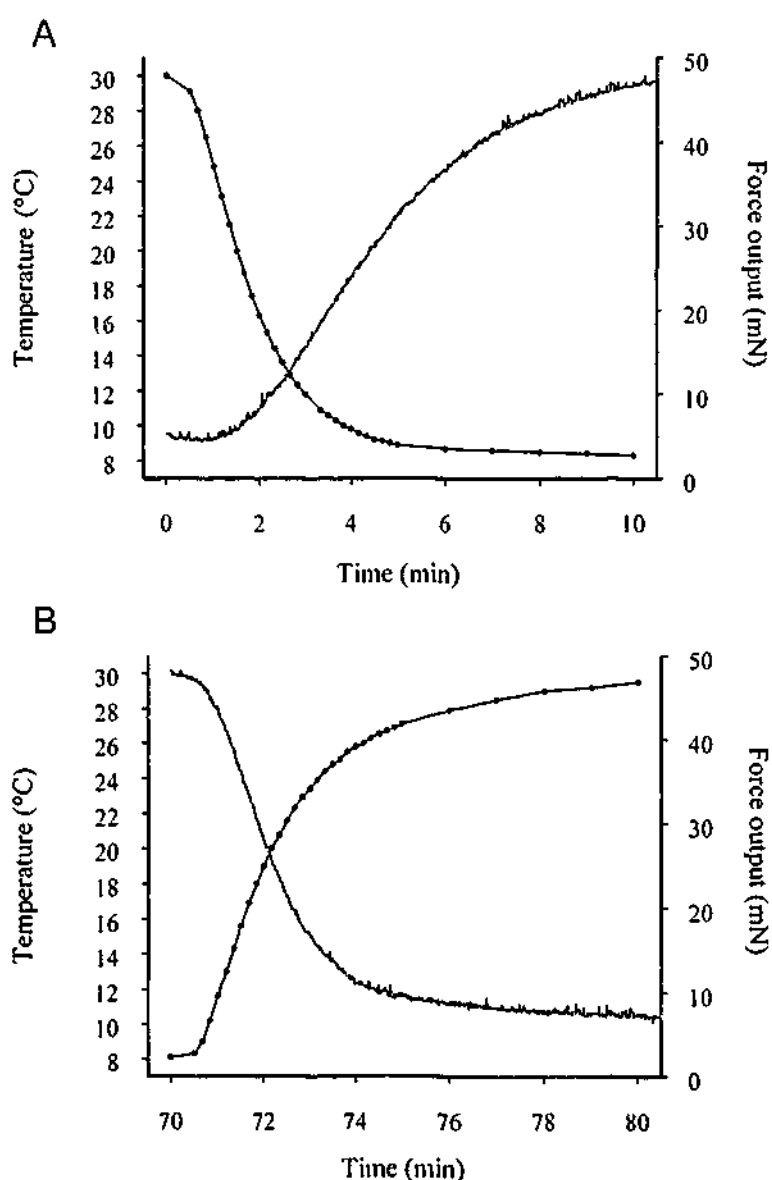
Figure 5.2 Effects of changing temperature on passive tension

A representative example of the changes in passive tension associated with cooling a muscle from 30°C to 8°C is shown in **A** and rewarming the muscle from 8°C to 30°C in **B**. Temperature changes are shown in black and passive tension changes are shown in grey. Temperature (°C) was manually noted from the block temperature every 10 s for the first 5 min and every 1 min thereafter until 10 min. Force output was sampled at 1 Hz. In this example, the muscle was maintained at 8°C for 1 hr.

In Experiment 1, the mean passive tension of the preparations during the stabilisation period at 30°C was 8.1 ± 0.8 mN. As the muscles were cooled to 15°C, the tension increased, eventually stabilising at ~30 mN. In Experiments 2 and 3, where the muscles were cooled to 8°C, the tension increased from ~5-6 mN to ~50-60 mN (Figure 5.2). In all experiments, tension decreased during the rewarming period, eventually returning to a tension close to the original passive tension value in a temperature-dependent manner.

The same data used in Figure 5.2 were used to plot a graph of force output against muscle temperature change (Figure 5.3). This diagram allows an estimate of the temprrature below which the force output of the unstimulated muscle rises rapidly. The data indicate that during cooling force output increased rapidly once temperature decreased below ~20°C. Between 20 and 30°C, there was little variation in force output. Interestingly, during rewarming the relationship between force output and temperature differed from that observed during cooling; force output was higher during rewarming than cooling. Only at temperatures approaching 30°C did force return to its pre-cooling resting value.
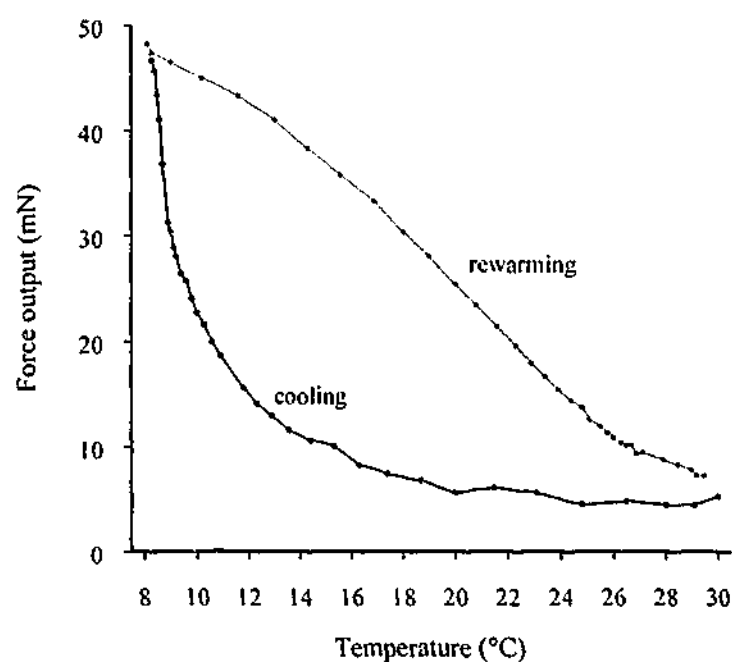
Figure 5.3 Changes in force output with temperature

This figure illustrates how the changing temperature influences muscle force output during cooling (black line) and rewarming (grey line). Cooling from 30 to 25°C had little effect on the force output and from 25 to 20°C, the force output began to increase. At temperatures below 20°C, muscle force output increased a relatively small amount to 15°C and then in greater amounts to 8°C. The force output was higher at each temperature during rewarming compared with the cooling relationship.

5.3.2 Effects of 1 hr, 15°C hypothermia on energetic variables

The effects of cooling papillary muscles to 15°C and maintaining this temperature for 1 hr on work output, enthalpy output and ε_{Net} following rewarming are shown in Figure 5.4.

Work output per twitch was significantly lower than the control value when first measured after rewarming but then recovered and was the same as the control value at the 30, 50 and 70 min post-rewarming time-points (Figure 5.4A). Following this recovery, work output per twitch again decreased and was significantly lower than control for the remainder of the experiment. At 130 min post-rewarming, the work output per twitch was ~86 % of the control value.

Enthalpy output per twitch did not vary in the same way as work output per twitch (Figure 5.4B). Although it appears that enthalpy output per twitch was reduced at the 10 min time-point, this change was not significant statistically. Enthalpy output per twitch did not differ significantly from the control value at any time-point other than at 50 and 70 min post-rewarming. At these times, the enthalpy output per twitch was increased significantly.
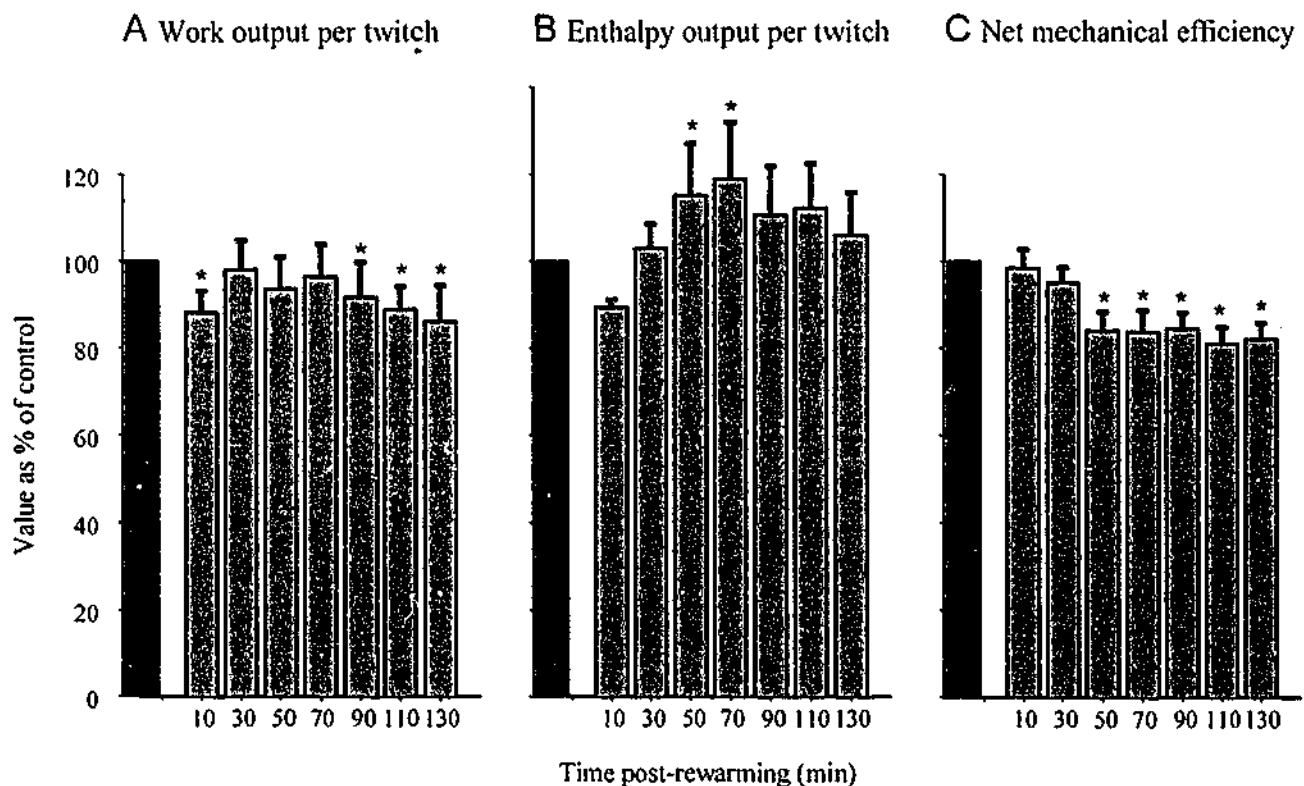
Figure 5.4 Effects of 1 hr, 15°C hypothermia on energetic variables

Effects of a 1 hr, 15°C period of hypothermia on work output per twitch (A), enthalpy output per twitch (B) and net mechanical efficiency (C) (n=8). All post-rewarming time-point values (grey columns) are expressed as a percentage of the control pre-cooling value (100 %, black columns). Asterisks indicate a statistically significant difference (p<0.05) from the control value.

The effects of the cold period on ε_{Net} are shown in Figure 5.4C. ε_{Net} was the same as the control value at 10 min post-rewarming due to significant decreases in both work output per twitch and enthalpy output per twitch. There was also no significant change to ε_{Net} at 30 min since, at this time, the work and enthalpy outputs per twitch were the same as their respective controls. For the remainder of the protocol, ε_{Net} was significantly decreased with respect to control. At 50 and 70 min post-rewarming, this decrease was due to an increase in the enthalpy output per twitch accompanied by no change in work output per twitch. At 90-130 min, the decrease in ε_{Net} was caused by a significant decrease in work output per twitch accompanied by no change in enthalpy output per twitch relative to control values.

5.3.3   Effects of 1 hr, 8°C hypothermia on energetic variables

The changes in work output following rewarming were relatively modest compared to some reported in the literature. For example, Belke reported a ~65 % decrease in cardiac work (averaged over 30 min rewarmed period) following a 2 hr period of hypothermia at 15°C. It was thought that perhaps the change in temperature used in the current study was not great enough to cause such changes, so muscle temperature was reduced to 8°C, rather than 15°C, to see if this caused more substantial decreases in work output and ε_{Net}. The effects of cooling to 8°C and maintaining this temperature for 1 hr, as before, on work output, enthalpy output and ε_{Net} following rewarming are shown in Figure 5.5.

Work output per twitch was significantly lower than the control value at all times following rewarming to 30°C (Figure 5.5A). Note that the work output did recover somewhat (30 and 50 min) following the first measurement, however this was not sustained. Work output per twitch was still only ~63 % of the control value at the final time-point (130 min post-rewarming). Enthalpy output per twitch was also significantly lower than the control value at every measured time-point following rewarming (Figure 5.5B) and followed the same general pattern of post-rewarming depression as the work output.

ε_{Net} was also significantly lower following rewarming compared to the control, pre-cooling value (Figure 5.5C). This was due to a greater depression in work output than in enthalpy output. The only value that did not differ statistically from the control value was the 50 min post-rewarming value. This was due to a further relative decrease in enthalpy output compared to work output at that time.

A Work output per twitch   **B** Enthalpy output per twitch   **C** Net mechanical efficiency

Time post-rewarming (min)
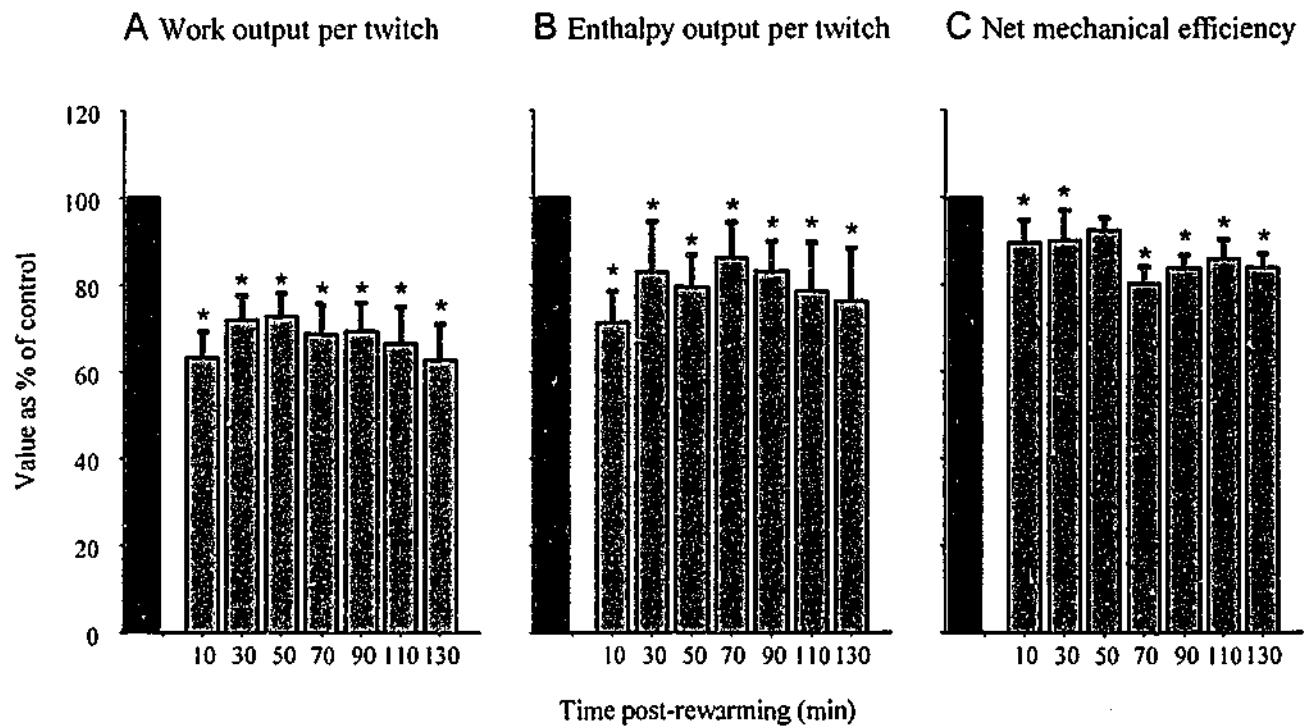
Figure 5.5 Effects of 1 hr, 8°C hypothermia on energetic variables

Effects of a 1 hr, 8°C period of hypothermia on work output per twitch (**A**), enthalpy output per twitch (**B**) and net mechanical efficiency (**C**) (n=5). All post-rewarming time-point values (grey columns) are expressed as a percentage of the control pre-cooling value (100 %, black columns). Asterisks indicate a statistically significant difference (p<0.05) from the control value.

5.3.4 Experimental recordings before and after a period of hypothermia

Typical records of length change, force output, muscle temperature change and cumulative work, heat and enthalpy outputs over a contraction protocol are shown in Figure 5.6 for a control, pre-hypothermia recording and another made 30 min following rewarming to 30°C.

The first point to note is that the passive tension was lower following the cooling and rewarming. An advantage of determining work output using the work loop technique is that changes in passive tension do not of themselves affect calculations of net work output. Note that the length of the muscle was held constant during this period. In addition to the lower passive tension evident in this example is the change in pattern of force output. Although the peak force output in the first post-rest twitch was high in both recordings, the peak force output in the subsequent twitches in the post-rewarming recording did not follow the usual positive staircase pattern exhibited in Figure 5.6A and Figures 3.3 and 4.4

in earlier studies in this thesis. The force output in Figure 5.6B was relatively constant following the high force output of the first twitch.

The temperature change and the heat output of the muscle over the contraction protocol were reduced markedly following cooling and rewarming. The enthalpy output was also reduced due to the lower work and heat outputs.
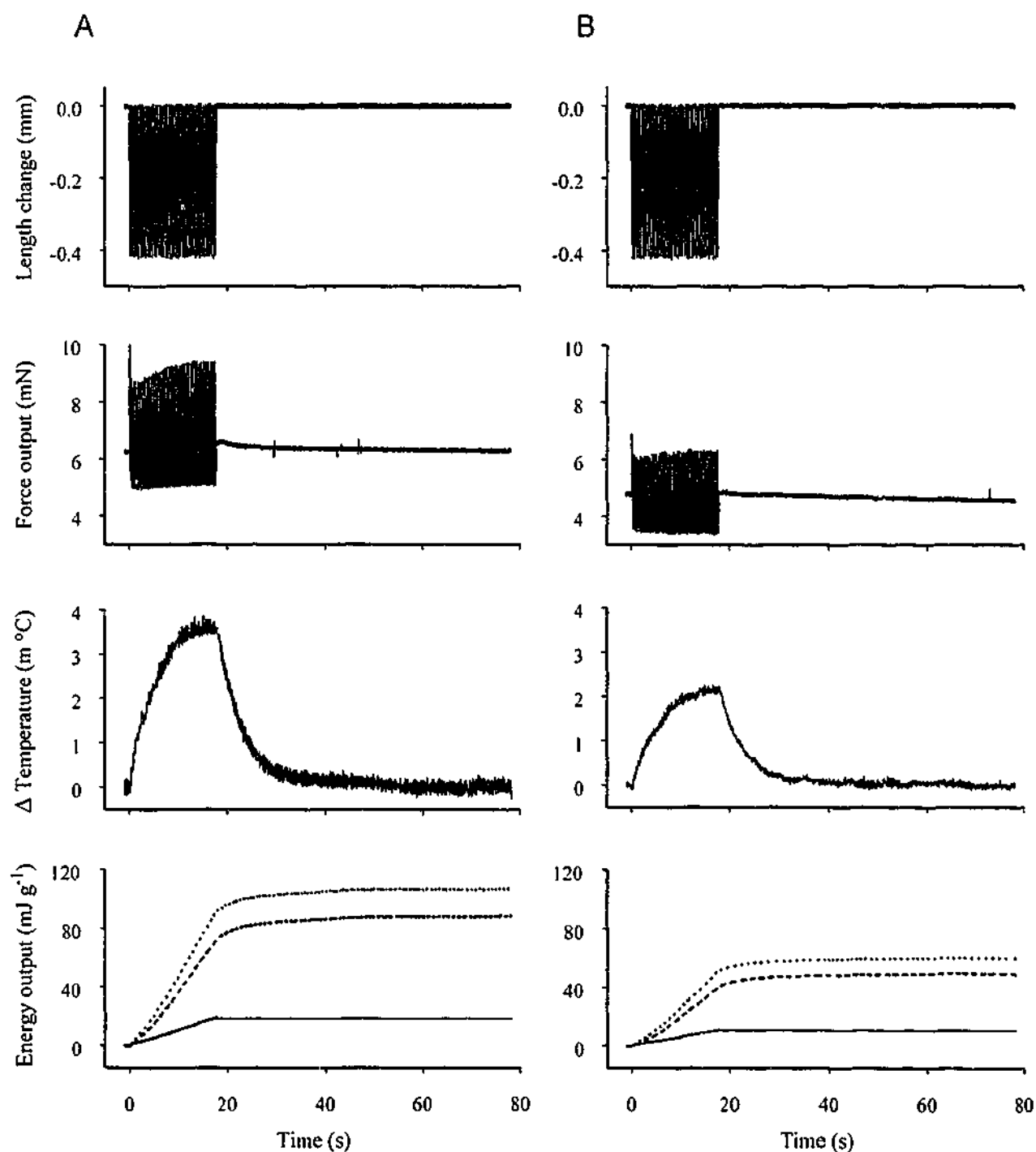
Figure 5.6 Examples of typical recordings before and after hypothermia

Records shown (from top to bottom) are change in muscle length from L_{max}, force output, change in muscle temperature and cumulative work (solid line), heat (dashed line) and enthalpy (dotted line) outputs. The panels shown in **A** are taken from a muscle prior to the period of hypothermia and those in **B** are taken from the same muscle at the 30 min post-rewarming time-point following a 1 hr, 8°C period of hypothermia. (Muscle mass, 2.21 mg; length, 4.1 mm, CSA, 0.51 mm^2).

The first 4 s of the force and enthalpy output records are shown on an expanded scale in Figure 5.7. Again, it is clear that the muscle produced less force and enthalpy per twitch following the 1 hr, 8°C period of hypothermia.
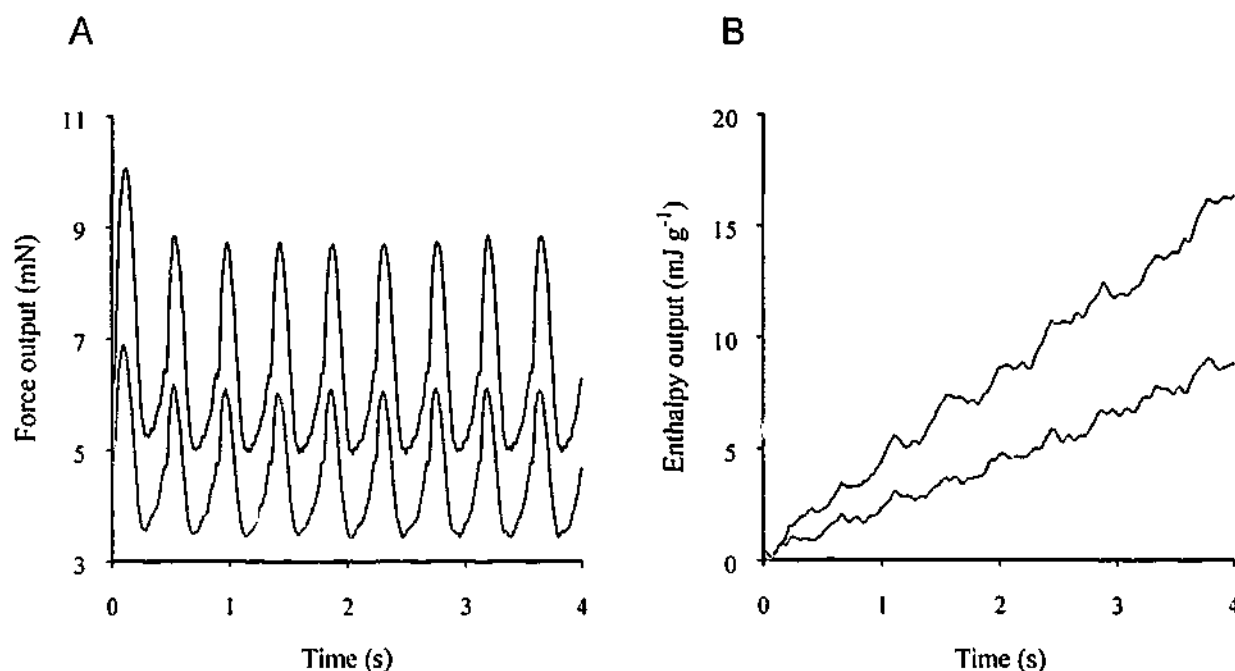
Figure 5.7 Comparison of force and enthalpy outputs before and after a period of hypothermia

The first 4 s of the force records shown in Figure 5.6 are shown in **A**. The control, pre-hypothermia recording is shown in black and the 30 min post-rewarming recording is in grey. The corresponding enthalpy outputs are shown in **B**.

5.3.5   Effects of hypothermia on work loops

In these experiments, net work output was calculated by integrating force output with respect to muscle length change. This is equivalent to calculating the area enclosed by a plot of force output against muscle length change. Work loops are shown in Figure 5.8 (A and B).

The loops shown are taken from recordings made on the same muscle. Following cooling and rewarming, the muscle developed less force during the initial isometric period. The muscle subsequently produced less force during shortening (Figure 5.8, A and B). To provide a direct comparison of the active force outputs before and after cooling, the passive force was removed from the records by subtracting the appropriate force output at the end of the relengthening period (equivalent to the end-diastolic force) from each record (Figure 5.8C). Further, to determine if the difference in active force output was due simply to a scaling of force output or was also due to a change in the force-velocity profile

of the muscle, the active force record was normalised by peak force (Figure 5.8D). The results of this analysis indicate that the active force-generating ability of the muscle was reduced (Figure 5.8C) and, furthermore, the force-velocity properties also appear to have been altered as indicated by the lower normalised force during the shortening phase in the post-rewarming recording (Figure 5.8D). Remember that shortening in this protocol occurred at a constant velocity.
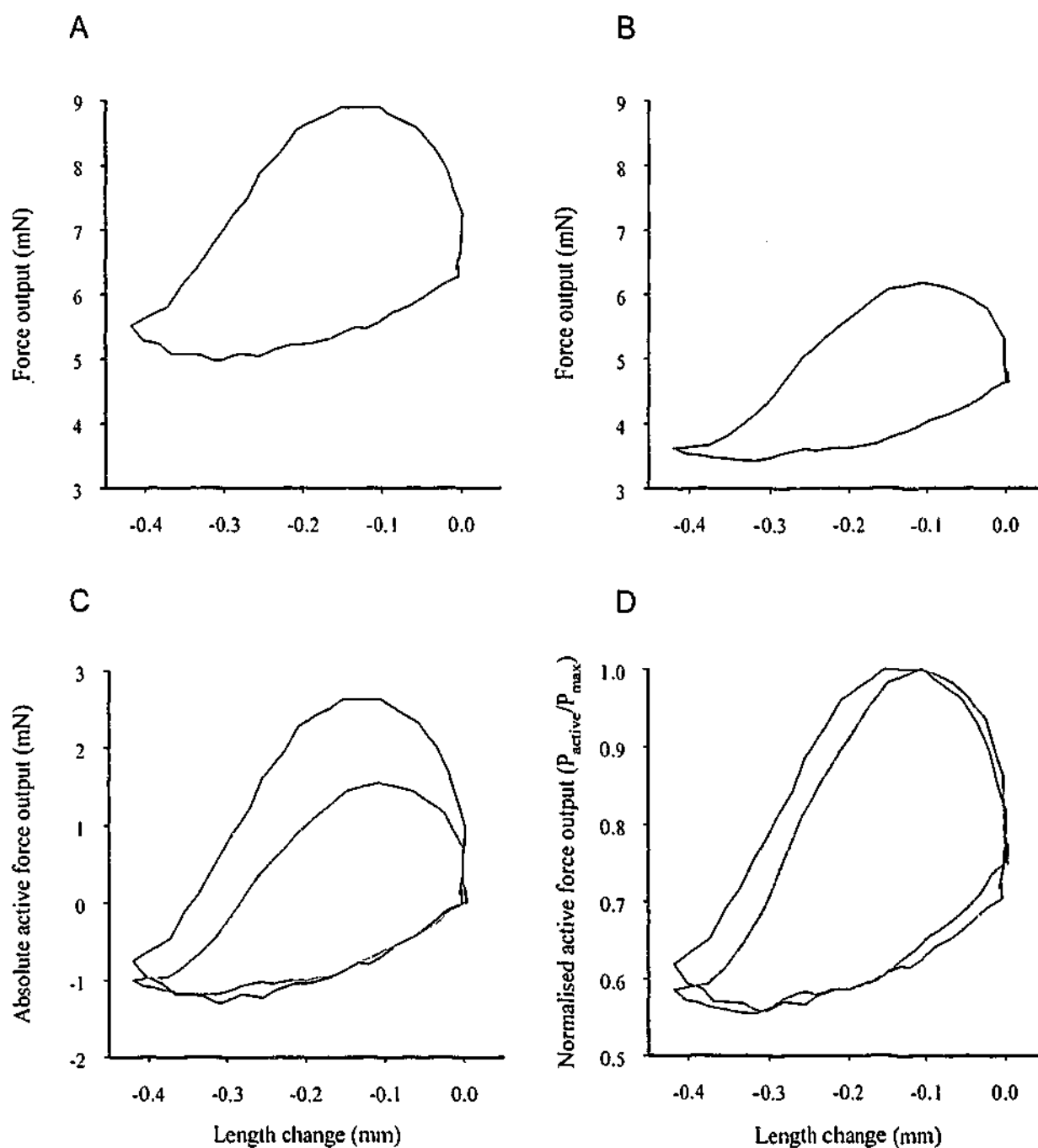
Figure 5.8 Comparison of work loops from control and post-rewarming recordings

These work loops are taken from the 13th twitch of the control (A) and the 30 min post-rewarming recordings (B) shown in Figure 5.6. In C, the records were normalised by subtracting the force at the end of the relengthening period just prior to contraction. In D, the records were normalised by peak contraction force. In C and D, the black traces are the control records and the grey traces are the 30 min post-rewarming records.

5.3.6 Effects of 2 hr, 8°C hypothermia on energetic variables

As a final test of the effects of hypothermia on the energetics of isolated papillary muscles, muscle temperature was again decreased from 30 to 8°C but was maintained at this temperature for 2 hr instead of 1 hr to determine if the time spent at the lower temperature was an important factor in the depression of energetic variables. The effects of cooling to 8°C and maintaining this temperature for 2 hr on work output, enthalpy output and ε_{Net} following rewarming are shown in Figure 5.9.
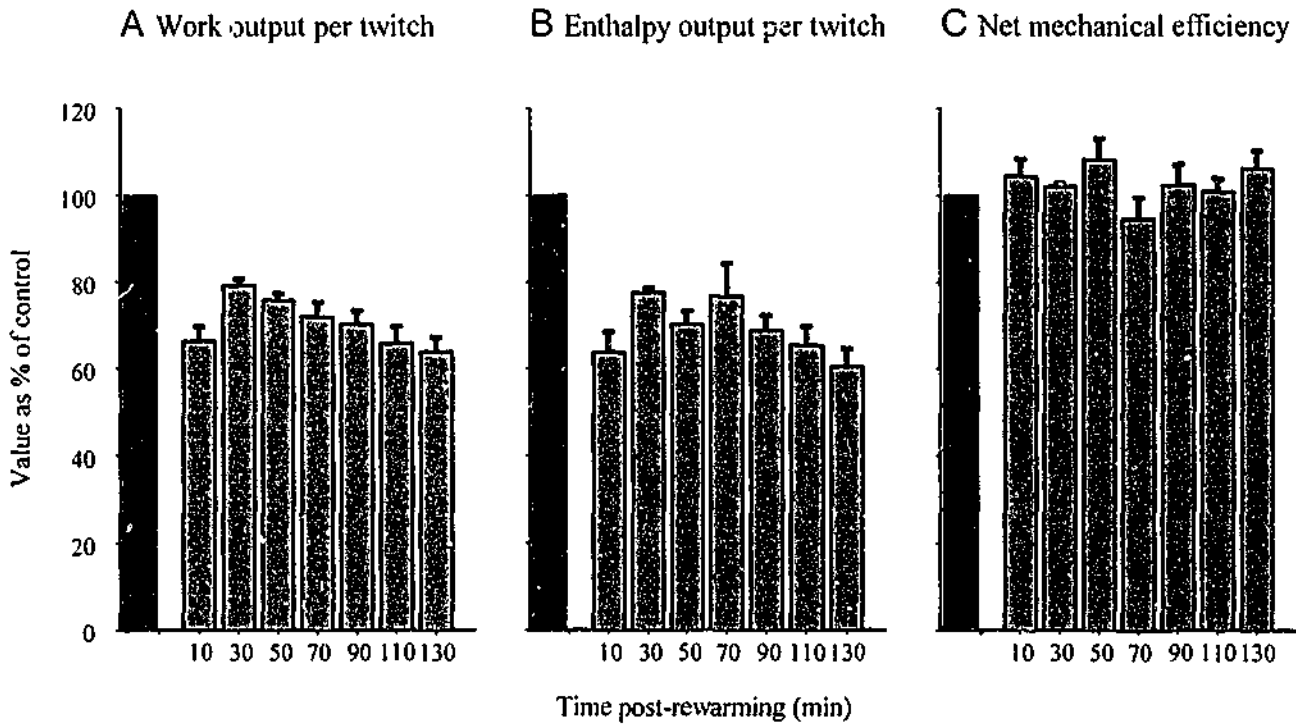
Figure 5.9 Effects of 2 hr, 8°C hypothermia on energetic variables

Effects of a 2 hr, 8°C period of hypothermia work output per twitch (**A**), enthalpy output per twitch (**B**) and net mechanical efficiency (**C**) (n=3). All post-rewarming time-point values (grey columns) are expressed as a percentage of the control pre-cooling value (100 %, black columns). Note that a statistical comparison was not made due to the small number (n=3) of muscles in this group.

It is evident from Figure 5.9 that the pattern of changes in work output per twitch following rewarming was similar to that in Experiment 2 (Figure 5.5). At the final time-point, work output per twitch was ~64 % of the control value (in Experiment 2, the corresponding value was ~63 %). It appears that the enthalpy output per twitch was more depressed than in Experiment 2 but this is inconclusive due to the small number of muscles included in the data set (n=3). Note, however, that the error bars in Figure 5.9 are very small indicating that the 3 muscles in this group responded to the period of hypothermia in a very similar manner. The decrease in work output compared to the

control, pre-hypothermia value was similar to that found in Experiment 2. However, the further depression in enthalpy output resulted in ε_{Net} remaining closer to the control, pre-hypothermia value.

5.4 Discussion

The current study investigated the effects of hypothermia on isolated rat papillary muscles. An important aspect of this study was the avoidance of hypoxia which is usually a consequence of the ischaemic periods inherent in most cardiac surgery. The muscles used in this study were supplied with oxygen throughout the experiment and during the period of hypothermia the muscle was immersed in solution that was agitated by the carbogen supply. Solution was removed from the chamber when measurements were made during the control and rewarming periods. This is equivalent to transient ischaemia but, very importantly, without hypoxia. The muscle was not stimulated for the majority of time during these periods. It should be noted that in the experiments reported in Chapters 3 and 4, these periods did not affect the energetics of the muscle over the course of an experiment. It has also been reported that cardiac muscle function is not affected by ≤ 20 min periods out of solution as long as the muscle is constantly supplied with oxygen (Allen *et al.*, 1989).

The main finding of this study was that the work and enthalpy outputs were decreased following 1-2 hr hypothermia at 8°C. These decreases caused relatively small changes to ε_{Net}.

5.4.1 Changes in passive tension during cooling

Large magnitude changes in passive tension accompanied cooling of the papillary muscles from 30°C to both 15 and 8°C. Liu *et al.* (1990) also observed an increase in the resting force of isolated rat papillary muscles, although they report this increase for temperatures below 15°C whereas the increase was observed at temperatures below ~20°C in the current study. This type of response has also been observed in whole heart studies. For instance, Aasum and Larsen (1999) reported an increase in left ventricular end-diastolic pressure during hypothermia. In that study, the heart was continuously perfused with oxygenated Krebs-Henseleit solution. Buckberg *et al.* (1977) reported a decrease in diastolic compliance during cooling. Again, the hearts were supplied with oxygenated saline throughout the experiment.

5.4.2 Could increased passive tension reflect temperature-dependent properties of parallel elastic elements?

In the simple, but nonetheless useful, model of muscle as a contractile element in series with an elastic element and in parallel with another elastic element, it is generally envisaged that passive tension arises from the extension of the parallel elastic element. Is it possible that a decrease in temperature could increase the tension in parallel elastic elements without altering the length of the element? Such an effect does indeed exist: the thermoelastic effect. Thermoelasticity refers to the thermal changes that accompany a change in stress on a given material.

Hill (1952) has investigated the thermoelastic properties of passive skeletal muscle. He found that passive muscle, in contrast to active muscle, has rubber-like thermoelasticity; that is, a decrease in temperature would tend to increase the tension in the elastic elements giving rise to passive force, as observed in the current study. However, the magnitude of the change in tension from thermoelastic properties would probably be much smaller than that observed in the current study. For example, if the change in heat content of the muscles upon cooling and the increase in passive force were used to estimate the thermoelastic coefficient (R) then R would have to be $\sim 1 \times 10^3$ which is $\sim 10^6$-fold larger than that found experimentally in muscle (Hill, 1952). It is, therefore, highly improbable that the increased passive tension with decreasing temperature observed in the current study could be accounted for by thermoelasticity.

5.4.3 Could the observed increase in passive tension be the result of ATP depletion?

Another mechanism by which muscles can develop sustained high forces is through ATP depletion. In this situation, attached cross-bridges are unable to detach. Contracture caused by ATP depletion can lead to serious and irreversible consequences (Stringham et al., 1992). Doherty et al. (1992) reported an increase in coronary resistance, indicating contracture, when oxygen was not present in the perfusate. In the experiments reported in this chapter, muscles remained immersed in oxygenated solution containing 10 mM glucose while the muscle was cold and the tension was high. It was assumed, therefore, that the muscle was not ATP-depleted due to oxygen deprivation or inadequate substrate supply. This idea was supported by the observations that the force declined immediately upon rewarming and contractile function did recover following hypothermia.

5.4.4 Is the passive tension observed in cold conditions really active tension?

Since the large increase in passive tension is unlikely to reflect changes in the properties of the parallel elastic element or ATP depletion, it could be a consequence of the active force-generating process, cross-bridge cycling. This would mean that the observed increase in tension might actually be active, rather than passive, tension. There is strong evidence to support this view.

It has been demonstrated that $[Ca^{2+}]_i$ increases progressively with cooling. This is due to a combined impairment of Ca^{2+}-regulating processes including the SR Ca^{2+}-release channels, SR Ca^{2+}-ATPase, Na^+/K^+-ATPase, Mg^+-ATPase and the Na^+/Ca^{2+} exchanger (Liu et al., 1991a; Liu et al., 1997; Liu et al., 1991b; Thurston et al., 1978). In the current experiments, the tension produced by the muscle during the 8°C period of hypothermia was greater than that produced at 15°C. This suggests a greater impairment of Ca^{2+}-extruding mechanisms at 8°C than at 15°C.

The high tension produced by the muscles during hypothermia in the current study (see Figure 5.2) suggests that the $[Ca^{2+}]_i$ must have remained high throughout the period of hypothermia. This, in turn, would allow cross-bridges to remain attached throughout the cold period. However, the low rate of oxygen consumption of hypothermic cardiac muscle (Buckberg et al., 1977) suggests that cross-bridges must cycle very slowly, if at all, during this period. To provide experimental verification of this idea, cross-bridge kinetics during hypothermia could be characterised using a length perturbation method like that described by Rossmanith et al. (1986). Those authors monitored the rate of cross-bridge cycling by observing the time-course of force redevelopment after application of fast, small amplitude decreases in muscle length.

In all muscles studied, the cold contracture was reversed upon rewarming the muscle to 30°C, with the tension decreasing in a temperature-dependent manner. As muscle temperature was increased, cellular enzymes would be expected to regain their capacity for normal function. The decrease in $[Ca^{2+}]_i$ expected to accompany the increase in temperature would allow the tension of the muscle to decrease to its original, passive value, as observed in the current study. It is interesting to note that the time-course of tension change during rewarming was different to that during cooling (Figure 5.3). This may be indicative of a sustained alteration in SR Ca^{2+}-ATPase function.

5.4.5 The time spent at the cold temperature was less important than the magnitude of the temperature decrease

The current study demonstrated that the temperature of the superfusing solution had marked effects on recovery of mechanical function following rewarming. Following a 1 hr, 15°C hypothermic period, work output per twitch recovered to ~86 % of the pre-hypothermia value compared to ~63 % when the muscle was subjected to a 1 hr, 8°C hypothermic period. Increasing the period of hypothermia from 1 to 2 hr at 8°C appeared to have no further detrimental effect on work output per twitch. Hence, it seems that the magnitude of hypothermia is more important than the duration of the hypothermic period in recovery of mechanical function following rewarming to 30°C. In all experimental conditions tested in this study, work output per twitch recovered somewhat following the first post-rewarming recording, but then decreased again for the remainder of the experiment.

5.4.6 Possible explanations for impaired work output

The results of the current study, especially the results of the 1 and 2 hr, 8°C periods of hypothermia, indicate that the main post-hypothermia impairment was the inability of the muscle to do work. This is supported by the relatively modest changes in ε_{Net} indicating that enthalpy output was scaled appropriately to work output. This suggests that mitochondrial function post-hypothermia was adequate. This is supported by the time-course of the decrease in temperature following completion of the contractions in Figure 5.6. The time-course appears to be much the same in both the pre- and post-hypothermia measurements indicating that there was no fundamental change in the recovery process following hypothermia.

The impairment in the ability of the muscle to do work post-hypothermia is illustrated in Figure 5.8. It appears from the work loops shown that two factors contributed to the decreased work output. Firstly, active force output was depressed following the period of hypothermia (Figure 5.8C). This indicates that either fewer cross-bridges were attached during this time or that the same number of cross-bridges were attached but each cross-bridge produced less force. Fewer attached cross-bridges could be the result of a decrease in $[Ca^{2+}]_i$ during twitches following the period of hypothermia, although this cannot be determined from the current results. Less force output per cross-bridge could be the result of changes in the intracellular milieu, such as increased levels of P_i and H^+ (see explanation in Chapter 4, Section 4.4.1). An increase in P_i would occur if the levels of

ATP and PCr decreased. Aasum and Larsen (1999) reported that intracellular concentrations of ATP and PCr were well-maintained during a period of hypothermia (40 min at 10°C) but then, once the muscle was rewarmed, declined to ~50 % of the pre-cooling values (measured over 30 min). In that study, isolated hearts were perfused continuously with oxygenated saline containing both glucose and palmitate. It is possible that levels of H^+ could increase as a result of actions of other sarcolemmal ion exchangers. The Na^+/Ca^{2+} exchanger would assist in lowering the $[Ca^{2+}]_i$ during rewarming which would cause an increase in $[Na^+]_i$. Some of the increased Na^+ may be extruded from the cytoplasm via the Na^+/K^+ and Na^+/H^+ exchangers which may result in a higher $[H^+]_i$.

Secondly, the force-velocity relation of the muscle changed following the period of hypothermia as indicated by the lower force along the downward slope of the work loop in Figure 5.8D. The strain protocol used in the current study ensured that the muscle shortened at the same velocity during all recordings. Following hypothermia, relative force output at that velocity was lower. Thus, both isometric force was lower and force during shortening was depressed, even more than isometric force, relative to the pre-hypothermia response. These changes could be due to either a decrease in V_{max} (i.e. relative velocity has changed) or to an increased curvature of the force-velocity relation. Further experiments using a range of shortening velocities to establish the force-velocity relations under the conditions tested in the current study would be required to distinguish between these possibilities.

5.4.7 Comparison to previous experimental findings

There have been several studies investigating the effects of hypothermia on cardiac muscle using either isolated or *in situ* whole heart preparations (*e.g.* Belke *et al.*, 1997; Buckberg *et al.*, 1977). Some studies have incorporated both ischaemia and hypothermia, again making it difficult to distinguish between the effects of these two variables (*e.g.* Ericsson *et al.*, 1999). While some studies have looked at substrate metabolism during and after a period of hypothermia (Belke *et al.*, 1997; Orme and Kelly, 1977), others have concentrated on functional consequences (Suga *et al.*, 1988) or ion exchange and pumping (Liu *et al.*, 1991a; Liu *et al.*, 1997; Liu *et al.*, 1991b; Thurston *et al.*, 1978). Species differences in tolerance of hypothermia have also been investigated (Aasum and Larsen, 1999; Liu *et al.*, 1991a; Liu *et al.*, 1990a; Liu *et al.*, 1990b).

In an interesting study comparing the effects of hypothermia on a hibernating and a non-hibernating species, Belke *et al.* (1997) showed that the hibernating species (ground

squirrel) exhibited a substantially better recovery of cardiac output than the rat (non-hibernating species) following 2 hr at 15°C. That study used an isolated working heart model in which the heart was continuously perfused with oxygenated solution at constant pressure. Although the coronary flow rate decreased during hypothermia, which could result in areas of ischaemic tissue due to collapse of smaller vessels, the authors concluded that the substantially reduced cardiac output following a period of hypothermia in the rat reflected the effects of hypothermia rather than ischaemia. This conclusion was based on the stability of endogenous substrates (glycogen and triacylglycerol) indicating that the supply and oxidation of exogenous substrates was adequate to meet the metabolic requirements of the heart. Belke *et al.* (1997) proposed that the poor functional recovery of rat hearts following rewarming might be due to a decrease in efficiency although they did not make any direct measurements of mechanical efficiency. Their measurements of cardiac output and acetyl CoA production suggested that efficiency may have decreased by as much as 50 %. This was based on a decrease in cardiac output accompanied by a steady production of acetyl CoA compared with pre-cooling data.

The data from the current study showed a smaller decline in work output than that observed by Belke *et al.* (1997) and also a smaller change in efficiency than they suggested. Thus, the current results support the idea that the primary effect of hypothermia is on cross-bridge processes rather than metabolic processes.

5.5 Conclusion

This study has shown that the mechanical function of rat papillary muscles was impaired by a period of hypothermia. Following rewarming, the net mechanical efficiency of the muscles was relatively close to pre-cooling values indicating that energy consumption was still closely coupled to work output. This study has demonstrated the utility of the contraction protocol developed in Chapter 4 for investigating the effects on cardiac energetics of a physiological insult similar to that experienced by the heart during some clinical procedures. The protocol has proved to be a useful tool for identifying the nature of energetic changes associated with this disruption to cellular homeostasis and in precisely locating the muscle characteristics that must underlie the altered function.

Chapter 6: Concluding comments

This thesis describes the development of the first contraction protocol for use with mammalian papillary muscle *in vitro* that closely resembles the actual movements and contraction rates of these muscles *in vivo*. The protocol can be adjusted to mimic most aspects of cardiac mechanical performance that alter under pharmacological or pathological influences. This gives the new protocol the potential to provide quite detailed and sophisticated analyses of the effects of various interventions on cardiac muscle function. Accurate measurements of work output and energetic cost, such as is possible with this protocol and isolated muscles, cannot be made using whole hearts.

The final set of experiments described in this thesis were an example of an application of the protocol to a particular intervention (hypothermia) known to alter cardiac function. It was clear from the analysis of the data obtained from the cyclic, realistic protocol that the major influence of a hypothermic insult was impaired work output as a result of both decreased force-generating ability and altered force-velocity properties. Despite the relatively preliminary nature of these experiments, the scope of the analysis possible using this protocol is evident.

The major experimental finding of this thesis was that the net mechanical efficiency of rat papillary muscles was independent of experimental protocol and, furthermore, was between 10 and 15 % rather than 20-25 % as suggested in some recent studies. The cause of this discrepancy was the inclusion of the load supported by passive elements in the 'net'

work calculation of afterloaded isotonic contractions. This finding does, however, pose the question of why the efficiency of the muscle, as measured in the current studies, should be so much lower than that of the whole, beating heart (typically between 20 and 30 %). An indication of one factor that may be influencing efficiency can be seen by comparing the efficiencies reported in Chapters 3 and 4 (27°C) with the efficiency calculated for the experiments in Chapter 5 in which the experimental temperature was 3°C higher. In Chapter 3, ε_{Net} was 10-15 % for the afterloaded isotonic and sinusoidal contraction protocols while in Chapter 4, ε_{Net} was ~12 % when using the realistic strain protocol with a shortening amplitude of 10 % and a contraction frequency of 2 Hz. In Chapter 5, ε_{Net} was ~17.7 % at 30°C using the same protocol but at a contraction frequency of 2.2 Hz. Upon observing this apparent effect of temperature on ε_{Net}, a single experiment was performed at an experimental temperature of 37°C. At this temperature, ε_{Net} was ~20 % using the same protocol again but at a contraction rate of 4 Hz. The idea that temperature may have a substantial effect on ε_{Net} warrants further investigation.

Considering the above proposition, it would be informative to conduct an investigation of the energetics of cardiac muscle using the realistic protocol developed in Chapter 4 in conjunction with a physiological temperature (37°C) and an appropriate contraction rate (~5-6 Hz). This type of study would require preparations of very small CSA to allow sufficient diffusive oxygen supply. Additionally, such a study could be performed using mouse papillary muscles. The mouse would be a particularly useful model for the study of cardiac energetics due to the variety of knock-out species available. This would enable the effects on cardiac energetics of known molecular alterations to be investigated using a realistic strain protocol.

The investigation into the effects of hypothermia on cardiac muscle also raised some interesting possibilities for future studies. Further investigation into the impairment of work output following hypothermia is required. Specifically, the mechanisms underlying the decreased isome ic force output and the exact nature of the alteration in the force-velocity relation of the muscle need to be elucidated. It would also be interesting to test whether the post-hypothermia impairment to work output is related to the high tension observed during the cold period. One method of testing this possibility would be to prevent cross-bridge cycling during the period of hypothermia. This could be readily accomplished by, for example, including BDM in the chamber solution during just the period of hypothermia.

A final, important observation was that the enthalpy output per twitch was more-or-less independent of the protocols used in this study. This is consistent with the idea that the energetic cost of a cardiac twitch, under normal conditions (*i.e.* no inotropic influences), is constant. In the current studies, this was true for different types of contraction that caused substantial changes to work output. Thus, the efficiency of the muscle was altered, due to the variation in work output, but the enthalpy output was constant. If this is also a feature of the working heart during normal activity then it would enable the rate of mitochondrial ATP production to proceed at a fairly constant rate and avoid the need for substantial, short-term alterations in the rate of substrate oxidation. This phenomenon would then provide a mechanism for the matching of energy supply to energy demand during much of normal cardiac activity.

References

Aasum, E. and Larsen, T. S. (1999). Different tolerance to hypothermia and rewarming of isolated rat and guinea pig hearts. *Cryobiology* **38**, 243-249.

Allen, D. G., Cairns, S. P., Turvey, S. E. and Lee, J. A. (1993). Intracellular calcium and myocardial function during ischemia. *Adv Exp Med Biol* **346**, 19-29.

Allen, D. G., Lee, J. A. and Smith, G. L. (1989). The consequences of simulated ischaemia on intracellular Ca^{2+} and tension in isolated ferret ventricular muscle. *J Physiol* **410**, 297-323.

Altringham, J. D. and Johnston, I. A. (1990). Scaling effects on muscle function: power output of isolated fish muscle fibres performing oscillatory work. *J Exp Biol* **151**, 453-467.

Armour, J. A. and Randall, W. C. (1970). Electrical and mechanical activity of papillary muscle. *Am J Physiol* **218**, 1710-1717.

Askew, G. N. and Marsh, R. L. (1997). The effects of length trajectory on the mechanical power output of mouse skeletal muscles. *J Exp Biol* **200**, 3119-3131.

Backx, P. H., Gao, W. D., Azan-Backx, M. D. and Marban, E. (1994). Mechanism of force inhibition by 2,3-butanedione monoxime in rat cardiac muscle: roles of $[Ca^{2+}]_i$ and cross-bridge kinetics. *J Physiol* **476**, 487-500.

Barclay, C. J. (1994). Efficiency of fast- and slow-twitch muscles of the mouse performing cyclic contractions. *J Exp Biol* **193**, 65-78.

Barclay, C. J. (1999). A weakly coupled version of the Huxley crossbridge model can simulate energetics of amphibian and mammalian skeletal muscle. *J Muscle Res Cell Motil* **20**, 163-176.

Barclay, C. J., Arnold, P. D. and Gibbs, C. L. (1995). Fatigue and heat production in repeated contractions of mouse skeletal muscle. *J Physiol* **488**, 741-752.

Baxi, J., Barclay, C. J. and Gibbs, C. L. (2000). Energetics of rat papillary muscle during contractions with sinusoidal length changes. *Am J Physiol* **278**, H1545-1554.

Belke, D. D., Wang, L. C. H. and Lopaschuk, G. D. (1997). Effects of hypothermia on energy metabolism in rat and Richardson's ground squirrel hearts. *J Appl Physiol* **82**, 1210-1218.

Bigelow, W. G., Lindsay, W. K. and Greenwood, W. F. (1950a). Hypothermia. *Ann Surg* **132**, 849-866.

Bigelow, W. G., Lindsay, W. K., Harrison, R. C., Gordon, R. A. and Greenwood, W. F. (1950b). Oxygen transport and utilization in dogs at low body temperatures. *Am J Physiol* **160**, 125-137.

Brady, A. J. (1971). A measurement of the active state in heart muscle. *Cardiovasc Res* **1**, Suppl 1:11-17.

Buckberg, G. D., Brazier, J. R., Nelson, R. L., Goldstein, S. M., McConnell, D. H. and Cooper, N. (1977). Studies of the effects of hypothermia on regional myocardial blood flow and metabolism during cardiopulmonary bypass. I. The adequately perfused beating, fibrillating and arrested heart. *J Thorac Cardiovasc Surg* **73**, 87-94.

Capasso, J. M., Remily, R. M. and Sonnenblick, E. H. (1982). Alterations in mechanical properties of rat papillary muscle during maturation. *Am J Physiol* **242**, H359-364.

Chambers, D. J., Braimbridge, M. V. and Hearse, D. J. (1991). Perfusate calcium: effect on cardiac stability and response to ischemia and reperfusion. *Can J Cardiol* **7**, 410-418.

Chapman, J. B. (1976). Heat and fluorescence changes in cardiac muscle: effects of substrate and calcium. *J Mol Cell Cardiol* **8**, 545-558.

Close, R. I. (1981). Activation delays in frog twitch muscle fibres. *J Physiol* **313**, 81-100.

Cook, D. J. (1999). Changing temperature management for cardiopulmonary bypass. *Anesth Analg* 88, 1254-1271.

Cronin, R., Armour, J. A. and Randall, W. C. (1969). Function of the in-situ papillary muscle in the canine left ventricle. *Circ Res* 25, 67-75.

Curtin, N. A. and Woledge, R. C. (1993). Efficiency of energy conversion during sinusoidal movement of white muscle fibres from the dogfish *Scyliorhinus Canicula*. *J Exp Biol* 183, 137-147.

Dijkema, F. K., Elzinga, G. and Holewijn, A. J. (1985). Measurement of temperature changes in muscle contraction with a thermopile and amplifier designed to improve signal-to-noise ratio and resolution in time and place. *Proc R Soc Lond B* 366, 4P.

Doherty, N. E., Turocy, J. F., Geffin, G. A., O'Keefe, D. D., Titus, J. S. and Daggett, W. M. (1992). Benefits of glucose and oxygen in multidose cold cardioplegia. *J Thorac Cardiovasc Surg* 103, 219-229.

Donald, T. C., Reeves, D. N. S., Reeves, R. C., Walker, A. A. and Hefner, L. L. (1980). Effect of damaged ends in papillary muscle preparations. *Am J Physiol* 238, H14-23.

Drexler, H., Flaim, S. F., Fields, R. H. and Zelis, R. (1985). Effects of nisoldipine on cardiocirculatory dynamics and cardiac output in conscious rats at rest and during treadmill exercise. *J Pharmacology Experi Thera*, 376-381.

Elliott, A. C., Smith, G. L. and Allen, D. G. (1994). The metabolic consequences of an increase in the frequency of stimulation in isolated ferret hearts. *J Physiol* 474, 147-159.

Elzinga, G. and Westerhof, N. (1980). Pump function of the feline left heart: changes with heart rate and its bearing on the energy balance. *Cardiovasc Res* 14, 81-92.

Ericsson, A. B., Takeshima, S. and Vaage, J. (1999). Warm or cold continuous blood cardioplegia provides similar myocardial protection. *Ann Thorac Surg* 68, 454-459.

Frampton, J. E., Harrison, S. M., Boyett, M. R. and Orchard, C. H. (1991). Ca^{2+} and Na^+ in rat myocytes showing different force-frequency relationships. *Am J Physiol* 261, C739-750.

Gaillard, D., Bical, O., Paumier, D. and Trivin, F. (2000). A review of myocardial normothermia: its theoretical basis and the potential clinical benefits in cardiac surgery. *Cardiovasc Surg* 8, 198-203.

Geddes, L. A. and Baker, L. E. (1968). Criteria for the faithful reproduction of an event. In *Principles of Applied Biomedical Instrumentation*, New York: Wiley.

Gibbs, C. L. (1978). Cardiac energetics. *Physiol Rev* 58, 174-254.

Gibbs, C. L. and Barclay, C. J. (1995). Cardiac efficiency. *Cardiovasc Res* 30, 627-634.

Gibbs, C. L. and Barclay, C. J. (1998). Efficiency of skeletal and cardiac muscle. *Adv Exp Med Biol* 453, 527-535.

Gibbs, C. L. and Chapman, J. B. (1979a). Cardiac energetics. In *Handbook of Physiology - The Cardiovascular System I*, vol. 1 (ed. R. M. Berne, N. Sperelakis and S. Geiger), pp. 775-804. Maryland, MD: American Physiological Society.

Gibbs, C. L. and Chapman, J. B. (1979b). Cardiac heat production. *Annu Rev Physiol* 41, 507-519.

Gibbs, C. L. and Gibson, W. R. (1970). Energy production in cardiac isotonic contractions. *J Gen Physiol* 56, 732-750.

Gibbs, C. L. and Loiselle, D. S. (2001). Cardiac basal metabolism. *Jap J Physiol* 51, 399-426.

Gibbs, C. L., Mommaerts, W. F. and Ricchiuti, N. V. (1967). Energetics of cardiac contractions. *J Physiol* 191, 25-46.

Gibbs, C. L., Papadoyannis, D. E., Drake, A. J. and Noble, M. I. (1980). Oxygen consumption of the nonworking and potassium chloride-arrested dog heart. *Circ Res* 47, 408-417.

Gorman, J. H., Gupta, K. B., Streicher, J. T., Gorman, R. C., Jackson, B. M., Ratcliffe, M. B., Bog, D. K. and Edmunds, L. H. (1996). Dynamic three-dimensional imaging of the mitral valve and left ventricle by rapid sonomicrometry array localization. *J Thorac Cardiovasc Surg* 112, 712-726.

Gwathmey, J. K., Hajjar, R. J. and Solaro, R. J. (1991). Contractile deactivation and uncoupling of crossbridges. Effects of 2,3- butanedione monoxime on mammalian myocardium. *Circ Res* 69, 1280-1292.

Hajjar, R. J., Ingwall, J. S. and Gwathmey, J. K. (1994). Mechanism of action of 2,3-butanedione monoxime on contracture during metabolic inhibition. *Am J Physiol* 267, H100-108.

Hartree, W. and Hill, A. V. (1928). The energy liberated by an isolated muscle during the performance of work. *Proc R Soc Lond B* **104**, 1-27.

Harwood, C. L., Young, I. S. and Altringham, J. D. (1998). Influence of cycle frequency, muscle strain and muscle length on work and power production of rainbow trout (*Oncorhynchus mykiss*) ventricular muscle. *J Exp Biol* **201**, 2723-2733.

Hearse, D. J. (1990). Ischemia, reperfusion, and the determinants of tissue injury. *Cardiovasc Drugs Ther* **4**, Suppl 4: 767-776.

Hearse, D. J. and Bolli, R. (1992). Reperfusion induced injury: manifestations, mechanisms, and clinical relevance. *Cardiovasc Res* **26**, 101-108.

Henderson, A. H., Craig, R. J., Sonnenblick, E. H. and Urschel, C. W. (1970). Species differences in intrinsic myocardial contractility. *Proc Soc Exptl Biol Med* **134**, 930-932.

Hibberd, M. G., Dantzig, J. A., Trentham, D. R. and Goldman, Y. E. (1985). Phosphate release and force generation in skeletal muscle fibers. *Science* **228**, 1317-1319.

Hill, A. V. (1931). Myothermic experiment on a frog gastrocnemius. *Proc R Soc Lond B* **109**, 267-303.

Hill, A. V. (1937). Methods of analyzing the heat production of muscle. *Proc R Soc Lond B* **124**, 114-136.

Hill, A. V. (1949). The energetics of relaxation in a muscle twitch. *Proc R Soc Lond B* **136**, 211-219.

Hill, A. V. (1952). The thermodynamics of elasticity in resting striated muscle. *Proc R Soc Lond B* **139**, 464-497.

Hirakawa, S., Sasayama, S., Tomoike, H., Crozatier, B., Franklin, D., McKown, D. and Ross, J., Jr. (1977). In situ measurement of papillary muscle dynamics in the dog left ventricle. *Am J Physiol* **233**, H384-391.

Hisano, R. and Cooper, G. (1987). Correlation of force-length area with oxygen consumption in ferret papillary muscle. *Circ Res* **61**, 318-328.

Holroyd, S. M. and Gibbs, C. L. (1992). Is there a shortening-heat component in mammalian cardiac muscle contraction? *Am J Physiol* **262**, H200-208.

Hunter, P. J., McCulloch, A. D. and ter Keurs, H. E. (1998). Modelling the mechanical properties of cardiac muscle. *Prog Biophys Mol Biol* **69**, 289-331.

Huxley, A. F. (1973). A note suggesting that the cross-bridge attachment during muscle contraction may take place in two stages. *Proc R Soc Lond B* **183**, 83-86.

Jennings, R. B. and Reimer, K. A. (1991). The cell biology of acute myocardial ischemia. *Annu Rev Med* **42**, 225-246.

Josephson, R. K. (1985). Mechanical power output from striated muscle during cyclic contraction. *J Exp Biol* **114**, 493-512.

Josephson, R. K. (1993). Contraction dynamics and power output of skeletal muscle. *Annu Rev Physiol* **55**, 527-546.

Karas, S. and Elkins, R. C. (1970). Mechanism of function of the mitral valve leaflets, chordae tendineae and left ventricular papillary muscles in dogs. *Circ Res* **26**, 689-696.

Kaye, G. W. C. and Laby, T. H. (1973). Tables of physical and chemical constants. London: Longmans.

Kentish, J. C. (1991). Combined inhibitory actions of acidosis and phosphate on maximum force production in rat skinned cardiac muscle. *Pflugers Arch* **419**, 310-318.

Kiriazis, H. and Gibbs, C. L. (1995). Papillary muscles split in the presence of 2,3-butanedione monoxime have normal energetic and mechanical properties. *Am J Physiol* **269**, H1685-1694.

Kiriazis, H. and Gibbs, C. L. (2000). Effects of aging on the work output and efficiency of rat papillary muscle. *Cardiovasc Res* **48**, 111-119.

Kotsanas, G., Holroyd, S. M., Wendt, I. R. and Gibbs, C. L. (1993). Intracellular Ca^{2+}, force and activation heat in rabbit papillary muscle: effects of 2,3-butanedione monoxime. *J Mol Cell Cardiol* **25**, 1349-1358.

Kretzschmar, K. M. and Wilkie, D. R. (1972). A new method for absolute heat measurement, utilizing the Peltier effect. *J Physiol* **224**, 18P-21P.

Kretzschmar, K. M. and Wilkie, D. R. (1975). The use of the Peltier effect for simple and accurate calibration of thermoelectric devices. *Proc R Soc Lond B* **190**, 315-321.

Layland, J., Young, I. S. and Altringham, J. D. (1995). The effect of cycle frequency on the power output of rat papillary muscles *in vitro*. *J Exp Biol* **198**, 1035-1043.

Leblanc, N., Chartier, D., Gosselin, H. and Rouleau, J. L. (1998). Age and gender differences in excitation-contraction coupling of the rat ventricle. *J Physiol* **511**, 533-548.

Lichtenstein, S. V., Abel, J. G. and Salerno, T. A. (1991a). Warm heart surgery and results of operation for recent myocardial infarction. *Ann Thorac Surg* **52**, 455-460.

Lichtenstein, S. V., Ashe, K. A., el Dalati, H., Cusimano, R. J., Panos, A. and Slutsky, A. S. (1991b). Warm heart surgery. *J Thorac Cardiovasc Surg* **101**, 269-274.

Liu, B., Arlock, P., Wohlfart, B. and Johansson, B. W. (1991a). Temperature effects on the Na and Ca currents in rat and hedgehog ventricular muscle. *Cryobiology* **28**, 96-104.

Liu, B., Belke, D. D. and Wang, L. C. (1997). Ca^{2+} uptake by cardiac sarcoplasmic reticulum at low temperature in rat and ground squirrel. *Am J Physiol* **272**, R1121-1127.

Liu, B., Wang, L. C. and Belke, D. D. (1991b). Effect of low temperature on the cytosolic free Ca^{2+} in rat ventricular myocytes. *Cell Calcium* **12**, 11-18.

Liu, B., Wohlfart, B. and Johansson, B. W. (1990a). Effects of low temperature on contraction in papillary muscles from rabbit, rat, and hedgehog. *Cryobiology* **27**, 539-546.

Liu, B., Wohlfart, B. and Johansson, B. W. (1990b). Mechanical restitution at different temperatures in papillary muscles from rabbit, rat, and hedgehog. *Cryobiology* **27**, 596-604.

Loiselle, D. (1985a). A theoretical analysis of the rate of resting metabolism of isolated papillary muscle. *Adv Myocardiol* **6**, 205-216.

Loiselle, D. S. (1979). The effects of temperature on the energetics of rat papillary muscle. *Pflugers Arch* **379**, 173-180.

Loiselle, D. S. (1982). Stretch-induced increase in resting metabolism of isolated papillary muscle. *Biophys J* **38**, 185-194.

Loiselle, D. S. (1985b). The rate of resting heat production of rat papillary muscle. *Pflugers Arch* **405**, 155-162.

Loiselle, D. S. and Gibbs, C. L. (1979). Species differences in cardiac energetics. *Am J Physiol* **237**, H90-98.

Mahler, M., Louy, C., Homsher, E. and Peskoff, A. (1985). Reappraisal of diffusion, solubility, and consumption of oxygen in frog skeletal muscle, with applications to muscle energy balance. *J Gen Physiol* **86**, 105-134.

Marsh, R. L. (1999). How muscles deal with real-world loads: the influence of length trajectory on muscle performance. *J Exp Biol* **202**, 3377-3385.

Martin, T. D., Craver, J. M., Gott, J. P., Weintraub, W. S., Ramsay, J., Mora, C. T. and Guyton, R. A. (1994). Prospective, randomized trial of retrograde warm blood cardioplegia: myocardial benefit and neurologic threat. *Ann Thorac Surg* **57**, 298-304.

Marzilli, M., Sabbah, H. N., Goldstein, S. and Stein, P. D. (1985). Assessment of papillary muscle function in the intact heart. *Circulation* **71**, 1017-1022.

Marzilli, M., Sabbah, H. N., Lee, T. and Stein, P. D. (1980). Role of the papillary muscle in opening and closure of the mitral valve. *Am J Physiol* **238**, H348-354.

Mast, F. and Elzinga, G. (1988). Recovery heat production of isolated rabbit papillary muscle at 20°C. *Pflugers Arch* **411**, 600-605.

Mast, F. and Elzinga, G. (1990). Heat released during relaxation equals force-length area in isometric contractions of rabbit papillary muscle. *Circ Res* **67**, 893-901.

Mauney, M. C. and Kron, I. L. (1995). The physiologic basis of warm cardioplegia. *Ann Thorac Surg* **60**, 819-823.

Melrose, D. G., Dreyer, B., Bentall, H. H. and Baker, J. E. (1955). Elective cardiac arrest. *Lancet* **2**, 21-22.

Miyazaki, S., Guth, B. D., Miura, T., Indolfi, C., Schulz, R. and Ross, J. (1990). Changes of left ventricular diastolic function in exercising dogs without and with ischemia. *Circulation* **81**, 1058-1070.

Moon, T. W., Altringham, J. D. and Johnston, I. A. (1991). Energetics and power output of isolated fish fast muscle fibres performing oscillatory work. *J Exp Biol* **158**, 261-273.

Mulieri, L. A., Hasenfuss, G., Ittleman, F., Blanchard, E. M. and Alpert, N. R. (1989). Protection of human left ventricular myocardium from cutting injury with 2,3-butanedione monoxime. *Circ Res* **65**, 1441-1449.

Mulieri, L. A., Hasenfuss, G., Leavitt, B., Allen, P. D. and Alpert, N. R. (1992). Altered myocardial force-frequency relation in human heart failure. *Circulation* **85**, 1743-1750.

Mulieri, L. A., Luhr, G., Trefry, J. and Alpert, N. R. (1977). Metal-film thermopiles for use with rabbit right ventricular papillary muscles. *Am J Physiol* **233**, C146-156.

Mullin, W. J., Herrick, R. E., Valdez, V. and Baldwin, K. M. (1984). Adaptive responses of rats trained with reductions in exercise heart rate. *J Appl Physiol* **56**, 1378-1382.

Orme, S. K. and Kelly, G. A. (1977). Glucose metabolism in the hypothermic perfused rat heart. *Life Sci* **20**, 597-608.

Palmer, S. and Kentish, J. C. (1996). Developmental differences and regional similarities in the responses of rat cardiac skinned muscles to acidosis, inorganic phosphate and caffeine. *J Mol Cell Cardiol* **28**, 797-805.

Paul, R. J. (1983). Physical and biochemical energy balance during an isometric tetanus and steady state recovery in frog sartorius at 0°C. *J Gen Physiol* **81**, 337-354.

Perreault, C. L., Mulieri, L. A., Alpert, N. R., Ransil, B. J., Allen, P. D. and Morgan, J. P. (1992). Cellular basis of negative inotropic effect of 2,3-butanedione monoxime in human myocardium. *Am J Physiol* **263**, H503-510.

Peterson, J. N., Hunter, W. C. and Berman, M. R. (1989). Control of segment length or force in isolated papillary muscle: an adaptive approach. *Am J Physiol* **256**, H1726-1734.

Press, W. H., Teukolsky, S. A., Vetterling, S. A. and Flannery, B. P. (1992). Numerical Recipes in C. New York: Cambridge University Press.

Ravens, U. (1992). Post-rest potentiation and its decay. In *The Interval-Force Relationship of the Heart: Bowditch Revisited*, (ed. M. I. M. Noble and W. A. Seed), pp. 245-258. Great Britain: Cambridge University Press.

Rayhill, S. C., Daughters, G. T., Castro, L. J., Niczyporuk, M. A., Moon, M. R., Ingels, N. B., Stadius, M. L., Derby, G. C., Bolger, A. F. and Miller, D. C. (1994). Dynamics of normal and ischemic canine papillary muscles. *Circ Res* **74**, 1179-1187.

Rossmanith, G. H., Hoh, J. F., Kirman, A. and Kwan, L. J. (1986). Influence of V_1 and V_3 isomyosins on the mechanical behaviour of rat papillary muscle as studied by pseudo-random binary noise modulated length perturbations. *J Muscle Res Cell Motil* **7**, 307-319.

Sagawa, K., Maughan, L., Suga, H. and Sunagawa, K. (1988). Cardiac contraction and the pressure-volume relationship. New York: Oxford University Press, Inc.

Sellin, L. C. and McArdle, J. J. (1994). Multiple effects of 2,3-butanedione monoxime. *Pharmacol Toxicol* **74**, 305-313.

Semafuko, W. E. B. and Bowie, W. C. (1975). Papillary muscle dynamics: in situ function and responses of the papillary muscle. *Am J Physiol* **228**, 1800-1807.

Sonnenblick, E. H. (1962). Implications of muscle mechanics in the heart. *Fedn Proc* **21**, 975-993.

Sonnenblick, E. H. (1964). Series elastic and contractile elements in heart muscle: changes in muscle length. *Am J Physiol* **207**, 1330-1338.

Stephenson, E. R., Jayawant, A. M., Baumgarten, C. M. and Damiano, R. J. (2000). Cardioplegia-induced cell swelling: prevention by normothermic infusion. *Ann Thorac Surg* **69**, 1393-1398.

Stringham, J. C., Southard, J. H., Hegge, J., Triemstra, L., Fields, B. L. and Belzer, F. O. (1992). Limitations of heart preservation by cold storage. *Transplantation* **53**, 287-294.

Suga, H. (1990). Ventricular energetics. *Physiol Rev* **70**, 247-277.

Suga, H., Goto, Y., Igarashi, Y., Yasumura, Y., Nozawa, T., Futaki, S. and Tanaka, N. (1988). Cardiac cooling increases E_{max} without affecting relation between O_2 consumption and systolic pressure-volume area in dog left ventricle. *Circ Res* **63**, 61-71.

Syme, D. A. (1994). The efficiency of frog ventricular muscle. *J Exp Biol* **197**, 143-164.

Syme, D. A. and Josephson, R. K. (1995). Influence of muscle length on work from trabecular muscle of frog atrium and ventricle. *J Exp Biol* **198**, 2221-2227.

Taylor, T. W., Goto, Y. and Suga, H. (1993). Variable cross-bridge cycling-ATP coupling accounts for cardiac mechanoenergetics. *Am J Physiol* **264**, H994-1004.

Thurston, J. T., Burlington, R. F. and Meininger, G. A. (1978). Effect of low temperatures on rat myocardial Mg-ATPase and NaK-ATPase. *Cryobiology* **15**, 312-316.

Ullrick, W. C. (1964). Characteristic force-velocity equation of rat heart muscle. *Am J Physiol* **206**, 1285-1290.

Wang, S. N., Wyeth, R. P. and Kennedy, R. H. (1998). Effects of gender on the sensitivity of rat cardiac muscle to extracellular Ca^{2+}. *Eur J Pharmacol* **361**, 73-77.

Watkins, M. W., Slinker, B. K., Goto, Y. and LeWinter, M. M. (1992). 2,3-Butanedione monoxime increases contractile efficiency in the rabbit ventricle. *Am J Physiol* **263**, H1811-1818.

Wendt, I. R. and Loiselle, D. S. (1981). The effect of external calcium concentration on activation heat in cardiac muscle. *J Mol Cell Cardiol* **13**, Suppl 3: 8P.

West, J. M. and Stephenson, D. G. (1989). Contractile activation and the effects of 2,3-butanedione monoxime (BDM) in skinned cardiac preparations from normal and dystrophic mice (129/ReJ). *Pflugers Arch* **413**, 546-552.

Woledge, R. C. (1998). Techniques for muscle energetics. In *Current Methods in Muscle Physiology: Problems and Limitations*, (ed. H. Sugi), pp. 343-370. Oxford: Oxford University Press.

Woledge, R. C., Curtin, N. A. and Homsher, E. (1985). Energetic aspects of muscle contraction. London: Academic Press.

Woledge, R. C. and Reilly, P. J. (1988). Molar enthalpy change for hydrolysis of phosphorylcreatine under conditions in muscle cells. *Biophys J* **54**, 97-104.

Wong, A. Y. (1973). Some proposals in cardiac muscle mechanics and energetics. *Bull Math Biol* **35**, 375-399.